Optical vapour pressure monitoring and mass transport control during bulk CdTe crystal growth in a novel multi-tube PVT system

Alabert, Josep Carles

Optical Vapour Pressure Monitoring and Mass Transport Control during Bulk CdTe Crystal Growth in a Novel Multi-Tube PVT System

by

Josep Carles Alabert

A thesis presented in candidature for the degree of

Doctor of Philosophy

in the

University of Durham

UK

Department of Physics

April 1998

ABSTRACT

This work is concerned with the development of a new vapour growth system for the growth of high quality bulk CdTe crystals, and, in particular, the study of mass transport control and *in situ* vapour pressure monitoring during growth in this system.

The Multi-tube Physical Vapour Transport (MPVT) apparatus designed in Durham incorporates several modifications and improvements from past PVT methods. The U-shaped system, which is based on the Markov design, consists of three main parts, namely the source, crossmember and growth tubes, and allows to some extent decoupling of the temperature fields between source and growth regions. The introduction of the crossmember is effectively the technological key that enables the use of a flow restrictor to control mass transport and the introduction of a non-intrusive optical absorption technique capable of monitoring the partial vapour pressures of the vapour elemental constituents, i.e. Cd atoms and Te_2 molecules, as growth proceeds.

The optical absorption in the near UV and Visible spectrum of Cd and Te_2 vapours has been quantitatively studied. The non-overlapping of the tellurium and the cadmium absorption bands allowed the use of a simple and compact light and detection system for *in situ* monitoring of vapour partial Cd and Te_2 pressures independently during growth in the MPVT apparatus. In particular, the optical absorption system is capable of monitoring, after suitable calibration, cadmium vapour pressures in the range 0.01-20 mbar and tellurium vapour pressures in the range 0.1-18 mbar

The use of porous silica discs for use as flow restrictors is quantitatively studied both using theory and experiment. The transport properties of these discs as a function of intrinsic parameters (porosity, dimensions and specific surface area) and extrinsic parameters (temperature, pressure and molecular weight of the gas) are evaluated experimentally in detail. The experimental results are found to agree with the predictions of standard theoretical expressions. In particular, for the case of a multicomponent vapour, i.e. Cd and Te_2 vapour mixture, it is experimentally found that the porous silica flow restrictor can also set the stoichiometry of the vapour to a smaller value than that expected under congruent CdTe sublimation.

It is shown that use of a porous silica disc in conjunction with dynamic pumping during growth allows the mass transport rate to be set to the desired value, and permits diffusionless transport. Modelling of the transport process under several possible flow regimes encountered during normal growth conditions is also presented. The model, which assumes that diffusion mechanisms are unimportant, allows expressions to be obtained for the mass transport rate through the flow restrictor (porous disc or capillary) in the crossmember, the growth rate and the stoichiometry of the vapour above the source and crystal.

Optical monitoring during CdTe growth carried out in several growth runs confirms both the predictions of the model concerning the stoichiometry of the vapour and its usefulness as a possible tool to monitor the growth process and growth rate.

DECLARATION

I declare that all the work reported in this thesis was carried out by the candidate except when explicitly stated otherwise. I also declare that none of this work has been previously submitted for any degree and that it is not currently being submitted for any other degree.

Dr. A. W. Brinkman

Supervisor

Josep Carles Alabert

Candidate

ACKNOWLEDGEMENTS

I would like to firstly express my gratitude and thanks to my supervisor Dr. Andy W. Brinkman for his supervision and encouragement throughout the course of this work and for giving me the opportunity of doing this Ph.D. degree. I would also like to thank Dr. Rafael Rodriguez-Clemente for bringing to my knowledge the possibility of doing this work.

Many thanks also go to all the members and previous members of the II-VI Semiconductors & Ceramics group for their friendship and help during the course of this work. Special thanks go to Dr. S. Oktik and Dr. H. M. Al-Allak for helping me feel part of the group in the very beginning. I also thank K. Durose for stimulating and beneficial discussions. Many special thanks go to the fellow Ph.D. and M.Sc. students with whom a good companionship relation was established, in particular, Paul R. Edwards and Matt Hogan, as well as Dr. Simon Galloway. Some work in this thesis could have not been produced without the support of Dr. J. T. Mullins. I thank him for the technical help for some of my experiments as well as for allowing me to use some experimental data obtained by him. I am also grateful to Professor Brian Mullin for many helpful discussions and for sharing with me some of his almost infinite knowledge and experience in crystal growth. I am grateful to Norman Thompson, David Pattison and John E. Gibson for the technical support and help provided throughout the course of this work. I am also very grateful to the members of staff of the Mechanical and Electrical Workshop of the Engineering Department, in particular Harry Kelly, for his skilful technical help and always speedy help when most needed. Special thanks go to the glassblowers in the Chemistry Department Ray Hart and Gordon Haswell for their skilful glasswork, and Sergei Petrov for his russian translations of some papers. I would also like to thank all my friends in Roses, Barcelona and Durham who have helped me to maintain enthusiasm and for a great time during my stay in England. They know who they are. I wish to give many special thanks to all my family, specially mum and dad, for their love, extreme support and constant encouragement. I am indebted to the European Community for their financial help through the Brite-Euram Program, grant n° BRE2-CT94-3094 and Training and Mobility of Researchers scheme, grant n° FMBI-CT96-1625.

STATEMENT OF COPYRIGHT

This thesis is dedicated

to Mum and Dad

CONTENTS

CHAPTER THREE

The New "Multi-tube" PVT Apparatus for CdTe Growth.

CHAPTER FOUR

Cd and Te_2 Optical Absorption and Its Application to Vapour Pressure Monitoring.

Chapter One

Introduction

1.0 INTRODUCTION.

CdTe is a strategically important II-VI semiconductor with a range of uses in several areas. Its main application in the past was, due to its similar lattice parameter, as a substrate for the epitaxial growth of $Hg_{1-x}Cd_xTe$, a material of tuneable bandgap developed for infrared detection applications [1,2]. Presently CdTe has been replaced by $Cd_{1-x}Zn_xTe$ as the substrate material, since compositions containing ~ 4% of Zn are near-lattice matched to $Hg_{1-x}Cd_xTe$ for the important $Hg_{1-x}Cd_xTe$ compositions [2]. Despite improvements in the growth of bulk $Hg_{1-x}Cd_xTe$ [2], there is still a demand for high quality (low dislocation densities $\leq 10^4$ cm^{-2}, twin free, low concentrations of small size ($\leq$ 1-5 μm size) inclusions and no larger inclusions), high resistivity, highly uniform large ($\geq$ 50 mm) diameter wafers for use in X-ray and γ-ray solid state room temperature radiation detectors [3]. In addition, the large electro-optical coefficient of CdTe [4] has recently attracted much attention for use in optoelectronics.

Most of the applications mentioned above have been and still are constrained by the lack of large area CdTe wafers of consistent good quality. Commercially available CdTe or $Cd_{1-x}Zn_xTe$ is normally grown from the melt. The boules obtained are usually of poor quality (multigrained and twinned) and must be mined in order to obtain usable, normally small size ($\leq$ 40×60 mm) wafers. Some encouraging results have been obtained recently using melt methods [1], but in general there is a lack of consistency and reliability in the achievement of good quality CdTe crystals, mainly due to the intrinsic structural and thermodynamical properties of the material itself.

Although vapour growth offers a number of *a priori* advantages for the growth of CdTe high quality and large area substrates, it has been used in the past mainly to obtain small crystals for research and academic purposes, and as a consequence, the technology, with perhaps a few exceptions [5,6] is not fully understood *and* developed. In particular, run-to-run reproducibility is poor, despite numerous studies of the vapour growth of CdTe and II-VI compounds in general. Significant advances have been made in the vapour growth technology and fundamental physico-chemical aspects involved in it recently, but, disappointingly, for the production of another important semiconductor, SiC [7] and not CdTe or related II-VI compounds. However, the SiC work has demonstrated that the failure of vapour growth techniques to produce large single CdTe crystals is primarily due to the technology involved, rather than to any fundamental limitations of the process.

This thesis is an effort to demonstrate the usefulness and potential of vapour growth in obtaining high quality CdTe. The thesis describes the development of a new bulk vapour growth technique and its application to the growth of CdTe crystals and focuses on mass transport mechanisms and their modelling, and vapour pressure monitoring during the growth process. The growth system was designed as part of the Brite Euram II, Vapour*Cryst project, funded by the European Community (contract BRE2.CT94.0609), and titled *Advanced Vapour Growth Technology for High Quality Bulk Crystals for Optical, Substrate and Sensor Materials.*

Chapter two can be divided in two main parts. First, a brief review of those properties of CdTe which are relevant to the crystal grower is presented. The second part attempts to summarise past work in the vapour crystal growth of CdTe. Some

references to vapour growth techniques and results for other materials are also presented. In chapter two, the intention is not to review all the techniques and results available in the literature, but to highlight the main improvements, and perhaps most importantly, outline the advantages and disadvantages of each vapour growth technique. The chapter concludes with an analysis of CdTe properties and growth methods that should be taken into account in the design of a new growth system.

Chapter three describes the new "Multi-tube" vapour growth system based on the modified Markov [6] design and developed in Durham mainly by Dr. J. T. Mullins. The most innovative aspect of the "Multi-tube" PVT originated from the conceptually simple idea of bending the silica tube that contains the source and seed, forming a U-shaped ampoule. With this arrangement, the system is composed of three elements, namely the source side, the crossmember part and the growth side. As explained in chapter three, this configuration allows the temperatures of the source and growth sides to be controlled almost independently, but also constitutes the technological key that allows for the introduction of a flow restrictor (capillary or porous silica disc) designed to control the mass transport rate. The introduction of the crossmember also allows optical access to the surface of the crystal and source, thus permitting visual monitoring as well as, in principle, precise temperature monitoring of the crystal surface with a pyrometer. The crossmember also allows the introduction of an optical absorption technique that can monitor the partial vapour pressures of the elemental vapour constituents at both sides of the flow restrictor as the growth proceeds. Chapter three also describes several other modifications from traditional PVT systems that the Multi-tube PVT system incorporates, such as the ability to introduce a constant gas flow

during growth, and the constant removal of outgassing and volatile impurities through the use of dynamic pumping without diminishing significantly the crystal yield.

Chapter four describes the optical absorption technique and the compact apparatus developed for the monitoring of vapour pressures during growth. Fundamental optical absorption properties of the main constituents of the vapour, namely Cd atoms and Te_2 molecules are quantitatively studied and presented. Conclusions drawn from these quantitative results allowed the design and construction of a simple apparatus that can be used in conjunction with the Multi-tube PVT system to monitor reliably and in real time, the partial pressures of Cd and Te_2 at both the source and growth sides after a simple set of calibrations is obtained. In particular, the calibration expressions and curves obtained allowed reliable measurement of cadmium and tellurium partial pressures during typical vapour growth conditions.

Chapter five focuses on the use of a porous silica disc for use as a flow restrictor to control the mass transport rate of CdTe. The intrinsic nature of the porous disc may condition the flow regime and hence the dependency of the transport rate on the partial pressures. Quantitative analysis (using both theoretical expressions and experimental results) is described which details the ways in which the flow regime influences the partial pressure ratio of the elemental vapour constituents. It is shown that the porous silica disc replaces the need for a temperature gradient between source and growth locations, since the driving force to transport the vapour is provided by the pressure difference across the silica disc and dynamic pumping from the growth side. Chapter five ends by showing that relatively simple modelling of the flow properties of the silica disc can be used to estimate mass transport rates.

Chapter six presents a simple model to evaluate the transport and crystal growth rate in the Multi-tube PVT system, using known flow expressions. Although the model is comparatively simple and assumes that transport is not diffusion limited due to the use of a flow restrictor and dynamic pumping, it is seen to predict correctly the ratio of partial pressures in both source and growth sides and hence allows determination of transport and growth rates.

Chapter seven describes some growth experiments carried out in the Multi-tube PVT system. In particular, the optical monitoring system described in chapter 5 is used to obtain the partial pressure ratios during growth. The usefulness of the vapour monitoring system is also evaluated.

Finally, chapter 8 summarises the main results obtained in this work and gives an outline for further research and improvements of the MPVT system. A discussion on the possibilities of the MPVT system for research and production of CdTe and other compounds is also included.

REFERENCES FOR CHAPTER ONE

[1] *Widegap II-VI Compounds for Opto-Electronic Applications.* Electronic Materials Series, volume 1. Edited by H. E. Ruda. Chapman & Hall, London (1992).

[2] *Narrow-Gap II-VI Compounds for Optoelectronic and Electromagnetic Applications.* Electronic Materials Series, volume 3. Edited by P. Capper. Chapman & Hall, London (1997).

[3] *Semiconductors for Room Temperature Nuclear Detectors Applications.* Semiconductors and Semimetals Treatise, volume 43. Edited by T. E. Schelesinger and R. B. James. Academic Press, San Diego (1995).

[5] *Cadmium Telluride.* Semiconductors and Semimetals Treatise, Volume 13. Edited by R. K. Willardson and A. C. Beer. Academic Press, London (1978).

[4] J. Y. Moisan, P. Gravey, G. Picoli, N. Wolffer and V. Vieux. *"Potentiality of Photorefractive CdTe"*. Mat. Sci. Eng.. B16 (1993) 257.

[5] F. Rosenberger, M. Banish and M. B. Duval. *Vapour Crystal Growth Technology Development – Application to Cadmium Telluride.* NASA Technical Memorandum 103786 (1991).

[6] M. Laasch, T. Kunz, C. Eiche, M. Fierderle, W. Joerger, G. Kloess and K. W. Benz. *"Growth of Twin-Free CdTe Single Crystals in a Semi-Closed Vapour Phase System"*. J. Crystal Growth, **174** (1997) 696.

[7] D. Hofmann, R. Eckstein, M. Kölbl, Y. Makarov, St. G. Müller, E. Schmitt, A. Winnacker, R. Rupp, R. Stein and J. Völkl. *"SiC Bulk Growth by Physical Vapor Transport and Its Global Modelling"*. J. Crystal Growth, **174** (1997) 669.

Chapter Two

Vapour Crystal Growth and CdTe Related Properties

2.0 INTRODUCTION.

This chapter describes some important CdTe properties, knowledge of which is essential for controlled CdTe crystal growth from the vapour. A short historical review of the vapour techniques used in the past to grow cadmium telluride crystals is also presented. The intention here is not to produce a compilation of all the work done in this field to date, but to analyse some of the important results encountered and, more importantly, to draw conclusions on which to base possible improvements in the development of a system to grow high quality CdTe crystals reliably and consistently.

2.1 IMPORTANT CdTe PROPERTIES FOR CRYSTAL GROWTH FROM THE VAPOUR.

Here, several of the properties of CdTe that can influence the growth process are presented. Firstly, the thermodynamic data and the relationships between vapour and solid phases with respect to temperature, pressures and composition will be discussed. Then a brief summary will be given of those physical properties which can directly influence growth procedures.

2.1.1 Thermodynamic Properties: Phase Relationships.

Temperature versus Composition (*T-x*) Diagram.

The *T-x* projection of the Cd-Te phase diagram is shown in figure 1. The shape of the curve is very simple and characteristic of binary II-VI compounds, and shows that from the point of view of phase stability at the growth temperature versus room

temperature, any temperature can, in principle, be chosen for growth [1]. From figure 1, it can be seen that a source providing stoichiometric vapour is the only requirement to obtain a stoichiometric crystal. However, this picture is not so simple, since the vertical line that indicates the formation of CdTe is an oversimplification. In reality, there is a range of stability at both sides of the solidus line, the so called homogeneity region of existence of CdTe, due to solid solution formation with either impurities or excess of Cd or Te.

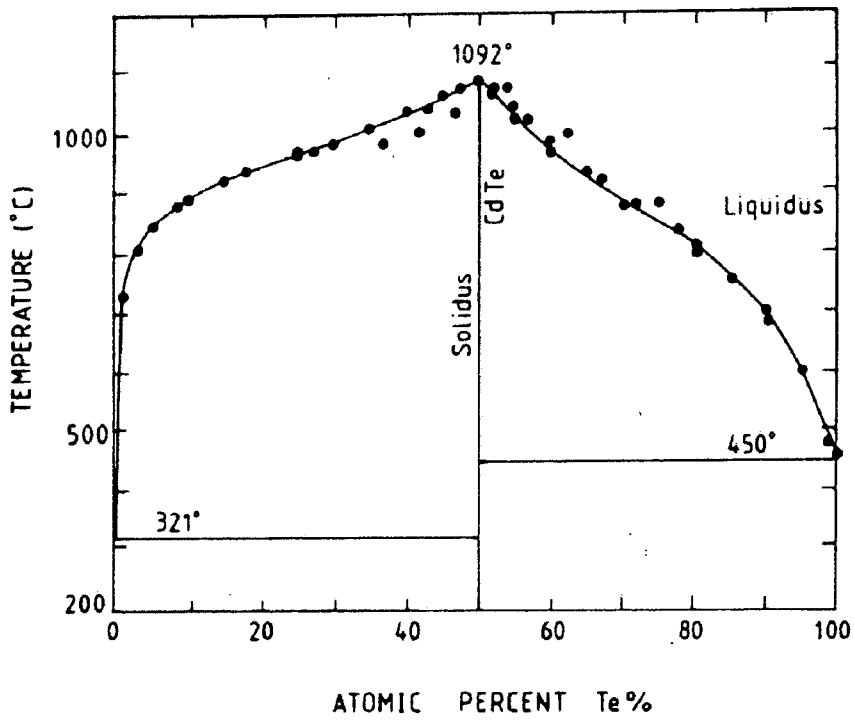

Figure 1. The *T-x* projection of the Cd-Te phase diagram (from [2]).

In the past, the range of homogeneity, which has important consequences on the electrical properties of the crystal, has been inferred from conductivity measurements assuming a specific defect model [2-4]. Recently, two different techniques have been used to obtain much more precise (since the techniques do not assume any particular defect model) limits of the stability region with good agreement [5-9]. As can be seen in figure 2, the range of stability for CdTe as a function of temperature, is asymmetrical

with respect to the 50 at. % line, and the asymmetry increases as the temperature increases. It also can be seen that congruent sublimation is a function of temperature, and that as the temperature increases, the composition of the solid that provides congruent sublimation shifts towards the Te-rich side. The tellurium non-stoichiometry region is wider than that of the cadmium for temperatures between 1100 and 1300 K approximately. The implications of this asymmetry for the crystal growth process are clear: the higher the growth temperature, the more probable that precipitates (specially tellurium) will form during the cooling down stages at the end of the growth process, since the stability range becomes extremely narrow below 800 K (retrograde solubility).

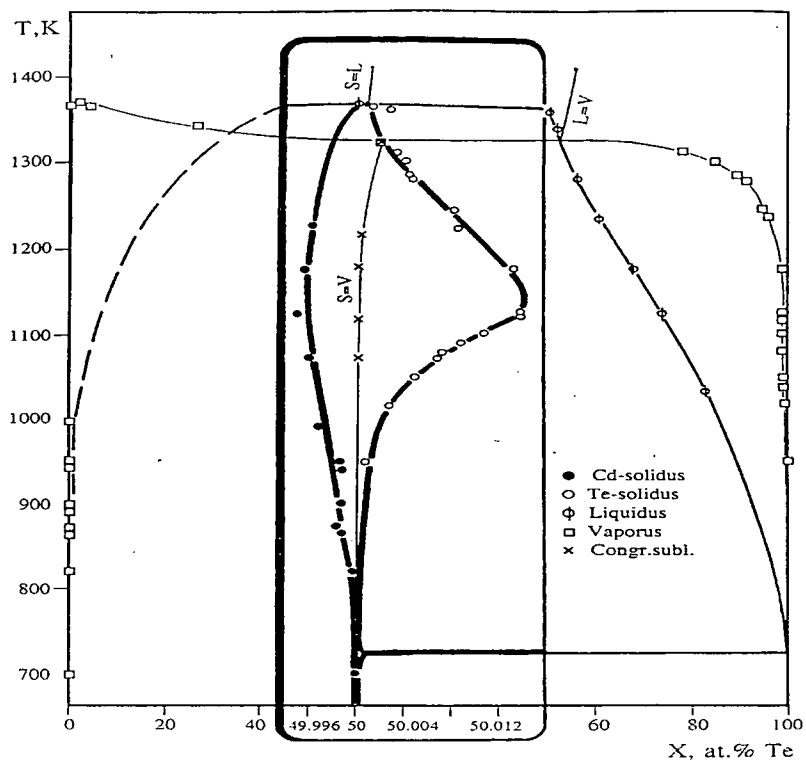

Figure 2. The range of homogeneity for CdTe as a function of temperature (after [9]). The $S=V$ line indicates congruent sublimation.

In principle, this can be minimised using a Cd rich source composition or a Cd reservoir, thus ensuring that the stoichiometry of the condensate lies within the narrow low temperature homogeneity region during growth temperatures [10]. In practice,

however, it is difficult to achieve the necessary accuracy and control particularly when using closed ampoules. Therefore, the growth temperature in vapour growth should be as low as possible, although in general a compromise has to be struck between the conflicting requirements of growth rate, acceptable precipitate density, and the maintenance of a stable interface due to supersaturation effects. In principle, according to the above figure, vapour crystal growth under conditions of congruent sublimation can only result in nonstoichiometric crystals [11].

Pressure versus Temperature (*P-T*) Diagram.

Mass spectrometric measurements [12] show that CdTe dissociates on heating, and that Cd and Te_2 are the only significant species present in the vapour (the presence of CdTe is ~2×10^{-3} % according to [13] at 1100 K and a total pressure of 4 mmHg). Accordingly, it follows from the equilibrium reaction,

$$CdTe_{(s)} \Leftrightarrow Cd_{(g)} + \tfrac{1}{2}Te_{2(g)} \tag{2.1}$$

(where *s* denotes solid and *g* denotes vapour) and the corresponding mass action law, (which assumes the activity coefficient of solid CdTe to be unity and that of the vapour components to be equal to the vapour pressure of these components)

$$K_{CdTe}(T) = P_{Cd}P_{Te_2}^{1/2} = e^{\frac{\Delta G}{RT}} \tag{2.2}$$

(where R is the ideal gas constant, ΔG is the free energy of formation and $K_{CdTe}(T)$ is the equilibrium constant of the reaction) that stoichiometric CdTe sublimes congruently and that the vapour is stoichiometric. Moreover, according to 2.1,

$$P_{Cd} = 2P_{Te_2} \tag{2.3}$$

and it can be shown [14,15] that under these circumstances, the total pressure is the minimum possible at a given temperature,

$$P_{total}^{\min} = \frac{3}{2} 2^{1/3} K_{CdTe}^{1/3}(T) \tag{2.4}$$

According to 2.2, at constant temperature, the two partial pressures are not independent: once one is fixed, the other is given by 2.2. Brebrick and Strauss [16] used an optical absorption technique to measure P_{Te_2} and P_{Cd} over congruently subliming CdTe in the range of temperature 780 - 939 °C, and obtained the relation,

$$\begin{aligned} \log P_{Te_2}(mbar) &= -\frac{1\times10^4}{T} + 9.351 \\ \log P_{Cd}(mbar) &= -\frac{1\times10^4}{T} + 9.652 \end{aligned} \tag{2.5}$$

and using 2.2, they obtained the free energy of formation, and the equilibrium constant,

$$\Delta G\left(\frac{Kcal}{mol}\right) = -68.64 + 44.94\times10^{-3}T \tag{2.6}$$

$$\log K_{CdTe}\left(mbar^{3/2}\right) = -\frac{1.5\times10^4}{T} + 19.003 \tag{2.7}$$

Again, equations 2.1 - 2.3 are an oversimplification. In general, equation 2.1 should include defect (vacancies/intersticials) concentrations, and from figure 2, any excess component. Equation 2.1 is not strictly correct and consequently equation 2.2 is concentration dependent. The uncertainty in the latter is however, very small since the range of homogeneity (figure 2) is extremely narrow [16], and equation 2.2 can always be applied, with caution, for compositions within the range of homogeneity [7]. Equation 2.3 will be obeyed when subliming a small volume amount of CdTe in a comparatively large vessel, or alternatively, after removal of the preferentially sublimed vapour that results from excess components in the source or from native surface oxides. Hence, in a typical closed vapour growth experiment, equation 2.3 does not hold normally and in general the relation between the partial pressures will be determined by the history and pre-treatment of the source, as shown recently by Su *et al.* [17] and Palosz *et al.*[18] and on the initial stoichiometry of the source as determined by

weighing errors [19-21] (see also appendix B). The consequences that this has on the mass transport and growth rates are discussed later, and can be seen in figure 6.

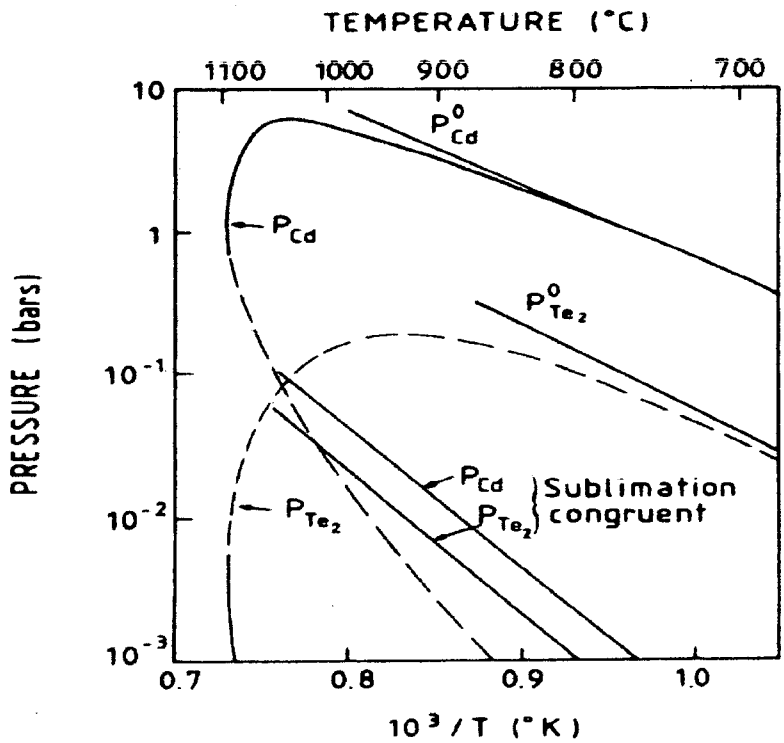

Figure 3. *P-T* projection of the Cd-Te phase diagram (from [2]). The straight lines labelled p^o_{Cd} and $p^o_{Te_2}$ correspond to elemental cadmium and tellurium respectively.

The *P-T* projection of the phase diagram is shown in figure 3, and its correspondence with the *T-x* projection in figure 4. Intuitively, equation 2.3 can only be obeyed for those temperatures where the pressure loops overlap [22] although this is a necessary but not sufficient condition. This has been shown experimentally by Greenberg [9], who also showed that there is a temperature, T=1051 °C, above which congruent sublimation does not occur. This can be seen in figure 2. Clearly, vapour crystal growth should not take place above this temperature, in order to avoid nonstoichiometric vapours.

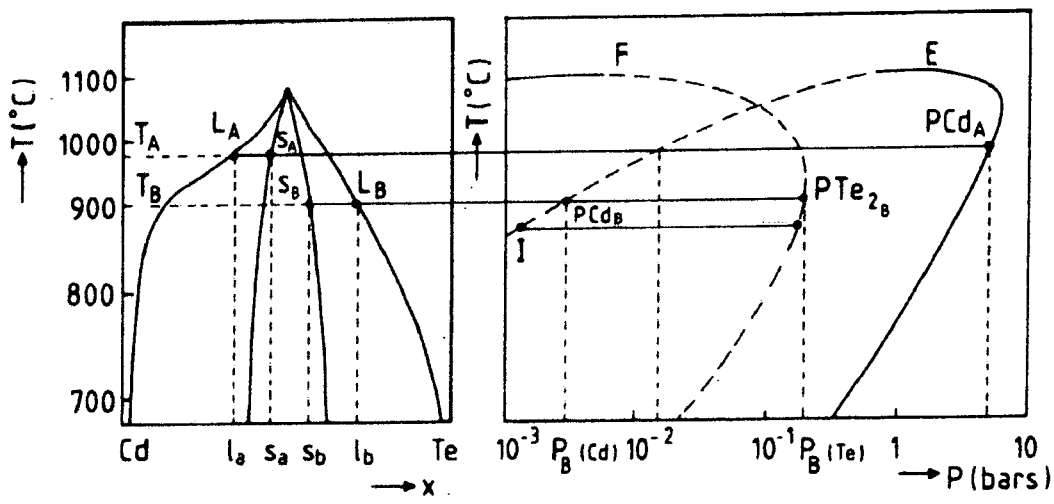

Figure 4. Schematic correspondence of *T-x* and *P-T* projections (from [2]). The solid portion of the vapour pressure curve *E* represents the Cd vapour pressure at equilibrium with the solid Cd rich side, S_A while the dashed portion give the Cd vapour pressure at equilibrium with the solid Te rich side, S_B. The same analogous connection applies to the tellurium vapour pressure curve *F*.

2.1.2 Mechanical Properties.

Knowledge of the mechanical properties of a crystal at the growth temperature and below is especially important for crystal growth, due to the strain induced by the crucible-crystal interaction and the thermal stress that occurs during the growth process. This is specially the case for CdTe, since it is mechanically weak and brittle at all temperatures (Knoop hardness 45 [23]), and has a low stacking fault energy (SFE) [11] and critical resolved shear stress (CRSS) [24] when compared to other typical semiconductors. Since dislocations can propagate and multiply when the stress applied to the crystal exceeds a value close to the CRSS, interaction with the ampoule or crucible where growth takes place should be minimised. Sharp thermal gradients during growth and cooldown should also be minimised in order to avoid twinning.

The mechanical properties of CdTe and CdZnTe have been reviewed by Williams [25] and calculated data is also available [26]. A recent study [24] showed that

for CdTe, the CRSS ranges from 5 MPa at 300 K to about 0.2 MPa at 1353 K, decreasing rapidly with increasing temperature up to 400 K, remaining nearly constant between 400 and 800 K and decreasing beyond 800 K. As a comparison, the CRSS of CdTe is about one order of magnitude lower than that of Si, Ge or III-V compounds at the melting point [27]; from this point of view alone, one would expect the dislocation density to be higher for CdTe.

The linear thermal expansion coefficient, α_{CdTe} (T) of CdTe has been experimentally determined by several authors, although only one [28] gives data (for amorphous CdTe) for normal growth temperatures. Hartmann *et al.* [11] recommends a constant value of 5.5×10^{-6} °C^{-1} between 25 and 800 °C, meanwhile Woods [15] gives an average value of 4.9×10^{-6} °C^{-1}. Both are in reasonable qualitative agreement with the data of Williams [29] in the range 20-420 °C,

$$\alpha_{CdTe}(T) = 4.932\times10^{-6} + 1.165\times10^{-9}T + 1.428\times10^{-12}T^2 \quad (^{\circ}C^{-1}) \qquad (2.8)$$

which results in values ranging between 4.96×10^{-6} and 5.67×10^{-6} °C^{-1}. The linear thermal expansion coefficient for silica is approximately constant in the range of temperatures 20 and 1400 °C [30], with an average value of 5.5×10^{-7} °C^{-1}, i.e. about one order of magnitude lower than that of CdTe [10]. This would be ideal as thermal straining would be eliminated [31], except that CdTe does normally adhere to the ampoule walls due to the existence of native surface oxides of CdTe, such as CdO or TeO_2 [10,32] (unavoidable either due to contamination during source handling or outgassing from the silica container). Some tensile strain and associated stress can hence be expected during the cooling down process (experimentally, this stress can be realised by simply listening to the *cracking sounds* during the cooling down of CdTe in a capillary after a sublimation process). The correlation between sticking and etch pit

density in the crystal has been experimentally demonstrated by Shetty *et al* [33], who established a correspondence between the mean etch pit density and the wetting contact angle of molten CdTe for several ampoule materials.

Although the tensile stress associated with the sticking can in principle be estimated [34,35] using the elastic constants of CdTe [11,36], the unpredictability and variable extent of the sticking areas mean that such a stress would represent an upper limit. The thermal stress associated with thermal gradients can be more readily qualitatively estimated using the Young's modulus E, which has been recently estimated by Kurilo *et al.* [36] at room temperature for different planes and CdTe crystals grown by several methods. The averaged value of E is,

$$\langle E \rangle = 4.52 \times 10^{10} \qquad \text{(Pa)} \tag{2.9}$$

Using the above value, it can be qualitatively shown (see appendix A) that small temperature differences between different parts of the crystal as little as 2 °C can produce stresses higher than the CRSS during growth temperatures.

2.1.3 Thermal Properties.

The thermal properties of CdTe have been reviewed recently by Maleki *et al.* [37]. The thermal conductivity of CdTe at the melting point (0.013 $W.cm^{-1}.K^{-1}$) is about one order of magnitude smaller than that of group IV or III-V semiconductors, making control of interface shape and crystal diameter difficult in melt growth techniques [27]. The thermal conductivity is also an important property in vapour crystal growth since it affects the thermal coupling between the crystal and the furnace [38]. Moreover, as the crystal grows, the latent heat formed at the interface has to be transported away [14,39] in order to avoid superheating conditions and hence morphological instabilities.

The value of the thermal conductivity $\lambda(T)$ as given by Abousehly *et al.* [40] in the range 300-700 K is given by the following expression,

$$\lambda(T) = 11.7477 - 1.522207 \times 10^{-2} T + 8.306916 \times 10^{-6} T^2 \quad (\mathrm{W.m^{-1}.K^{-1}}) \quad (2.10)$$

which shows that the thermal conductivity decreases slowly as the temperature increases. The influence of the growth container on the curvature of the crystal interface and crystal morphology due to different thermal conductivities has been discussed previously by Schonherr [41]. When the thermal conductivity of the ampoule is higher than that of the crystal, the interface tends to be concave, and convex when the contrary occurs [33,41,42]. The latter is generally desirable since it reduces the risk of unwanted parasitic nucleation at the ampoule walls.

Besides thermal conductivity, the emissivity of CdTe as a function of temperature, $\varepsilon(T)$ can also influence the growth process. The influence of radiative heat exchange between parts of the furnace and the crystal on the mass transfer-surface kinetics and growth rate has been extensively studied for HgI_2 [43-46]. Radiative heat transport can stop growth abruptly even under conditions of apparent supersaturation. The emissivity of CdTe for temperatures in the range 827-1104 K at wavelengths between 0.6 and 1.8 μm has been recently obtained by Mullins *et al.* [47]. The emissivity was observed to increase as a function of the temperature as expected, and it was also found that in general the crystal behaved like a grey body rather than a perfect black body. The same study showed the well known influence of the surface conditions on the emissivity [48], and suggested its use as a measure of the surface quality and stoichiometry during vapour growth.

2.2 CdTe CRYSTAL GROWTH FROM THE VAPOUR AND TECHNIQUES USED IN THE PAST.

A short review of the many techniques used to grow CdTe crystals from the vapour phase is presented. Several extensive reviews can be obtained from the literature [3,11,49,50].

2.2.1 Advantages and Disadvantages of Vapour Growth.

Presently, all commercially available CdTe is grown using modified Bridgman techniques or gradient freezing methods, with possibly one exception [51]. Boules of up to 100 mm diameter are routinely grown, and single crystal substrates are obtained by mining the boules for suitable single grains. According to Asashi *et al.* [52], the main reasons for the failure to consistently obtain good quality crystals are the low thermal conductivity and low values of SFE and CRSS. Rudolph *et al.* [53] also point out that a nearly stoichiometric melt evaporates incongruently, and hence unless the vapour pressures over the melt are controlled, the melt is always Te-rich. The high degree of association in the melt [3] and the liquidus shape further complicates the melt growth process [53]. Vapour growth offers a considerable number of advantages over melt growth:

i) The relatively high vapour pressures below the melting point allow growth to take place at low temperatures. This in principle, leads to a reduction in the density of precipitates (see figure 2) and inclusions (due to temperature fluctuations) as well as limiting the amount of thermal stress applied to the crystal.

ii) Contamination from the crucible should be smaller than in melt techniques due to the lower temperatures used.

iii) Non-volatile impurities present in the source charge are not transported to the crystal, i.e. the growth process is to some extent also a purifying one.

Although the above advantages have been realised in the past (see for example references [10] and [54]), and high quality CdTe crystals have been obtained, considerable technical difficulties have been encountered. The technology of crystal growth from the vapour has not been fully developed, and in general is only used to obtain crystals for research and academic purposes. It is only recently [55] that new techniques are being introduced mainly for SiC growth with impressive results. The main problems associated with vapour crystal growth are the difficulties of controlling seeding, and vapour and source stoichiometry, which in turn results in low growth rates, complex mass transport mechanisms and irreproducibility of results, as well as difficulty in doping. However, as pointed out by Rosenberger *et al.* [10], failure to obtain, consistently and reliably, high quality single CdTe crystals is a consequence of the traditional sublimation methods employed. Consequently, current bulk vapour growth methods, which will be reviewed here, have not yet fully realised the expected advantages.

2.2.2 Closed Physical Vapour Transport Techniques.

Closed silica ampoules have been extensively used in the past, because of their simplicity of fabrication and operation, but were abandoned as control of vapour stoichiometry and gaseous impurities could not be achieved. The apparently simple process of sealing the ampoule alone, introduces residual gases, and in addition considerable outgassing might take place during growth [56]. All closed PVT techniques are a modification of the sublimation method devised by Czyzak *et al.* [57],

improved by Greene *et al.* [58] and established by Piper and Polich [59] for CdS unseeded bulk growth. In contrast with other sublimation methods [60,61], this technique allows relatively large crystals, typically a few cm^3 to be obtained. In this method, sintered powder or polycrystalline material of the same type as the crystal is charged at one end of a silica tube which is tapered to a conical tip at the other end. Growth proceeds in a horizontal furnace by imposing a suitable, simple parabolic-like gradient. Vapours formed from the source in the hot zone are transported down the gradient to deposit on the conical tip to grow a single crystal. The design of the silica tube at the source end is such that it is normally not tightly sealed in the initial state, but gradually sealed with condensing vapours during preheating. This design allows for a constant slow flow of an inert gas if necessary. The kinetics of vapour growth in the Piper-Polich method were studied early on by Toyama [62].

Several modifications of the original Piper-Polich have been used (see [3,11,49, 50]), but the main modification was introduced by Hoschl *et al.* [63], who used molten cadmium to control the partial pressure and the sublimation rate to obtain ~$1cm^3$ crystals in a sealed capsule. Igaki *et al.* [64] used a similar approach to demonstrate the dependence of the growth rate on the partial pressure of the controlling constituent element. Effects due to supersaturation and deviation of source stoichiometry were later studied by Mochizuki [65,66], who concluded that the *history* of the source determines the growth rate. The technique was further developed by the Durham group (see for example [67-70]) for growth of several II-VI compounds (see figure 5). Unseeded growth proceeded in a tipped vertical ampoule which was connected via a narrow orifice to a long tail containing one of the elemental constituents. The tail was maintained, independently of the growth and source temperature, at a lower temperature

and was normally adjusted to provide a vapour pressure in the ampoule close to the partial pressure which would result if p_{min} conditions had been established. Growth proceeded as the ampoule was pulled through an appropriate temperature gradient. Using this technique CdTe boules of up to 35 cm^3 were routinely grown. However, all of them (over a hundred) were multigrained and contained at least one twin [71]. The lack of correspondence between growth conditions and crystal quality as well as the transport rate (sometimes as long as several weeks) were related to the existence of residual gases during the seal-off of the capsule , which indirectly caused diffusional limitations [68]. The high content of precipitates compared with the Piper-Polich method was attributed to the long time periods of growth [72].

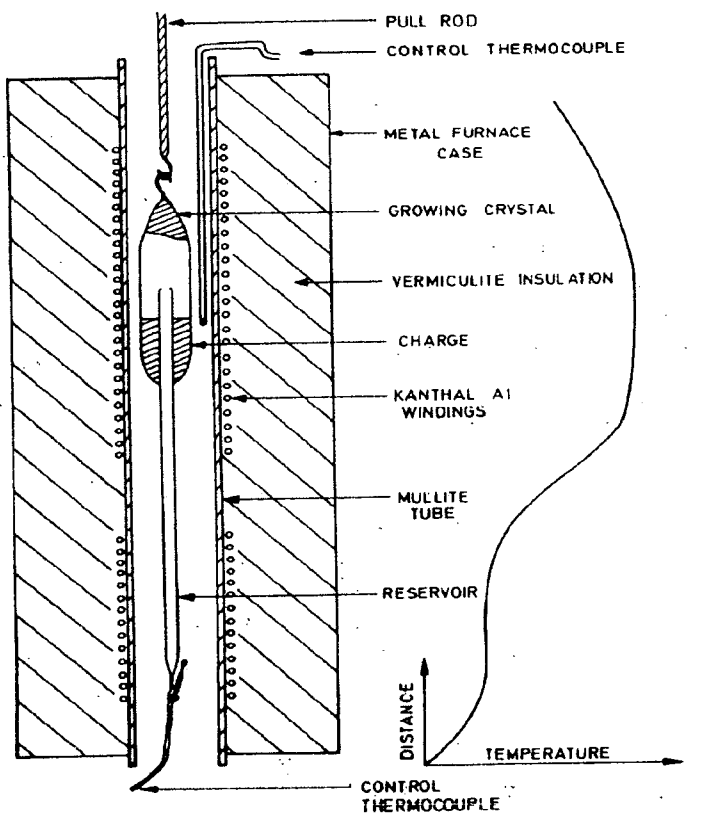

Figure 5. Experimental arrangement for the growth of II-VI compounds used by the Durham group (after [68]).

The limitations of closed ampoule growth where highlighted early on in several theoretical descriptions of dissociative sublimation by Faktor *et al.* [73-76] and Rosenberger and co-workers [77,78], who also modelled vapour transport in closed ampoules. Despite this, several workers [79,80] have continued using closed (seeded and unseeded) vapour growth techniques. Yellin *et al.* [19-21] used a vertical, unseeded growth method (devised by Tamari *et al.* [81]) to study the dependence of the growth rate on the stoichiometry of the source. The method introduced the use of a silica rod heat pipe to control nucleation. The most important result, however, was that the growth rate was found to be strongly dependent on the Te or Cd excess present in the growth charge (see figure 6), and they explained this result by assuming noncongruent sublimation of CdTe. The importance of source stoichiometry (and pre-treatment before growth) has been confirmed subsequently [17,18].

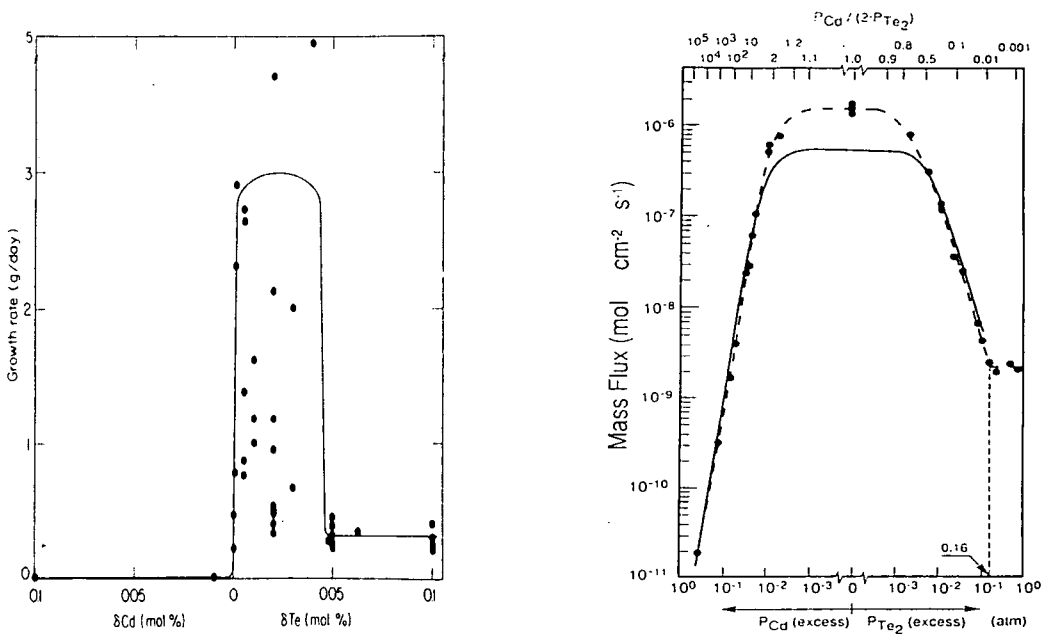

Figure 6. Right: dependence of the CdTe mass transport rate on source stoichiometry and its influence on the partial pressure ratio (after [18]). Left: dependence of source stoichiometry on growth rate for the vertical unseeded CdTe vapour growth of Yellin *et al.* (after [20]).

Another closed ampoule technique worthy of mention is the sublimation travelling heater method (STHM), introduced by Triboulet *et al.* [82]. The method replaces the Te-rich molten zone in the typical THM technique by a vapour zone. Stoichiometry is controlled by connecting a capillary to the sublimation chamber whose upper end stays at room temperature. Large, multigrained and twinned boules are routinely obtained. The technique has been adapted by other researchers to obtain undoped [83] and halogen doped [84] CdTe crystals, but the quality of the crystals was not further improved.

2.2.3 Semiopen Physical Vapour Transport Techniques.

The use of semiopen* ampoules has been extensively studied in the past for several semiconductors [41]. The concept was pioneered in fact by Piper and Polich for CdS growth [59] and fully understood and developed by Faktor *et al.* [85], who realised the importance of evacuating continuously the growth capsule in order to obtain stable growth and maintain a constant partial pressure ratio. The authors incorporated small, calibrated *effusion* holes in the walls of the growth ampoule, which was surrounded by a vacuum jacket or alternatively, by a determined pressure of one of the elemental constituents or an inert gas. The method was further developed by Rosenberger *et al.* who obtained growth rates up to three orders of magnitude higher than in closed ampoules for the growth of KCl and KBr [86,87]. Using an ingenious design, seeded growth took place without contact with the walls. Kuwamoto [88] and Dierssen and Gabor [89] used a very similar design (except that the former used a light heat pipe to support and supposedly cool the crystal) to grow quite large (>18 cm^3) CdTe and CdS

* Here, the term *semiopen* describes, besides the obvious meaning, an arrangement that allows mass transport between the growth region and a *sink* located within the same container.

crystals respectively, the former at temperatures in the range 680-850 °C. Kuwamoto reported on the existence of thin voids oriented parallel to the growth direction and attributed this to too high growth rates. He also noticed that in order to obtain single crystals, the seed had to be kept under high argon pressure until the operating growth temperature of the furnace had been reached. Failure to do so resulted in a polycrystal, due to multigrain recrystallisation of the seed. The importance of the seed crystallographic orientation was studied earlier [61].

A similar technique was developed earlier by Markov and Davydov [90,91] for the growth of II-VI compounds. In this technique, the seed was supported by a sapphire rod, which was enclosed in the vertical growth ampoule. A small gap between the rod and the silica ampoule walls allowed, not only contact free growth, but also deposition of any excess constituent element at the bottom of the ampoule, which was held at room temperature. In this way an effective sink or cold trap for volatile impurities, equivalent to pumping, was obtained. A relation between the necessary length of the rod and the vapour pressure at the source and seed areas was also given. The length of the rod appeared to be crucial in order to obtain wall free growth conditions. The technique seemed to have passed unadvertised until Golacki *et al.* [92] used it to obtain CdTe crystals. Unfortunately their quality was not reported.

Lauck *et al.* [93] made theoretical studies on the purification during unseeded, horizontal CdS and CdTe vapour growth in semiclosed ampoules with effusion holes, and demonstrated experimentally [94] that impurities with a segregation coefficient $k < 1$ are not incorporated to the crystal, meanwhile for those with $k > 1$, no purification takes place. Apart from this, studies of the leakage through the *effusion* holes showed

that deviation from the stoichiometry of the crystal depended not only on the leakage loss but also on the leakage kinetics (flow regime).

A horizontal arrangement was used by Boone *et al.* [95] for seeded growth under argon atmosphere of p-type CdTe crystals (up to 100 cm^3, 50 mm diameter) with etch pit densities in the range $3\text{-}7\times10^4$ cm^{-2}. No visual or X-ray detectable twins or grain boundaries were found, although the outer parts of the crystal, which were in contact with the ampoule, displayed considerably poorer quality. Interestingly, it was found empirically that crystals with lengths larger than the radii of the crystal could not be obtained due to parasitic nucleation at the walls; this was attributed to the difficulty in transferring heat away from the centre of the growing crystal.

Grasza *et al.* [96,97] devised an original and novel method for in-situ nucleation before CdTe growth. The technique, based on the design of Markov [90], uses thermal gradients to produce a single crystal seed that sticks to the surface of the silica rod. Once the seed is formed, the thermal gradient profile of the furnace is optimised for the growth process, and the crystal grows without contact with the wall. Conductivity was controlled by using different source stoichiometries. Although high quality but twinned crystals, up to 8 cm^3, with EPD's as low as 2×10^3 cm^{-2} were obtained, the technique returned vapour crystal growth to the status of a *"black art"*, due to the skill required to obtain successful seeding.

The most promising method for CdTe and II-VI solid solutions bulk vapour growth seems to be a modified Markov method, also called the free growth method [98-100] (see figure 7) where growth takes place under a helium or argon-hydrogen

mixture. The seed is placed at the end of a silica rod, which also acts as a heat remover and forms a sharper gradient in order to locate the condensation of vapours onto the seed. The silica rod is carefully located at the centre of the growth tube, to ensure a narrow gap between wall and crystal in order to maximise crystal yield. The transport of vapours from the top located source is controlled by calibrated holes and sometimes a "quartz net". Large diameter crystals, up to 100 mm are routinely grown. The crystals however are always short (~1 cm). Although not reported by Korostelin *et al.* [99-100], it seems that heat transfer precludes any further growth, in accordance with the empirical results of [95].

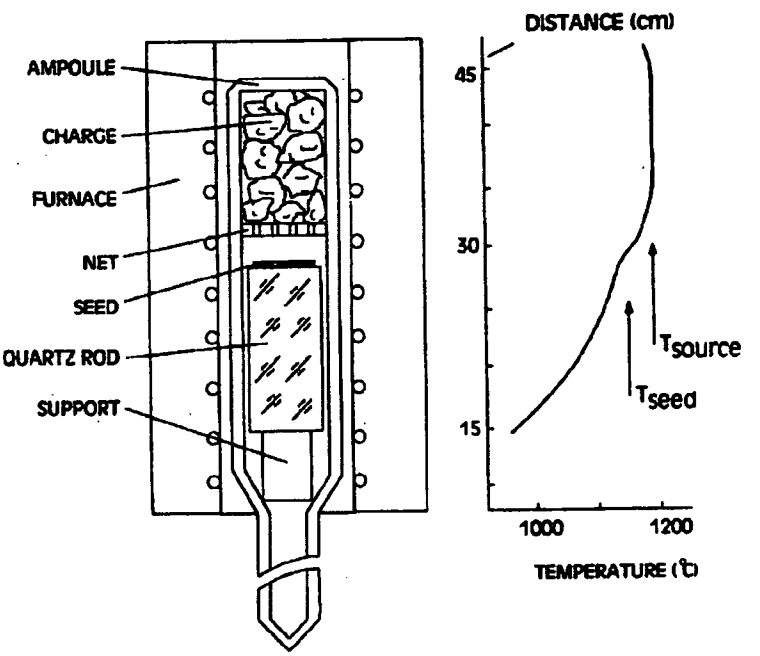

Figure 7. Growth ampoule design for the modified Markov (free growth method) (after [99]).

The modified Markov growth technique has been used by Laasch *et al.* [101] to produce twin free seeded and unseeded single CdTe crystals. They also used a birefringence technique to compare the strain of crystals grown with and without contact with the walls ampoule. The latter showed virtually no stress evidence. These

authors stress the importance of maintaining the sink at room temperature in order to obtain good quality twin-free crystals. Furthermore, they experimentally showed that the stoichiometry of the source does not influence the vapour composition at the growing front as long as the sink remains at room temperature.

A study on bulk vapour growth of CdTe by Rosenberger *et al.* [10], perhaps the most extensive and concise to date, resulted in the development of a growth technology that embraces and assimilates all the results and lessons from the research carried in the past and briefly described above. The effusive ampoule physical vapour transport (EAPVT) technique is one largely based on the Markov design, which allows for growth seeded or unseeded, free of contact with the walls, and continuous removal of vapour excess and impurities, as well as the use of a cadmium or tellurium reservoir. One of the improvements was the use of a capillary placed between source and crystal in order to independently control the mass transport rate. Special emphasis was placed on using a temperature "hump" between source and crystal to avoid spurious nucleation, as well as on temperature stability. Although unseeded growth was not successful, seeded growth of ~20 cm^3 crystals showed very low EPD (~2×10^3 cm^{-2}), among the lowest reported in the literature.

2.3 CONCLUSIONS.

A short review on the properties of CdTe important for vapour growth together with several significant bulk vapour growth techniques has been presented. The aim here has been to present and highlight substantial contributions for the improvement of CdTe bulk vapour growth. Several important conclusions may be drawn from past work

that can help in the further design and improvement of growth conditions. From the point of view of CdTe properties:

- The narrow, retrograde range of homogeneity counsels the use of low growth temperatures in order to avoid the occurrence of precipitates.

- Preferential sublimation of any excess constituent and noncongruent sublimation due to the history, pre-treatment and difficulty of synthesis (see appendix B), suggests the need for both a compact (and hence low specific surface area) and high purity source and careful source preparation, due to the strong interdependence of the constituents' partial pressures.

- The low stacking fault energy favours twinning. Therefore, temperature fluctuations during growth should be minimised and high temperature gradients during the cooldown process avoided.

- The extremely low critical resolved shear stress combined with the different thermal expansion coefficients of CdTe and SiO_2 can produce dislocations and cracks in the crystal. Consequently, interaction between crystal and ampoule should be minimised, and high thermal stresses eliminated (see appendix A).

- The low thermal conductivity can influence the interface shape and hence the morphological stability during growth. Accordingly radial gradients should be minimised and radiative heat transfer taken into account and promoted (for example, using a heat pipe) to some extent.

From the point of view of vapour growth techniques:

- Sealed ampoules introduce too many uncertainties in the growth process. The sealing process itself and outgassing during growth both introduce foreign gases. Therefore, reproducibility of growth experiments and results is difficult due to the very

sensitive dependency of growth rates on the partial pressure ratio of the constituent elements.

- Introduction of a reservoir with an elemental constituent in a closed system can alleviate nonstoichiometry source related mass transport problems, and, in principle, allows *p* or *n*-type CdTe to be obtained. In reality however, accurate control of the vapour pressure is unattainable.

- The use of physically semiopen ampoules allows for continuous removal of volatile impurities, excess components and outgassing products. This permits the total pressure to be maintained close to the p_{min} conditions, hence ensuring high growth rates.

- The use of cold trap – semiopen ampoules also allows for 3), but seal-off and outgassing products are still present during growth. In this case, careful ampoule seal-off and baking pre-treatment is necessary.

- The semiopen Markov and modified arrangements allows simultaneously for the crystal to grow without wall contact, the use of a seed and the introduction of a heat pipe which acts also as a support. The technique allows for dynamic pumping or cold trap, but more importantly it allows backfilling with inert gases during growth.

- Seeding is generally difficult and time consuming. Seeded growth is more reliable as long as the seed is monocrystalline and its polarity well chosen; however, thermal etching and recrystallisation of the seed should be avoided.

REFERENCES FOR CHAPTER TWO

[1] J.W. Nielsen and R. R. Monchamp. *"The Use of Phase Diagrams in Crystal Growth"* in *Phase Diagrams, Materials Science and Technology.* Volume 6-III. Edited by A. M. Alper. Academic Press, New York (1970).

[2] M. Hage-Ali and P. Siffert. *"Growth Methods of CdTe Nuclear Detector Materials"* in *Semiconductors for Room Temperature Nuclear Detectors Applications*, volume 43 (Semiconductors and Semimetals Treatise). Edited by T. E. Schelesinger and R. B. James. Academic Press, San Diego (1995).

[3] K. Zanio. *Cadmium Telluride.* Semiconductors and Semimetals Treatise, Volume 13. Edited by R. K. Willardson and A. C. Beer. Academic Press, London (1978).

[4] A. Albers . *"Physical Chemistry of Defects"* in *Physics and Chemistry of II-VI Compounds.* Edited by M. Aven and J. S. Prener. North Holland, Amsterdam (1967).

[5] J. H. Greenberg, V. N. Guskov and V. B. Lazarev. *"P-T-X Phase Diagram Cadmium-Tellurium"*. Mat. Res. Bull., **27** (1992) 997.

[6] J. H. Greenberg, V. N. Guskov, V. B. Lazarev and O. V. Shebershneva. *"Vapor Pressure Scanning of Nonstoichiometry in CdTe"*. J. Solid State Chem. **102** (1993) 382.

[7] R. Fang and R. F. Brebrick. *"CdTe I: Solidus Curve and Composition-Temperature-Tellurium Partial Pressure Data for Te-Rich $CdTe_{(s)}$ from Optical Density Measurements"*. J. Phys. Chem. Solids, **57** (1996) 443.

[8] R. F. Brebrick and R. Fang. *"CdTe II: Defect Chemistry"*. J. Phys. Chem. Solids, **57** (1996) 451.

[9] J. H. Greenberg. *"P-T-X Phase Equilibrium and Vapor Pressure Scanning of Non-Stoichiometry in CdTe"*. J. Crystal Growth, **161** (1996) 1.

[10] F. Rosenberger, M. Banish and M. B. Duval. *Vapour Crystal Growth Technology Development – Application to Cadmium Telluride.* NASA Technical Memorandum 103786 (1991).

[11] H. Hartmann, R. Mach and B. Selle. *"Wide Gap II-VI Compounds as Electronic Materials"* in *Current Topics in Materials Science.* Volume 9. Edited by E. Kaldis. North-Holland, Amsterdam (1982).

[12] P. Goldfinger and M. Jeunehomme. *"Mass Spectrometric and Knudsen Cell Vaporization Studies of Group 2B-6B Compounds"*. Trans. Faraday Soc., **59** (1963) 2851.

[13] A. P. Ubelis, in: *Radiation and Collisional Characteristics of Atoms and Molecules of Tellurium –A Collection of Scientific Papers.* Edited by A. P. Ubelis, R. S. Ferber and M. Ya. Tamanis. Latvian SSR Ministry of Public Education, P. Schutka Latvian University, Riga, Latvia (1989) (in Russian). (available in English: NASA TT-20831, 1990).

[14] F. Rosenberger. *Fundamentals of Crystal Growth I: Macroscopic Equilibrium and Transport Concepts.* Springer Series in Solid State Sciences. Edited by M. Cardona, P. Fulde and H. J. Queisser. Springer-Verlag, Berlin (1979).

[15] J. Woods. *"Group II-VI Semiconductors"* in *The Chemistry of the Semiconductor Industry.* Edited by S. J. Moss and A. Ledwith. Blackie & Son Ltd., Glasgow (1987).

[16] R. F. Brebrick and A. J. Strauss. *"Partial Pressures and Gibbs Free Energy of Formation for Congruently Subliming $CdTe_{(c)}$"*. J. Phys. Chem. Solids, **25** (1964) 1441.

[17] C. H. Su, Y. G. Sha, S. L. Lehoczky, H. C. Liu, R. Fang and R. F. Brebrick. *"Vapor-Phase Stoichiometry and Heat Treatment of CdTe Starting Material for Physical Vapor Transport"*. J. Crystal Growth, **183** (1998) 519.

[18] W. Palosz and H. Wiedemeier. *"Physical Vapour Transport of Cadmium Telluride in Closed Ampoules"*. J. Crystal Growth, **129** (1993) 653.

[19] N. Yellin, D. Eger and A. Shachna. *"Vertical Unseeded Vapour Growth of Large CdTe Crystals"*. J. Crystal Growth, **60** (1982) 343.

[20] N. Yellin and S. Szapiro. *"Vapor Transport of Nonstoichiometric CdTe in Closed Ampoules"*. J. Crystal Growth, **69** (1984) 555.

[21] N. Yellin and S. Szapiro. *"Calculation of the Partial Vapor Pressures of Tellurium and Cadmium Over Non-Stoichiometric CdTe in the Temperature Range 750-1050 °C"*. J. Crystal Growth, **73** (1985) 77.

[22] M. B. Panish. *"The Use of Phase Diagrams in Investigations of the Properties of Compound Semiconductors"* in *Phase Diagrams, Materials Science and Technology.* Volume 6-III. Edited by A. M. Alper. Academic Press, New York (1970).

[23] M. R. Squillante and K. S. Shah. *"Other Materials: Status and Prospects"* in *Semiconductors for Room Temperature Nuclear Detectors Applications*, volume 43 (Semiconductors and Semimetals Treatise). Edited by T. E. Schelesinger and R. B. James. Academic Press, San Diego (1995).

[24] R. Balasubramanian and W. R. Wilcox. *"Mechanical Properties of CdTe"*. Mat. Sci. Eng., **B16** (1993) 1.

[25] D. J. Williams. *"Mechanical Properties of CdTe and CdZnTe"* and *"Yield Stress and Hardness of CdTe and CdZnTe"* in *Properties of Narrow Gap Cadmium-based Compounds.* Emis Datareviews Series n° 10. Edited by P. Capper. Inspec (IEE), London (1994).

[26] V. Kumar, G. M. Prasad, A. R. Chetal and D. Chandra. *"Microhardness and Bulk Modulus of Binary Tetrahedral Semiconductors"*. J. Phys. Chem. Solids, **57** (1996) 503.

[27] R. N. Thomas, H. M. Hobgood, P. S. Ravishankar and T. T. Braggins. *"Meeting Device Needs Through Melt Growth of Large-Diameter Elemental and Compound Semiconductors"*. J. Crystal Growth, **99** (1990) 643.

[28] G. G. Gadzhiev, Sh. M. Ismailov and A. I. Dadashev. *"Thermal Properties of Ceramics Based on $A^{II}B^{VI}$ Compounds"*. High Temperature, **3** (1993) 468.

[29] M. G. Williams, R. D. Tomlinson and M. J. Hampshire. *"X-Ray Determination of the Lattice Parameters and Thermal Expansion of Cadmium Telluride in the Temperature Range 20-420 °C"*. Solid State Commun., **7** (1969) 1831.

[30] D. G. Holloway. *"The Physical Properties of Glass"*. Volume 24, *The Wykeham Science Series"*. Edited by N. Mott and G. R. Noakes. Wykeham Publications, London (1973).

[31] J. S. Shah, H. H. Wills. *"Creation, Measurement and Control of Crystal Growth Environment"*, in *Crystal Growth*, volume 6, series in the Science of Solid State. Edited by B. R. Pamplin. Pergamon Press, Oxford (1975).

[32] R. K. Bagai, R. D. S. Yadava, B. S. Sundersheshu, G. L. Seth, M. Anandan and W. N. Borle. *"A Study on Contaminations during Bulk Growth of CdTe Crystals"*. J. Crystal Growth, **139** (1994) 259.

[33] R. Shetty, W. R. Wilcox and L. L. Regel. *"Influence of Ampoule Coatings on Cadmium Telluride Solidification"*. J. Crystal Growth **153** (1995) 103.

[34] *Mechanical Behaviour of Materials at Elevated Temperatures.* Edited by J. E. Dorn. McGraw-Hill, New York (1961).

[35] W. Rosch and F. Carlson. *"Computed Stress Fields in GaAs during Vertical Bridgman Growth"*. J. Crystal Growth, **109** (1991) 75.

[36] I. V. Kurilo, V. P. Alekhin, I. O. Rudyi, S. I. Bulychev and L. I. Osypyshin. *"Mechanical Properties of ZnTe, CdTe, CdHgTe and HgTe Crystals from Micromechanical Investigation"*. Phys. Stat. Sol. (a), **163** (1997) 47.

[37] H. Maleki and R. L. Holland. *"Thermal Properties of Cd/Zn/Te/Se Compounds"* in *Properties of Narrow Gap Cadmium-based Compounds.* Emis Datareviews Series n° 10. Edited by P. Capper. Inspec (IEE), London (1994).

[38] M. Isshiki. *"Bulk Growth of Widegap II-VI Single Crystals"* in *Widegap II-VI Compounds for Opto-Electronic Applications"*. Edited by H. E. Ruda. Electronic Materials Series, volume 1. Chapman & Hall, London (1992).

[39] J. Nelson. *"Heat Conduction Problems in Crystal Growth from the Vapor"*. J. Crystal Growth, **132** (1993) 538.

[40] A. M. Abousehly, H. M. Basha and A. A. El-Sharkawy. *High Temperature – High Pressures*, Pion Publication **21** (1990) 178.

[41] E. Schonherr. "The Growth of Large Crystals from the Vapor Phase", in Crystals: Growth, Properties and Applications. Volume 2. Springer, Berlin (1980).

[42] P. Brunet, A. Katty, D. Schneider, A. Thomson-Carli and R. Triboulet. *"Horizontal Bridgman Growth of Large High Quality $Cd_{1-y}Zn_yTe$ Crystals"*. Mat. Sci. Eng., **B16** (1993) 44.

[43] E. Kaldis and M. Piechotka. *"Bulk Crystal Growth by Physical Vapour Transport"*, in *Handbook of Crystal Growth*, volume 2, part A: *Bulk Crystal Growth.* Edited by D. T. J. Hurle. North-Holland, Amsterdam (1993).

[44] A. A. Chernov, E. Kaldis, M. Piechotka and M. Zha. *"Conductive and Radiative Heat Transfer, Diffusion and Interface Kinetics in Spherically Symmetric Vapour Growth; Application to HgI_2"*. J. Crystal Growth, **125** (1992) 627.

[45] M. Piechotka. *"Mechanism of Vapour Growth and Defect Formation in Large Mercuric Iodide Crystals"*. J. Crystal Growth, **146** (1995) 1.

[46] A. Roux, A. Fedoseyev and B. Roux. *"Thermal Radiation and Low Temperature Vapour Growth of HgI_2 Crystal in Production Furnace"*. J. Crystal Growth, **130** (1993) 523.

[47] J. T. Mullins, J. Carles and A. W. Brinkman. *"High Temperature Optical Properties of Cadmium Telluride"*. J. Appl. Phys., **81** (1997) 6374.

[48] A. J. Strauss. *"The Physical Properties of Cadmium Telluride"*. Appl. Phys. Rev., **12** (1977) 167.

[49] P. Capper and A. W. Brinkman. *"Growth of CdTe, CdZnTe and CdTeSe by Bulk Methods"* in *Properties of Narrow Gap Cadmium-based Compounds.* Emis Datareviews Series n° 10. Edited by P. Capper. Inspec (IEE), London (1994).

[50] P. Capper. *"Bulk Growth Techniques"* in *Narrow-Gap II-VI Compounds for Optoelectronic and Electromagnetic Applications"*. Edited by P. Capper, Electronic Materials Series, volume 3. Chapman & Hall, London (1997).

[51] Cited by K. Durose, A. Turnbull and P. Brown. *"Structural Defects in Bulk and Epitaxial CdTe"*. Mat. Sci. Eng., **B16** (1993) 96. See also Atramet Inc. and Ramet Inc. catalogue.

[52] T. Asahi, O. Oda, Y. Taniguchi and A. Koyama. *"Characterization of 100 mm diameter CdZnTe single Crystals Grown by the Vertical Gradient Freezing Method"*. J. Crystal Growth, **149** (1995) 23.

[53] P. Rudolph and M. Muhlberg. *"Basic Problems of Vertical Bridgman Growth of CdTe"*. Mat. Sci. Eng., **B16** (1993) 8.

[54] N. R. Kyle. *"Growth of Semi-Insulating Cadmium Telluride"*. J. Electrochem. Soc., **118** (1971) 1790.

[55] V. Balakrishna, G. Augustine, H. McD. Hobgood, G. Dunne and R. H. Hopkins. *"Physical Vapor Transport of 4H-SiC Monocrystals: Growth and Properties"*. AACG Newsletter, **26**, n°2 (1997).

[56] W. Palosz, F. R. Szofran and S. L. Lehoczky. *"The Effect of Heat Treatment on the Magnitude and Composition of Residual Gas in Sealed Silica Glass Ampoules"*. J. Crystal Growth, **142** (1994) 215.

[57] S. J. Czyzak, D. G. Craig, C. E. McCain and D. C. Reynolds. *"Single Synthetic Cadmium Sulfide Crystals"*. J. Appl. Phys., **23** (1952) 932.

[58] L. C. Greene, D. C. Reynolds, S. J. Czyzak and W. M. Baker. *"Method for Growing Large CdS and ZnS Single Crystals"*. J. Chem. Phys., **29** (1958) 1375.

[59] W. W. Piper and S. J. Polich. *"Vapor Phase Growth of Single Crystals of II-VI Compounds"*. J. Appl. Phys., **32** (1961) 1278.

[60] I. Teramoto. *"Vapour Growth Patterns of CdTe Crystals"*. Phil. Mag., **8** (1963) 357.

[61] I. Teramoto and M. Inoue. *"Vapour Growth of Cadmium Telluride Crystals in the <111> Polar Directions"*. Phil. Mag., **8** (1963) 1593.

[62] M. Toyama. *"Kinetics of the Vapor Growth of II-VI Compounds Crystals"*. Jap. J. Appl. Phys., **5** (1966) 1204.

[63] P. Hoschl and C. Konak. *"Sublimation of Cadmium Telluride and Cadmium Selenide under a Vapour Pressure of one of their Components and the Equilibrium Form of Crystal Growth"*. Phys. Stat. Sol. **9** (1965) 167, and references cited therein.

[64] K. Igaki, N. Ohashi and K. Mochizuki. *"Vapor Phase of Cadmium Telluride under Controlled Partial Pressure of Constituent Element"*. Jap. J. Appl. Phys., **8** (1976) 1429.

[65] K. Mochizuki. *"Effect of Supersaturation on the Vapor Phase Transport of CdTe"*. J. Crystal Growth, **53** (1981) 355.

[66] K. Mochizuki. *"Effect of the Deviation from Stoichiometry of a Source Specimen on the Vapor Transport of CdTe"*. J. Crystal Growth, **51** (1981) 453.

[67] J. R. Cutter. *"The Crystal Growth and Properties of Some Chalcogenides of Zinc and Cadmium"*. Ph.D Thesis, University of Durham, UK (1977).

[68] G. J. Russell and J. Woods. *"The Growth of CdS in Sealed Silica Ampoules"*. J. Crystal Growth, **46** (1979) 323.

[69] K. Durose, G. J. Russell and J. Woods. *"Structural Properties of Crystals of CdTe Grown from the Vapour Phase"*. J. Crystal Growth, **72** (1985) 85.

[70] G. J. Russell, N. F. Thompson and J. Woods. *"The Incidence of Voids in Vapour Grown Crystals"*. J. Crystal Growth, **71** (1985) 621.

[71] K. Durose and G. J. Russell. *"Twinning in CdTe"*. J. Crystal Growth, **101** (1990) 246.

[72] K. Durose and G. J. Russell. *"Structural Defects in CdTe Crystals Grown by Two Different Vapour Phase Methods"*. J. Crystal Growth, **86** (1988) 471.

[73] M. M. Faktor, R. Heckingbottom and I. Garret. *"Growth of Crystals form the Gas Phase Part 1. Diffusional Limitations and Interfacial Stability in Crystal Growth by Dissociative Sublimation"*. J. Chem. Soc **A**, (1970) 2657.

[74] M. M. Faktor, R. Heckingbottom and I. Garret. *"Growth of Crystals form the Gas Phase Part 2. Diffusional Limitations and Interfacial Stability in Crystal Growth by Dissociative Sublimation, with and Inert Third Gas Present"*. J. Chem. Soc **A**, (1971) 1.

[75] M. M. Faktor, I. Garret and R. Heckingbottom. *"Diffusional Limitations in Gas Phase Growth of Crystals"*. J. Crystal Growth, **9** (1971) 3.

[76] M. M. Faktor and I. Garret. *"Interplay of Activation and Diffusion in Crystal Growth from the Vapour Phase"*. J. Crystal Growth, **9** (1971) 12.

[77] D. W. Greenwell, B. L. Markham and F. Rosenberger. *"Numerical Modeling of Diffusive Physical Vapor Transport in Cylindrical Ampoules"*. J. Crystal Growth, **51** (1981) 413.

[78] F. Rosenberger, J. Ouazzani, I. Viohl and N. Buchan. *"Physical Vapor Transport Revisited"*. J. Crystal Growth, **171** (1997) 270.

[79] W. Palosz, M. A. George, E. E. Collins, K. T. Chen, Y. Zhang, Z. Hu and A. Burger. *"Seeded Physical Vapor Transport of Cadmium-Zinc-Telluride Crystals: Growth and Characterization"*. J. Crystal Growth, **174** (1997) 733.

[80] H. Wiedemeier and G. H. Wu. *"Defects in CdTe Single Crystals Grown by Very Fast Vapor Growth Technique"*. J. Electron. Mater., **24** (1995) 1007.

[81] N. Tamari and H. Shtrikman. *"Non-Seeded Growth of Large Single $Pb_{1-x}Sn_xTe$ Crystals on a Quartz Surface"*. J. Crystal Growth, **43** (1978) 378.

[82] R. Triboulet and Y. Marfaing. *"CdTe Growth by Multipass THM and Sublimation THM"*. J. Crystal Growth. **51** (1981) 89.

[83] M. Bruder and R.Nitsche. *"Seeded Vapour Growth of Cadmium Telluride Using Focused Radiation Heating"*. J. Crystal Growth, **72** (1985) 705.

[84] M. Laasch, R. Schwarz, P. Rudolph and K. W. Benz. *"CdTe Crystal Growth by a Sublimation Traveling Heater Method"*. J. Crystal Growth, **141** (1994) 81.

[85] M. M. Faktor and I. Garret. *Growth of Crystals from the Vapour*. Chapman and Hall, London (1974).

[86] J. R. Abernathey, D. W. Greenwell and F. Rosenberger. *"Congruent (Diffusionless) Vapor Transport"*. J. Crystal Growth, **47** (1979) 145.

[87] F. Rosenberger and G. H. Westphal. *"Low-Stress Physical Vapor Growth (PVT)"*. J. Crystal Growth,**43** (1978) 148.

[88] H. Kuwamoto. *"Seeded Growth of Large Single-Grain CdTe from the Vapour Phase"*. J. Crystal Growth, **69** (1984) 204.

[89] G. H. Dierssen and T. Gabor. *"Seeded Growth of Large Single Crystals of CdS from the Vapour Phase"*. J. Crystal Growth, **43** (1978) 572.

[90] E. V. Markov and A. A. Davydov. *"Sublimation of CdS Crystals"*. Neo. Mater. 7 (1971) 575 (in russian). See Inorg. Mater 7 (1971) 503 for english translation.

[91] E. V. Markov and A. A. Davydov. *"Growth of Oriented Monocrystals of CdS from the Vapour Phase"*. Neo. Mater. **11** (1975) 1755 (in russian). See Inorg. Mater **11** (1975) 1504 for english translation.

[92] Z. Golacki, M. Gorska, J. Makowski and A. Szczerbakow. *"Vapour Phase Growth of CdTe"*. J. Crystal Growth, **56** (1982) 213.

[93] R. Lauck and G. Muller-Vogt. *"Vapour Transport of Impurities in Semi-Closed Ampoules I. Theory"*. J. Crystal Growth, **74** (1986) 513.

[94] R. Lauck and G. Muller-Vogt. *"Vapour Transport of Impurities in Semi-Closed Ampoules II. Doping Profiles, refining and Stoichiometry in Crystal Growth of II-VI Compounds"*. J. Crystal Growth, **74** (1986) 520.

[95] J. L. Boone, G. Cantwell, W. C. Harsch, J. E. Thomas and B. A. Foreman. *"Electrical and Crystallographic Characterization of CdTe Grown by the Transport Method"*. J. Crystal Growth, **139** (1994) 27.

[96] K. Grasza, U. Zuzga-Grasza, A. Jedrzejczak, R. R. Galazka, J. Majewski, A. Szadkowski and E. Grodzicka. *"A Novel Method of Crystal Growth by Physical Vapour Transport and Its Application to CdTe"*. J. Crystal Growth, **123** (1994) 519.

[97] K. Grasza, R. Schwarz, M. Laasch, K. W. Benz and M. Pawlowska. *"Surface Morphology of Vapour Phase Grown CdTe"*. J. Crystal Growth, **151** (1995) 261.

[98] A. A. Glebkin, A. A. Davydov and N. I. Garba. *"Growing Large Single Crystals of CdTe from the Vapor Phase"*. Inorg. Mater., **16** (1980) 19.

[99] Y. V. Korostelin, V.I. Kozlovsky, A. S. Nasibov and P. V. Shapkin. *"Vapour Growth of II-VI Solid Solution Single Crystals"*. J. Crystal Growth, 159 (1996) 181.

[100] Y. V. Korostelin, V.I. Kozlovsky, A. S. Nasibov and P. V. Shapkin. *"Vapour Growth and Characterisation of Bulk ZnSe Single Crystals"*. J. Crystal Growth, 161 (1996) 51.

[101] M. Laasch, T. Kunz, C. Eiche, M. Fierderle, W. Joerger, G. Kloess and K. W. Benz. *"Growth of Twin-Free CdTe Single Crystals in a Semi-Closed Vapour Phase System"*. J. Crystal Growth, 174 (1997) 696.

Chapter Three

The New "Multi-tube" PVT Apparatus for CdTe Growth

3.0 INTRODUCTION.

In this chapter, a description of the vapour growth experimental system used in Durham is presented. The system was mainly designed by Dr. J.T. Mullins, in particular the technical design, computer assisted thermal analysis and construction. Only a general description of the growth apparatus, with special emphasis on the innovative and relevant aspects for crystal growth rather than the engineering and technical elements of the system is presented.

3.1 DESIGN OF THE VAPOUR GROWTH APPARATUS.

3.1.1 General Design.

A sketch of the vapour growth system design is shown in figure 1. The design [1,2] is broadly a modification of the Markov technique, in the sense that the growth is seeded and proceeds without contact with the ampoule walls (thus avoiding sticking and stress related problems), but incorporates several innovative elements. The most striking feature is the inverted U-shape of the silica ampoule, which allows for the temperature of the source and growing crystals to be controlled independently. In essence, it consists of three separate zones: source, crossmember and growth regions. The introduction of the crossmember allows simultaneously the introduction of viewing ports to the surface of crystal and source (which can be used to monitor the nucleation and sublimation processes respectively) , measurement ports to measure the partial pressure by means of an optical absorption technique and an isothermal zone where a flow restrictor can be inserted in order to control the mass transport rate. The demountable and reusable silica glassware is surrounded by heat shields to provide thermal insulation and located in a

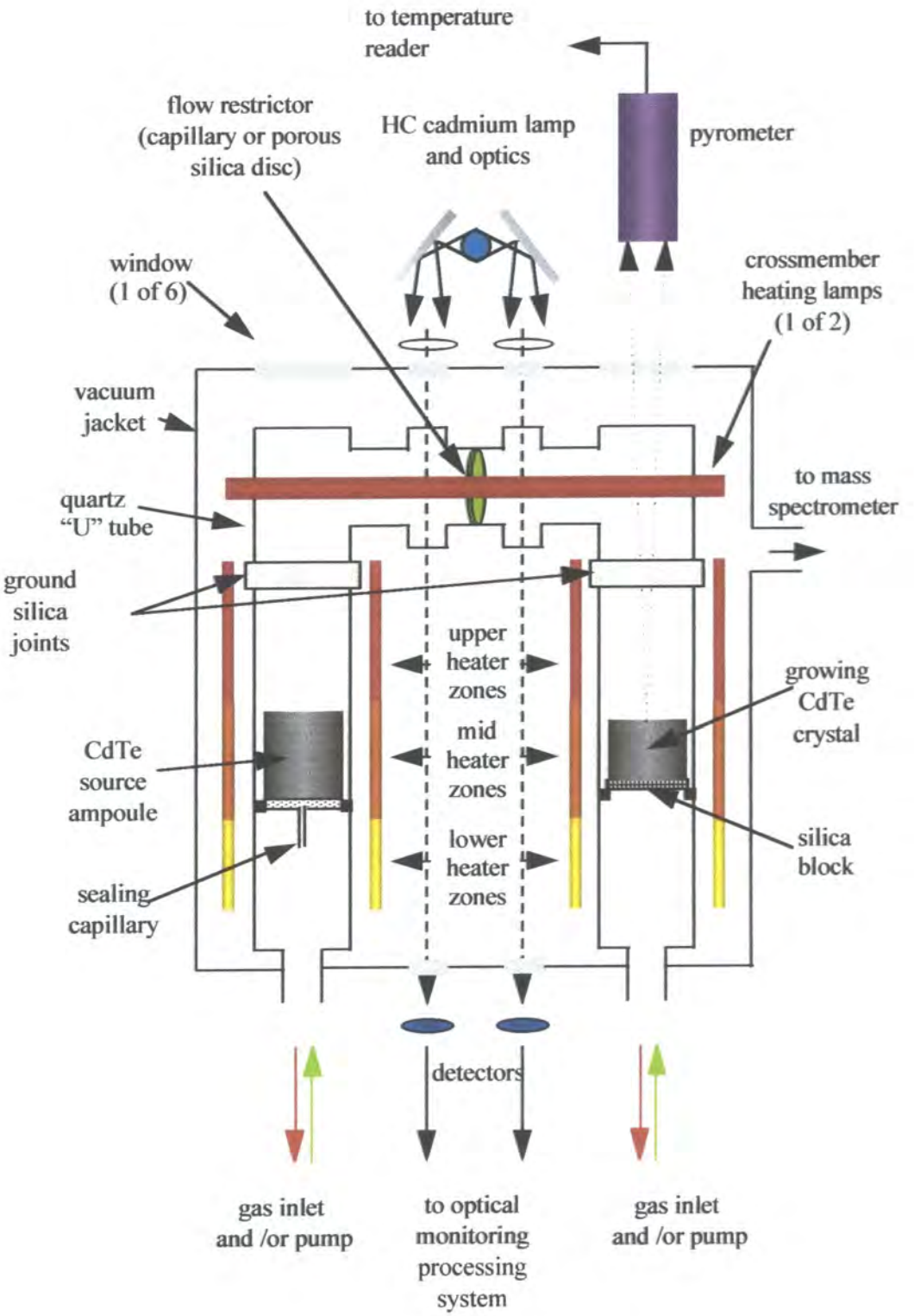

Figure 1. Design of the Multi-tube U-Tube Physical Vapour Transport Growth System.

vacuum jacket which is kept under dynamic pumping during operation. The source and seed can be easily introduced by removing the crossmember. The source zone has a small capillary which allows both the introduction of a constant flow of gas during or prior to growth as well as pumping of the ampoule. The design is such that if a gas flow is not introduced, the capillary is in principle sealed off by evaporation and transport of some CdTe from the top area of the source to the cooler bottom area during the initial stages of the sublimation process. Two growth tube designs have been used to date. The first is a Markov type arrangement: the 49 mm seed sits in a silica block, typically 1-5 cm long, which is tightly fitted in the growth tube, and held by three (permanently made) indentations in the growth tube. A narrow gap, always smaller than 0.1 mm, between the ampoule walls and the silica (and seed) block allows continuous removal of excess components, and more importantly, outgassing products and volatile impurities by dynamic pumping. The second arrangement is a modified Markov type also, but in this case the 29 mm seed sits on a flat-topped "plug" which fits into a glass socket. A gap of known dimensions (typically 25 μm) to allow dynamic pumping is allowed by inserting several platinum wires between the glass plug and the socket.

Both the source and growth tubes (49 mm inner diameter maximum) are heated independently by furnaces (made of pyrolitic boron nitride and using low copper content, high purity graphite contacts) consisting of three zones which can be independently computer controlled. The crossmember is heated by means of two 1000W quartz halogen lamps (QHL) the output power of which can be (independently of the source and growth furnaces) varied. Use of radiative heating is effectively the technological key that allows the introduction of windows for continuous visual supervision and diagnostic tools for non-destructive *in situ* monitoring. A pyrometer can

be used to determine accurately the surface temperature of the growing crystal, which, once the temperature gradient above the crystal is known, can allow direct measurement of the supersaturation growth conditions.

Figure 2. Photograph of the Durham growth system. Arrow numbers: 1) mass spectrometer, 2) turbomolecular pump, 3) PC control, 4) measuring and diagnostic instruments and 5) vacuum jacket.

The two central windows in the crossmember (see figure 1) allow for a straight optical path from the top to the bottom of the vacuum furnace. This is used to monitor the partial pressures of cadmium and tellurium simultaneously and independently (by optical absorption using a simple optics (see figure 6) and detector system described in chapter 5 and reference [3]) in both the source and growth sides when a flow restrictor is used. The latter, which can be a porous silica disc (the flow properties of which are

extensively studied in chapter five) or a simple capillary, allows precise control of the mass transport rate. The fact that it remains at a constant temperature (which is higher, but chosen independently than that of the source and growth areas) allows simple modelling of the flow regimes in the whole ampoule (see chapters five and six).

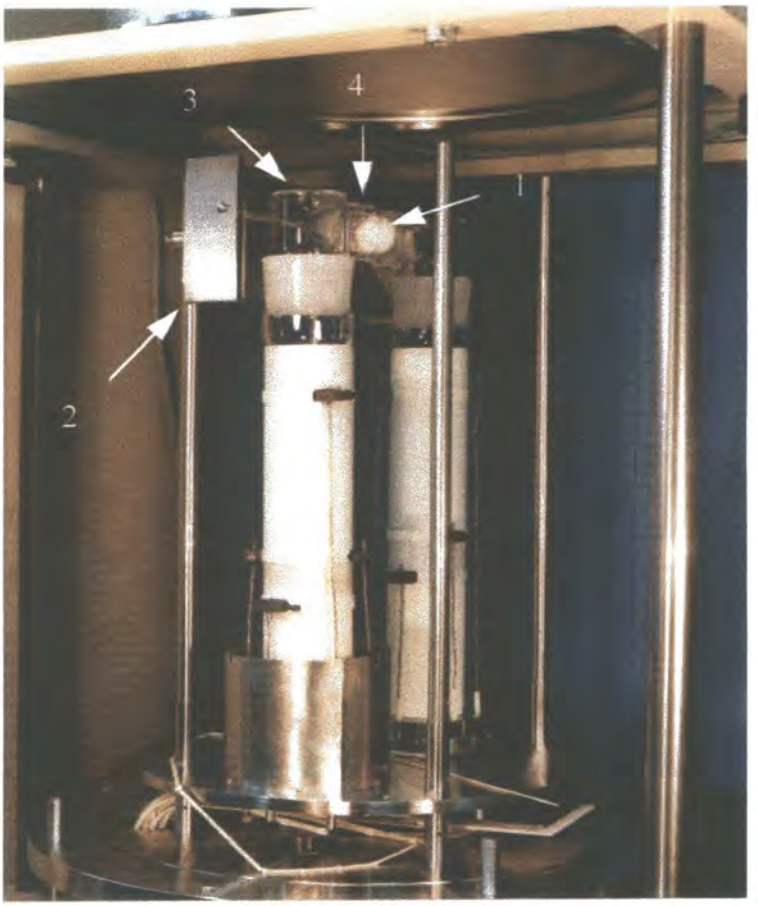

Figure 3. Photograph of the silica glassware (sitting on the base of the vacuum jacket) and the pyrolitic boron nitride heaters. The porous silica restrictor (1), one of the two crossmember heat shields (2), one of the optical access (3) and the four vapour monitoring (4) windows are visible.

Although the temperature distribution was computer modelled using a thermal modelling (I-DEAS^{TM}) program, the vacuum jacket is still constantly water cooled and ensures safe operation conditions. The vacuum jacket also allows the use of a quadrupole mass spectrometer for measuring the partial pressures of residual gases in

the system as well as the absolute pressure. In this way, the quality of the vacuum during operation and specially during growth can be monitored. The ampoule together with the heaters and mullite and molybdenum heat insulation shields (see figure 3 and 4) sit on the base of the vacuum jacket, which can be automatically lowered to provide access to the ampoule, source and seed before and after growth.

Figure 4. Photograph of the growth system of figure 3 after all the heat shields have been put in place. Three of the four stainless steel rods that support the QHL's and the molybdenum heat shields elements are visible.

3.1.2 Main features of the Multi-tube PVT apparatus.

From analysis of work done in the past and the conclusions outlined in chapter one, it can be seen that several features have been incorporated into the Multi-tube design in order to solve some of the problems encountered in the past.

With reference to the thermodynamics and mechanical properties of CdTe,

1) Interaction with the silica walls has been minimised by using the successful Markov technique.

2) The requirement for negligible (or at least small compared to the gradient above the crystal) temperature fluctuations has been taken into account by using independently controlled zones, by thermal analysis computer simulation and by the use of a pyrometer to monitor surface temperature (although the latter is difficult since calibration is needed [4,5]).

3) The use of two different furnace zones to some extent separates the temperature regimes in the source and crystal, effectively decoupling the evaporation and growth processes. Hence low temperatures, well within the narrower part of the homogeneity range can be used without the need to sacrifice high transport rates.

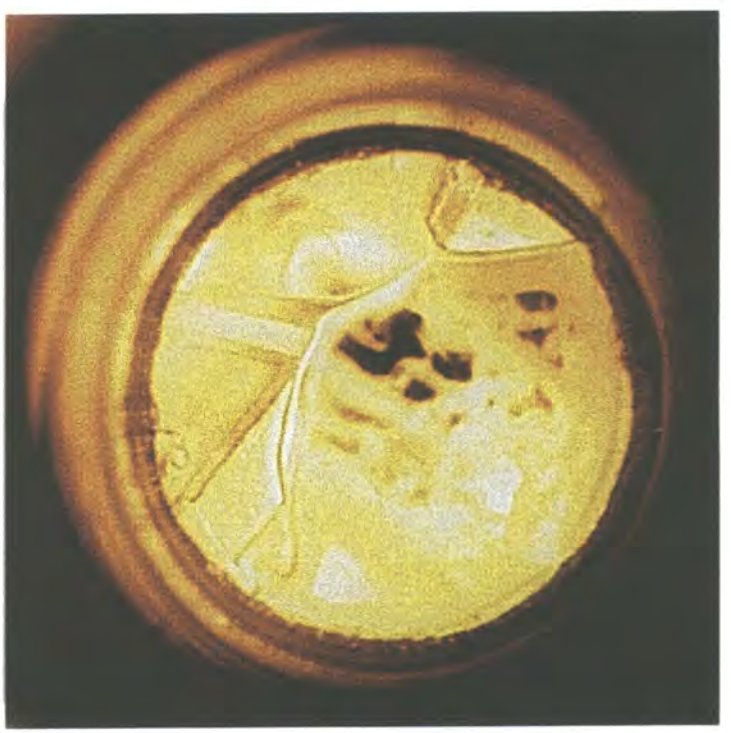

Figure 5. Photograph of a 49 mm CdTe crystal during growth. The polynucleation and thermal etching in the previous stages can be easily monitored: twin boundaries and subgrains are clearly visible, and follow the pattern of the multigrain seed.

From the technical point of view,

1) The source, crossmember and growth chambers are thermally decoupled. This allows the temperature in each region to be set independently, simplifying temperature control. Moreover the introduction of three zones, specially in the growth side allows in principle the adoption of growth-advantageous temperature profiles, which can be set independently of the source temperature. Temperature accuracy and stability is computer controlled.

2) The crucible is of simple design, is demountable for easy access to source and seed or crystal, and for cleaning and more importantly, can be re-used. The design allows for the introduction of further source tubes to grow ternary and multinary solid solutions (*octopus-like* shape) or of one or more elemental component reservoirs or of dopant sources.

3) The design allows for dynamic pumping of the ampoule during growth, thus ensuring continuous removal of excess components and outgassing residues. This allows mass transport to be more readily modelled, since the uncertainties due to residual, non-condensable vapours no longer exist. Furthermore it allows for the continuous flow of an inert gas or transport agent either during growth, or prior to growth to preserve the monocrystallinity of the seed and/or as a reducing agent.

4) The use of a flow restrictor further allows the sublimation and growth processes to be decoupled.

5) The U-shape design permits the use of a non-destructive, non-interacting diagnostics system to monitor the partial pressure ratio of Cd and Te_2 during growth, and hence the means to monitor growth conditions directly. It also allows visual access to the growing crystal (see figures 5 and 6) and, potentially, supervision of nucleation processes as well as the introduction of a pyrometer.

Figure 6. Photograph of the HC cadmium lamp and optics (1) and mechanical chopper (2) used for vapour pressure monitoring through the optical windows (5). The viewing ports (3) and (4) allow direct observation of the source and crystal respectively.

3.1.3 The U-tube design : transport test.

The innovative U-tube design was tested before construction of the Multi-tube growth system. In principle, there is no thermodynamical reason for the vapour originating at the source not to flow to the deposition zone through the crossmember. However, an experiment was set up in order to make sure transport would occur. A U-tube (see figure 7) was constructed. The inner diameter of the tube was 0.5 mm.. The closed end contained a small charge (1.868 gm) of CdTe, while a silica rod (~ 5 cm long) was inserted into the open end to provide nucleation (thus providing a Markov-like arrangement). The assembly was continuously pumped during the entire experiment through the space (<0.05 mm) left between the tube walls and the rod. The bent portion of the tube was kept at a higher temperature (800 °C) than the source (618 °C) and crystal (600 °C) zones. Full transport was achieved , as expected, and a polycrystal was

grown on the rod. A small amount of material and presumably some excess component was deposited downstream of the silica rod inserted, but none in the narrow gap (see figure 7). More importantly, the crystal was easy to remove, with no noticeable sticking to the glass walls. Apart from demonstrating the feasibility of the U-tube design, it also became clear that use of dynamic pumping (which provides both a constant pressure difference between source and crystal, and eliminates the build-up of excess components) speeds up the transport process, and hence a mass flow restrictor would have to be used in the Multi-tube growth system in order to control the mass transport rate.

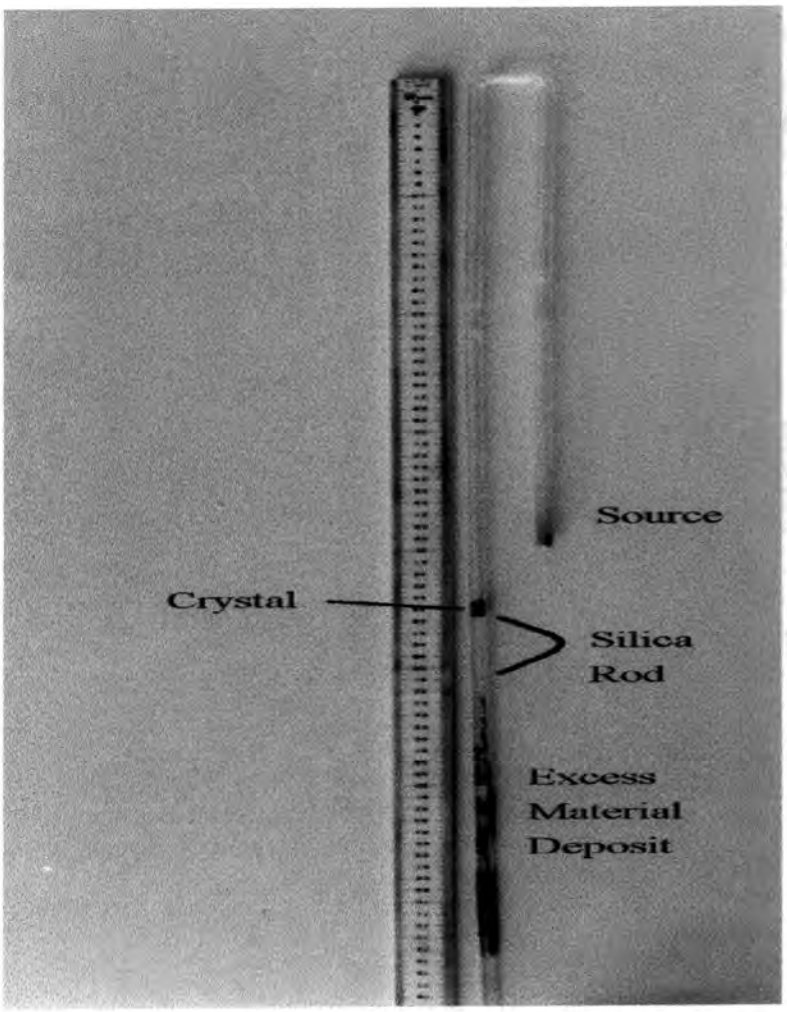

Figure 7. The U-tube used to test CdTe vapour transport. Absence of deposition along the length of the silica rod is clearly visible.

3.1.4 The source charge arrangement.

The importance of the charge has not been overlooked in the design of the growth apparatus. Contamination control during the various processing and handling steps prior to growth was partially achieved through the processing and synthesis of CdTe from its elemental constituents (99.9999 % purity) in a closed ampoule [6], which was placed in the source tube and opened just before growth. Technical furnace limitations did not allow for the source charge ampoule diameter to match that of the source tube, introducing some uncertainty in the rate of evaporation, since unless the three zones are kept at the same temperature, some vapour will condense in the gap left between the two containers. Consequently, the ideal situation in which the source material is completely compacted and has a constant surface area for evaporation which, at a given temperature, would provide a constant vapour flux, cannot be fully achieved in a reusable container. This situation however, was closely approached once the initial self-sealing process had been completed and the whole length of the source was maintained at a constant temperature.

3.2 GROWTH PROCEDURES.

Growth procedures have yet to be completely optimised due to the novelty and broad range of possibilities that the growth system offers. At the time of writing, the system has been in operation and available for experimentation for only a very limited period of time. Thus only a general overview of the generic steps are described here.

Once the system has been loaded, the crucibles and shields are put in place, the vacuum jacket is then closed, and pumping of the ampoule started. It is important to

evacuate the ampoule first to ensure that the pressure inside the glass ampoule is less than that in the vacuum jacket. Otherwise, a large positive pressure differential could force open the glass joints. This is achieved using a rotary pump connected to the source tube. Once the pressure in the ampoule is $< 10^{-1}$ mbar, evacuation of the main vacuum chamber is started using a turbomolecular pump. Pump down continues over a period of approximately a day, after which the vacuum is analysed using the mass spectrometer. Further removal of foreign gases, mainly water vapour, is achieved by simply setting the eight furnace zones to approximately 100 °C to bake out the ampoule. Special care is taken in order to avoid any deposition of hydrocarbons on the optical monitoring windows. After a period of approximately a day, the vacuum is again analysed and a second baking step is started by setting all the zones to 200 °C. After a few hours, the system is ready to proceed.

Ideally, inert gas should be admitted into the ampoule to preserve the integrity of the seed. However, this has yet been to be implemented due to the lack of time and the possible difficulty in ensuring the tightness of the glass joints. Normally, the crossmember temperature is raised first (600-800 °C) and then the source and growth tube temperatures are slowly increased. Special care has to be taken in order to avoid sublimation of the seed. Although thermal etching is unavoidable and to some extent beneficial in removing surface oxides to obtain a clean pre-growth surface, the temperature of the growth tube is kept as low as possible until an acceptable amount of vapour is present in the source side. After this step, the growth, source and crossmember temperatures are increased to the desired value. Temperatures throughout the whole growth experiment are accurately maintained (< 0.1 °C) under PC control.

On completion of growth, the temperature of the zones is decreased steadily and in a programmed manner. Normally care has to be taken to ensure that the temperature of the crossmember is always higher than that of the source and seed. This is specially the case since the thermal capacity of the crossmember is relatively low, and hence the cooling proceeds more rapidly than in the better insulated, higher heat capacity source and growth tube assemblies. Once the temperature has been reduced to room temperature, air is admitted slowly into the vacuum jacket, and the grown crystal can then be removed.

3.3 CONCLUSIONS.

The Multi-tube physical vapour transport (MPVT) growth apparatus developed in Durham (by Dr. J. T. Mullins) for the growth of large CdTe crystals has been briefly described. The innovative, conceptually simple design allows for the first time the introduction of simple diagnostic tools that in principle provide the means for determination of partial pressures of the vapour constituents, control of the mass transport and accurate determination of the supersaturation conditions over the crystal.

The MPVT growth apparatus takes into account previous experience and incorporates in its design novel features intended to minimise some of the growth problems that arise as a consequence of the intrinsic CdTe properties and the growth technology. In particular, decoupling of the sublimation and growth processes by the introduction of an independently temperature controlled crossmember allows for lower growth temperatures but is also the technological breakthrough that allows monitoring and control of the growth process.

Introduction of dynamic pumping allows not only strict control of growth pressures but also eliminates the presence and progressive build up of outgassing products as growth proceeds. These products can be monitored, in principle, throughout the growth process by the use of a mass spectrometer.

The potential of the growth process at this stage has not been fully developed, since, as shown in the following chapters, the main efforts have been directed to understanding the transport mechanisms, modelling and the development of state of the art optical monitoring tools. However, as shown in chapter 7, the precise control of the partial vapour pressures will allow further fundamental studies on vapour growth to be carried out. The Multi-tube growth system should be a promising technology for the industrial production of CdTe and other (including ternary and quaternary) II-VI compounds.

REFERENCES FOR CHAPTER THREE

[1] University of Durham. *"Improvements in and Relating to Crystal Growth"*. U.K. Patent Application n° 9717726.5 (1997).

[2] J.T. Mullins, J. Carles, N. M. Aitken and A. W. Brinkman. To be published.

[3] J. Carles, J. T. Mullins and A. W. Brinkman. *"Partial Pressure Monitoring in Cadmium Telluride Vapour Growth"*. J. Crystal Growth, **174** (1997) 740.

[4] T. R. Harrison. *Radiation Pyrometry and Its Underlying Principles of Radiant Heat Transfer"*. John Wiley & Sons, New York (1960).

[5] J. T. Mullins, J. Carles and A. W. Brinkman. *"High Temperature Optical Properties of Cadmium Telluride"*. J. Appl. Phys. **81** (1997) 6374.

[6] The source ampoule was produced by the Kristallographisches Institut, University of Freiburg, Germany. See for example, M. Laasch, T. Kunz, C. Eiche, M. Fierderle, W. Joerger, G. Kloess and K. W. Benz. *"Growth of Twin-Free CdTe Crystals in a Semi-Closed Vapour Phase System"*. J. Crystal Growth, **174** (1997) 696.

Chapter Four

Cd and Te_2 Optical Absorption and Its Application to Vapour Pressure Monitoring

4.0 INTRODUCTION.

The importance of maintaining a constant vapour pressure during growth has been discussed in previous sections and cannot be over emphasised. The Multi-tube vapour growth system was designed to accommodate a system capable of monitoring partial pressures throughout growth. Light absorption techniques provide a tool to investigate vapour composition without perturbing the growth process. Therefore, the absorption properties (and its relation with pressure) of vapours over solid CdTe had to be studied and understood. The chapter has two main sections. The first part presents the laws of light absorption in gases or vapours and reviews some of the theoretical background. The second part describes the absorption spectrum of Cd and Te_2 in the near UV-Visible range of wavelengths and discusses the applicability of the absorption laws to Cd atoms and Te_2 molecules. As will be seen, the relative simplicity of the spectra allows the construction of a very simple, compact and robust system to monitor *in situ* the optical absorption of Cd and Te_2 vapours independently, simultaneously and in real time during CdTe growth in the Durham vapour growth system. The chapter concludes with the calibration of the system as a function of vapour pressure for pure cadmium and tellurium, the results of which may be used to monitor the partial vapour pressures during growth.

4.1 THEORETICAL BACKGROUND.

4.1.1 Bouguert-Beer-Lambert Law of Absorption.

Quantitative analysis by absorption spectrometry techniques usually relies upon the Bouguert-Beer-Lambert (BBL) law of absorption [1], also commonly known as

Beer's law. This law is in fact a combination of several laws [2,3]. The BBL law states that, for a parallel beam of monochromatic light passing through a homogeneous, uniform medium of thickness l, in which the absorbing species have a concentration c, the intensity of transmitted light I and of incident light I_o are related by the expression,

$$I = I_o e^{-kcl} \tag{4.1}$$

where k is called the *absorption coefficient* of the medium. The BBL law is usually expressed in the form

$$D_\lambda \equiv \log\left(\frac{I_o}{I}\right) = \varepsilon_\lambda cl \tag{4.2}$$

where D_λ is the optical density or absorbance and ε_λ is called the *molar extinction coefficient*. The subscript λ denotes that both the optical density and extinction coefficient refer to monochromatic light of wavelength λ. The BBL law can be derived from the quantum theory of interaction of radiation with matter, using the Einstein coefficients of transition probability:

$$I = I_o e^{-\sigma(N_o - N_1)l} \tag{4.3}$$

where σ is the absorption cross section, the "effective area" that an absorber presents to a beam of photons, and N_o and N_1 are the number of absorbers per unit of volume in the ground and excited state respectively. The result [4] is equivalent to equation 4.1. Clearly ε_λ is closely connected with the transition probability, a large probability being associated with a large ε_λ and vice versa.

Since we are interested in absorption in vapours, we can rewrite equation 4.2 assuming that the vapours behave like an ideal gas:

$$D_\lambda = \frac{\varepsilon_\lambda pl}{RT_c} \tag{4.4}$$

or rearranging,

$$p = \frac{D_\lambda R T_c}{\varepsilon_\lambda l} \tag{4.5}$$

where p is the pressure of the vapour, T_c its temperature and R is the ideal gas constant. Therefore we can write,

$$p = C(\varepsilon_\lambda, T_c, l) D_\lambda \tag{4.6}$$

where $C(\varepsilon_\lambda, T_c, l)$ is a constant once ε_λ , T_c and l have been determined. The above equation states that when the BBL law is obeyed, the pressure is directly proportional to the optical density of the vapour. Therefore, in order to determine *in situ* vapour pressures during growth, it is necessary, once a suitable wavelength has been chosen, to determine the constant $C(\varepsilon_\lambda, T_c, l)$.

The relation between optical density and vapour pressure can be further developed once the cell temperature and path length is set. Since we are interested in cadmium and tellurium vapours, and these have well defined Clausius-Clapeyron vapour-solid or vapour-liquid equilibrium equations of the type,

$$\log(p) = \frac{a}{T_r} + b \tag{4.7}$$

where a and b are specific constants for each element at a determined range of temperatures, and T_r is the temperature of the reservoir, then, if the Beer's law is obeyed, for a given cell temperature and path length, a plot of $\log(D_\lambda)$ versus $1/T_r$ should give a straight line with slope a and intercept b':

$$\log(D_\lambda) = \frac{a}{T_r} + b' \tag{4.8}$$

Combining equations 4.7 and 4.8, the relation between p and D_λ is directly determined,

$$p = 10^{(b-b')} D_\lambda \tag{4.9}$$

or $$p = \alpha'_\lambda D_\lambda \tag{4.10}$$

where α'_λ is the experimentally determined value of $C(\varepsilon_\lambda, T_c, l)$ in equation 4.6. In the cases where the Beer's law is not obeyed, but the plot $\log(D_\lambda)$ versus $1/T_r$ still yields a straight line of slope a' and intercept b', it is still possible to relate the optical density to the pressure of the vapour for a given cell temperature and path length:

$$p = 10^{\left(\frac{ba'-b'a}{a'}\right)} D_\lambda^{a/a'} \tag{4.11}$$

or $$p = \alpha_\lambda D_\lambda^{\beta_\lambda} \tag{4.12}$$

4.1.2 Applicability of the Bouguert-Beer-Lambert Law.

Beer's law does not hold always. Although there are good theoretical reasons for supposing that the law should hold rigorously for monochromatic light, in practice the assumptions made in its derivation cannot be totally attained in the laboratory, and hence it is necessary to assess the dependence of optical density on the concentration. First, it is evident that ε_λ is a function of the wavelength λ, since this is the nature of an absorption spectrum. Secondly, an absorption band has a finite width, which can be due to natural, Doppler or collision broadening. The slits of the monochromator have a finite width, which means that the measured transmitted light is not monochromatic, but is comprised of a (normally narrow) wavelength band. The derivation of the exponential law connecting the fraction of light transmitted and the concentration shows that in this case, the law holds only when ε_λ is constant over the band [2]. This means that Beer's law holds in practice when ε_λ does not vary greatly over the portion of band selected by the slits, and it will not hold when the absorption band is narrow compared to the monochromator bandwidth, i.e. when the slit width does not provide sufficient resolving power. Other factors that might limit the validity of Beer's law are the diffusing or

scattering nature of the absorbing medium (which causes the rays to travel different path lengths), photoinduced chemical changes in the medium (which will produce a change in concentration of the absorbing species) or saturation effects in the case of large incident radiation flux [5].

These effects can only be recognised by means of experimental testing, and are normally rare. Other effects that should be taken into account, especially in our case, since we are dealing with vapours, is the broadening of the absorption lines due to natural, Doppler and pressure broadening. Broadening might have to be studied when the absorption band is extremely narrow, and hence, as discussed above, deviations from Beer's law are expected. In particular, Doppler broadening is a function of the vapour temperature [1].

This means that unless the absorption band is large enough so that ε_λ can still be considered to remain constant over the bandpass of the monochromator, every determination of ε_λ will be valid only for the vapour temperature used in the experiment, and equation 4.5 cannot be used to extrapolate ε_λ to other vapour temperatures. Apart from these effects, there still remains the experimentally related errors, which can be normally overcome, namely: i) the relative difficulty of collimating the light so that parallel rays travel perpendicular to the absorbing medium and the path length is the same for all of them ii) misalignment of the cell iii) stray light iv) length determination errors and v) the detection limit (signal to noise ratio) of the apparatus and sensitivity (size of the absorption signal) of the absorption line.

4.2 UV-VISIBLE ABSORPTION SPECTROSCOPY OF Cd ATOMS AND Te_2 MOLECULES.

In this section, the absorption spectra of Cd and Te_2 vapours are presented. It will be seen that as expected, the absorption features of the two vapours are very different. This is due to the fact that cadmium vapour is monoatomic [6], and hence transitions are expected to be electronic, resulting in extremely narrow absorption bands, while tellurium vapour is molecular [7], and hence broad vibrational absorption bands might appear in the absorption spectrum.

The full spectrum at different vapour pressures in the UV-Visible of Cd and Te_2 is needed in order to choose the optimum wavelengths for the optical density measurement. Clearly, it is desirable to choose those wavelengths that avoid any overlap between the absorption of Cd and Te_2, since this would complicate the conversion from optical density to vapour pressure.

4.2.1 Experimental Procedure.

The experimental arrangement used to obtain the spectra is shown in figure 1. A 50.1 mm long, 32 mm diameter silica transmission cell with a side arm containing a small charge of cadmium or tellurium was located in a two zone furnace which allowed the cell to be maintained at temperatures between 600 and 1100 °C while the temperature of the side arm could be varied between 120 and 950 °C to control the vapour pressure and hence density of the charge vapour. Charge material of at least 99.999 % purity was used, and in all cases this was first transported under dynamic vacuum prior to loading into the experimental cell to eliminate oxides and impurities

from the charge. The loaded ampoules were baked overnight at ~120 °C under vacuum to eliminate water vapour prior to sealing at a pressure of 10^{-5} mbar. Light from a 250W quartz halogen lamp was chopped and then collimated into the entrance of the furnace by silica lens 1. After passing through the silica transmission cell the light was collected and focused by silica lens 2 into the slits of one of the two monochromator and detector systems described below. Care was taken to ensure that no light was able to reach the detection system without passing through the ampoule and the vapour it contained.

Transmission spectra for tellurium vapour were recorded using an Oriel 1/8 m monochromator fitted with a 1200 lines/mm grating in conjunction with a Hamamatsu S1337-16BQ silicon photodiode and lock-in detection. The slits were set to give a wavelength resolution of approximately 5 nm. Transmission spectra for cadmium vapour were recorded using a Hilger & Watts, Monospek 1000 (1 meter focal length) monochromator fitted with a 1200 lines/mm grating together with a Hamamatsu R457 photomultiplier tube. Both the entrance and exit slits were set to give a resolution of 1 Å or better. The output of the lock-in amplifier was measured by a digital voltmeter and logged using a computer. In both cases it was necessary to correct for the wavelength dependence of the light sources, monochromator efficiency and photodiode response. In the cases of the tellurium vapour absorption measurements, optical densities were determined from the ratio of a spectrum taken with the desired pressure in the ampoule to a spectrum taken under the same light source and detection conditions but with a negligible vapour pressure ($p < 0.01$ mbar) in the transmission cell which gave the baseline I_o. For cadmium vapour absorption measurements, the baseline was determined from the same measurement as the absorption itself, by extrapolation from the non-absorbent tails on either side of the transmission line centre.

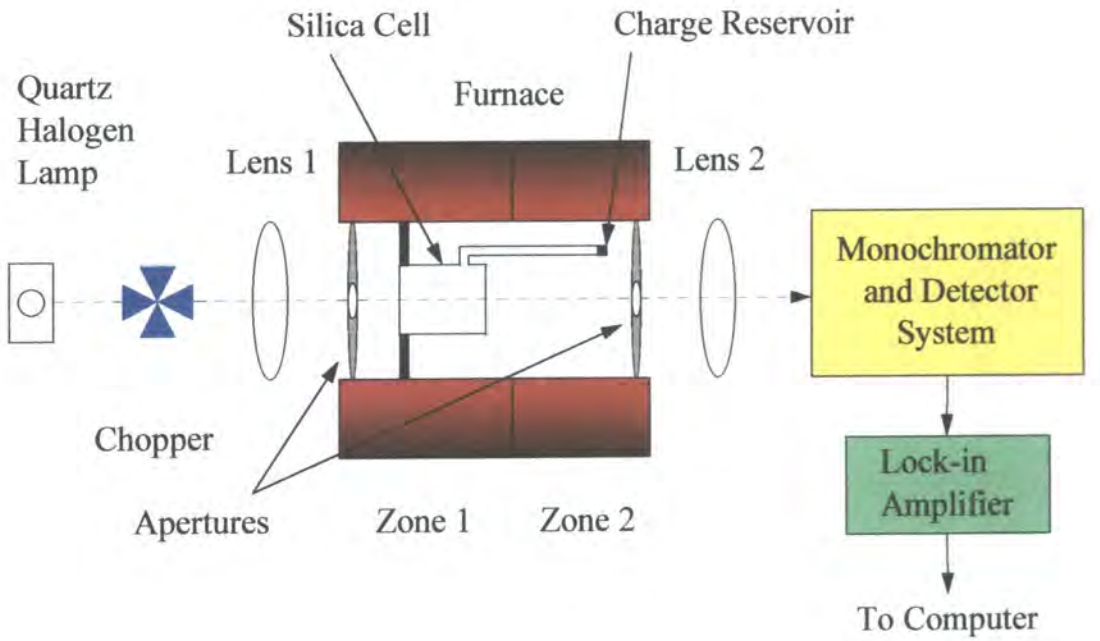

Figure 1. Experimental setup used to obtain transmission spectra of cadmium and tellurium vapours.

4.2.2 Tellurium Vapour Absorption Spectrum.

The tellurium vapour absorption spectrum in the range 300-650 nm is shown in figure 2 [8]. The temperature of the cell was maintained nearly constant, always in the range 793-823 °C. The range of tellurium vapour pressures varied from 0.3 mbar to 49.3 mbar corresponding to reservoir temperatures between 450 °C and 715 °C [9]. Specific values for each absorption curve are shown in table 1. The existence of a small temperature gradient in the reservoir (3-5 °C for the lower, 1-2 °C for the higher reservoir temperatures) introduces some uncertainty in the vapour pressure. The results shown in table 1 for vapour pressures were calculated in each case using the average reservoir temperature. However, the main intention here was to obtain a qualitative absorption spectrum for the typical vapour pressures encountered during vapour growth of CdTe.

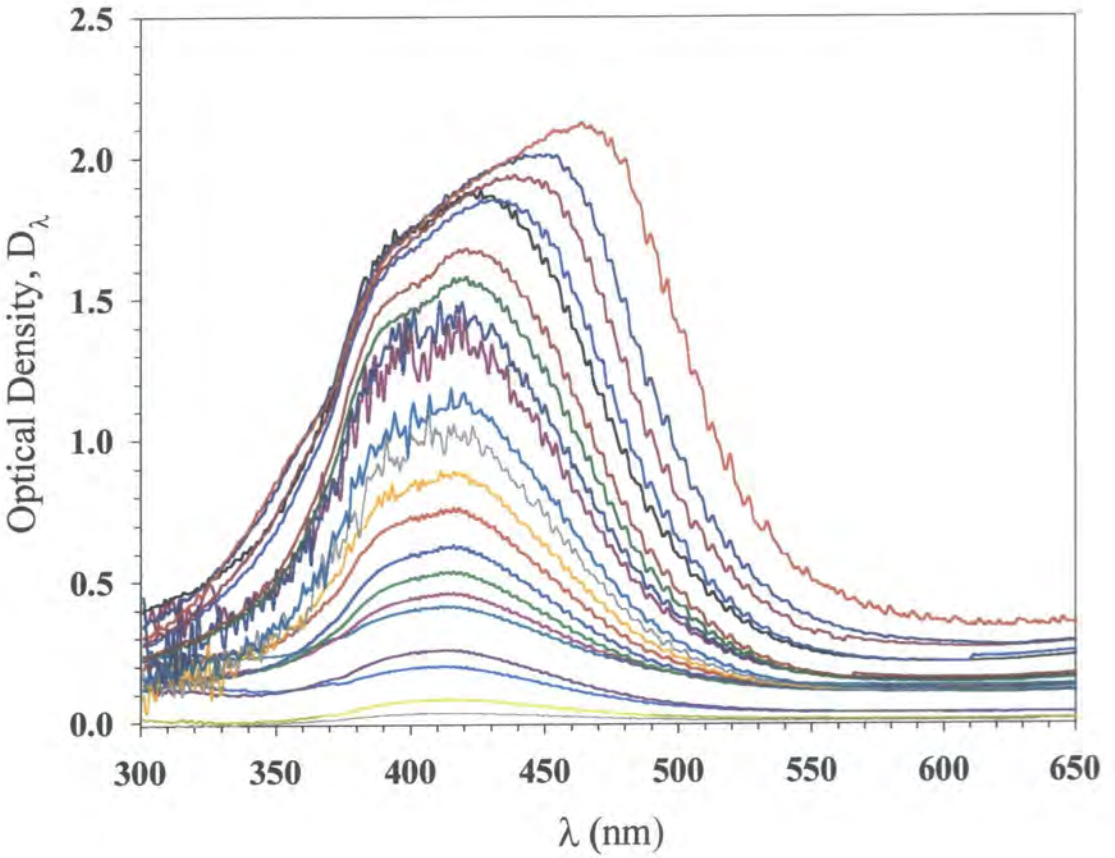

Figure 2. Absorption of tellurium vapour as a function of wavelength between 300 and 650 nm at an average vapour temperature T_c = 806 °C. See table 1 for T_r and p conditions.

In essence, the spectrum consists of a broadband absorption (in the near UV-visible region). Four main features are: 1) for all pressures below ~ 7 mbar, the bands have a maximum near 416 nm, while at higher pressures the maximum peak shifts towards the red due to pressure broadening effects, 2) as the pressure increases, the absorbance increases as expected, 3) structure due to vibrational absorption can be seen for wavelengths greater than 400 nm and 4) as the temperature increases, additional vibrational features appear due to ground state population changes. The results agree qualitatively with less extensive previous studies [10,11].

T_r	P_{Te_2}	D_{max}	λ_{peak}	T_r	P_{Te_2}	D_{max}	λ_{peak}
450	0.30	0.03	416	575	4.98	1.09	415
470	0.50	0.08	416	583	5.80	1.19	415
494	0.90	0.21	416	593	6.97	1.44	418
505	1.16	0.25	416	602	8.21	1.49	419
516	1.49	0.41	416	612	9.80	1.58	421
525	1.81	0.46	416	621	11.4	1.68	421
535	2.24	0.54	416	633	14.0	1.89	426
545	2.75	0.63	416	643	16.6	1.86	433
555	3.37	0.76	416	658	21.1	1.94	439
565	4.11	0.89	416	672	26.2	2.02	451
				715	49.3	2.13	464

Table 1. Reservoir temperature (°C), vapour pressure (mbar) and maximum optical density, D_{max}, of the absorption peak, λ_{peak} for the tellurium absorption curves in figure 2. The lowest T_r corresponds to the bottom curve, and the maximum T_r to the top curve.

Figure 3 shows a plot of the optical density for selected wavelengths as a function of vapour pressure. The "jumps" at vapour pressures of approximately 1 and 6 mbar are probably due to shifts in the baseline. For wavelengths closer to the blue side of the spectrum, the optical density at high pressures becomes saturated. This is due to both the nature of the spectrum itself and to the poor signal to noise ratio at such high optical densities (when the optical density has a value of two, the transmitted intensity I is only 1% of the incident intensity I_o). Importantly, it can be seen that equation 4.5 is approximately obeyed, i.e., a linear relation between D_λ and p exists, especially in the

wavelength range 470-510 nm, implying that the optical density is directly proportional to the pressure.

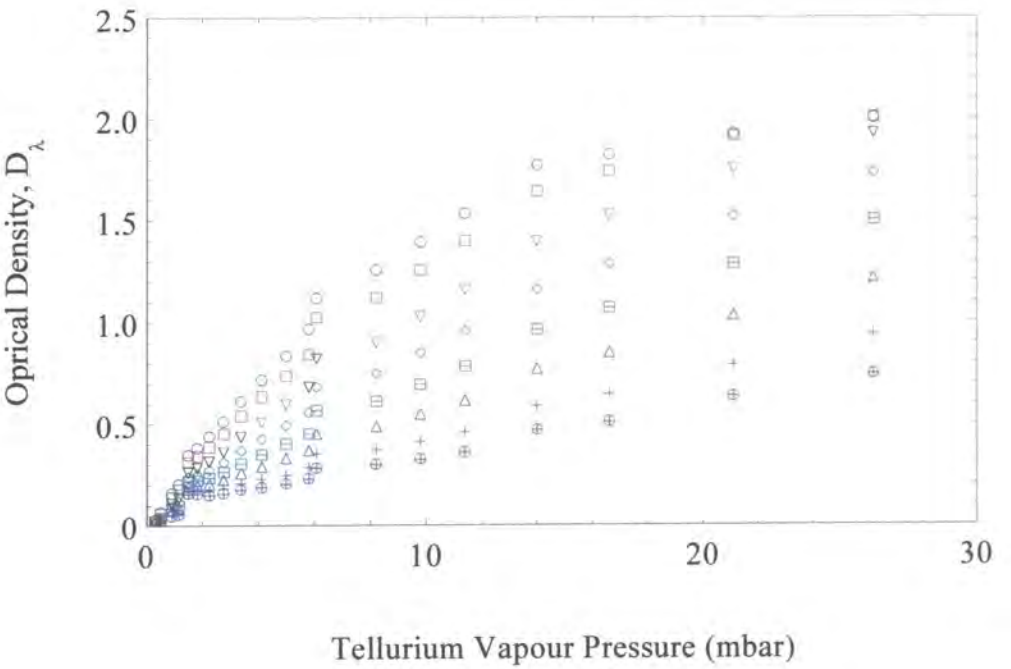

Figure 3. Optical density of tellurium vapour at selected wavelengths. From top to bottom: 440, 450, 460, 470, 480, 490, 500 and 510 nm.

In a typical CdTe vapour growth experiment, tellurium exists in the vapour almost entirely as dimers [12] and its vapour pressure may be up to several tens of mbar, depending on the stoichiometry of the source, although a value between 1 and 10 mbar, depending on the growth temperature, is appropriate when the source is nearly stoichiometric (see equation 2.5 of chapter two). For the higher pressures then, according to figure 3, only wavelengths between 470 and 510 nm may be used reliably. Pure tellurium vapour contains various polymer molecules, Te_n with n = 2-7, although at 723 K, the vapour consists mainly of diatomic molecules (95.88%) [7]. Since the present experiments were conducted at temperatures higher than 723 K, it is reasonable to assume that the tellurium vapour consisted of diatomic molecules and hence the

absorption spectrum of tellurium vapour over CdTe will be analogous excepting for possible absorption overlapping or interaction with Cd atoms.

4.2.3 Cadmium Vapour Absorption Spectrum.

The absorption spectrum of cadmium vapour has been studied extensively [13-15]. Cadmium vapour has two main atomic absorption lines due to electronic transitions: the 5^1S_o-5^1P_1 at 228.7 nm and 5^1S_o-5^3P_1 at 326.1 nm, both extremely narrow (at low pressures) and very sensitive (their absorption is measurable at cadmium vapour pressures as low as 10^{-4} mbar). These lines have been used extensively in the past to obtain extremely reliable thermodynamic data on both saturated vapour pressures over pure cadmium [16] and partial vapour pressures over several cadmium compounds [17-21]. The 228.7 nm line broadens extensively towards the red when the pressure is increased. The 326.1 nm line follows Beer's law accurately for the absorption peak in the range 0.02-1 atm pressure, according to Brebrick [22].

The 326.1 nm line was chosen for quantitative study. Using the experimental setup of section 4.2.1, several experiments were carried out to determine the absorption profile of the 326.1 nm line and investigate its behaviour at several pressures. Figures 4 and 5 show several representative high resolution absorption spectra for cadmium vapour at 614 and 800 °C respectively. It can be seen that at relatively high pressures, ~100 mbar, the absorption peak broadens towards the red, as expected, but even at these pressures the absorption profile remains extremely narrow (FWHM < 0.5 nm) so that the recorded profile is characteristic of the monochromator bandwidth (set by the slits) rather than by the natural shape of the absorption line. A total of seventy absorption experiments were carried out for vapour temperatures of 614 and 800 °C and for vapour

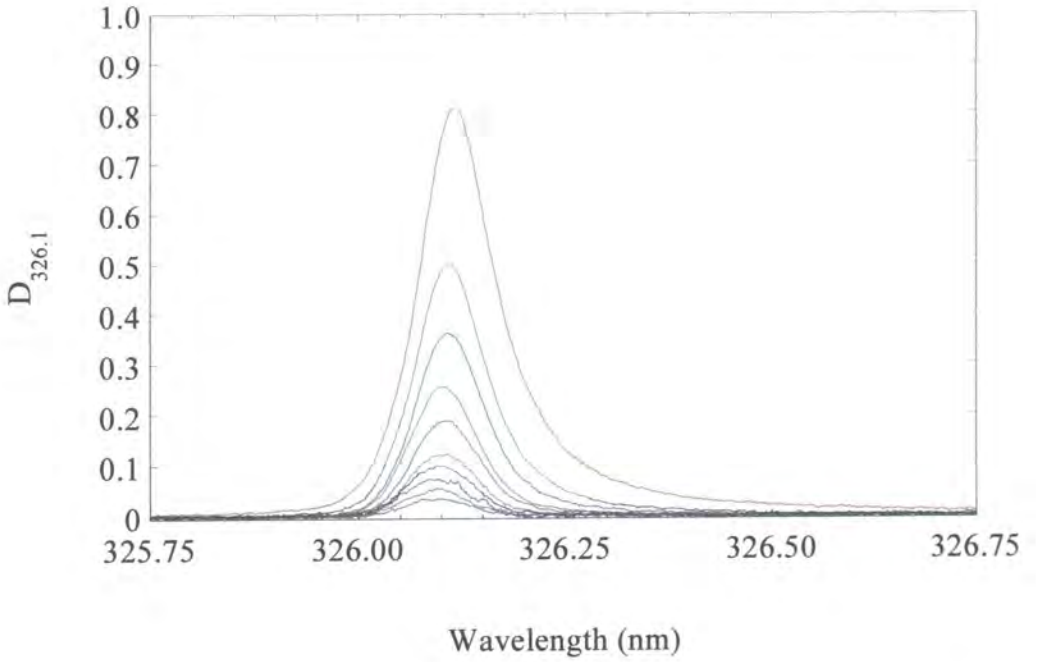

Figure 4. Cadmium vapour $D_{326.1}$ at 614 °C for vapour pressures, from top to bottom, of 88.9, 53.2, 37.7, 25.8, 17.6, 11.8, 9.7, 6.5, 3.7 and 2.1 mbar.

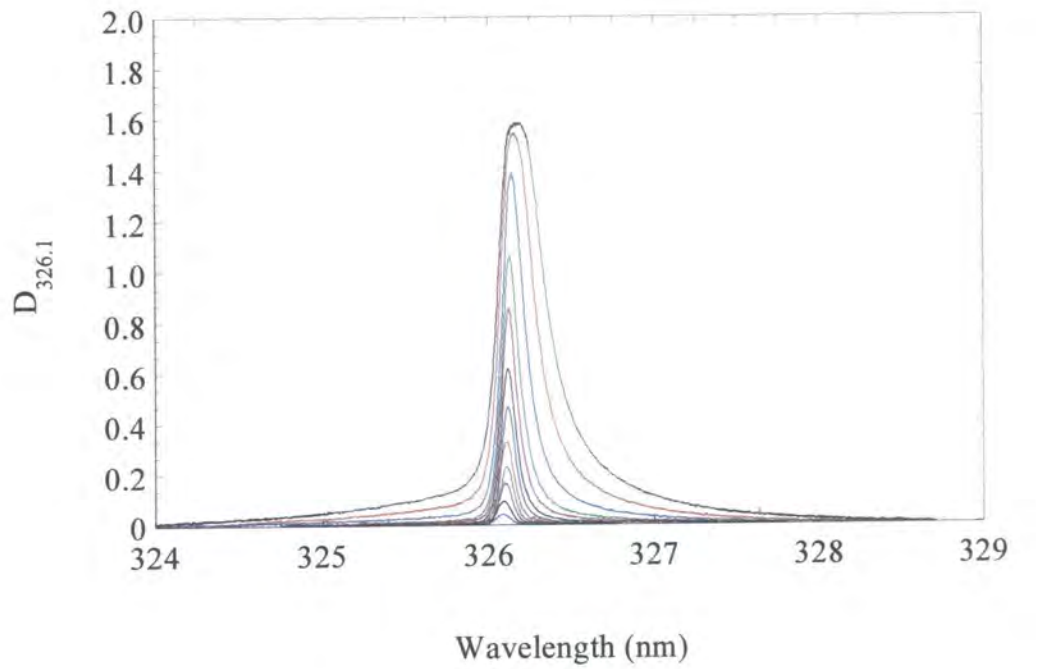

Figure 5. Cadmium vapour $D_{326.1}$ at 800 °C for vapour pressures, from top to bottom, of 461.8, 331.8, 221.1, 143.4, 106.3, 75.2, 56.1, 38.4, 25.3, 18.0, 8.5 and 3.3 mbar.

pressures in the range ~ 0.01 - 462 mbar. The peak optical density as a function of reservoir reciprocal temperature (which is proportional to vapour pressure, see equation 4.7) is plotted in figure 6 for the two cell temperatures. Three different features can be observed. For the highest reservoir temperatures at a vapour temperature of 800 °C, the optical density starts to saturate. This effect is attributed to both the broadening of the line due to Cd-Cd collisions, also called self-broadening, which causes a shift towards the red and to the (poor signal to noise ratio or saturation) detection limit: it can be shown [2] that for measured high optical densities, the combination of finite transmission bandwidth, the spectrum of the radiation and the spectral response of the detector, can cause a deviation from the effective optical density, resulting in the measured value of optical density falling below the effective value. It is not of concern here, since this pronounced departure from linearity only occurs at vapour pressures which are not normally encountered in vapour growth of CdTe (excepting possibly for growth with cadmium-rich sources in closed ampoules). A second feature is the high linearity for reservoir temperatures in the range 430-595 °C of the optical density as a function of the reciprocal of the reservoir temperature. Furthermore, according to section 4.1.1, if Beer's law is obeyed, the slope of the plot should be equal to the slope of a plot of cadmium vapour pressure versus reciprocal reservoir temperature. For the range of temperature 400-765 °C, the later is given by the expression (in mbar) [23]:

$$\log(p_{Cd}) = -\frac{5300}{T_r} + 8.118 \tag{4.13}$$

and the best fits for the 614 and 800 °C cell temperatures are respectively,

$$\log(D_{326.1}) = -\frac{4924}{T_r} + 5.635 \tag{4.14}$$

$$\log(D_{326.1}) = -\frac{4837}{T_r} + 5.473 \tag{4.15}$$

with a maximum deviation of 2 % for the 614 °C cell and 0.85 % for the 800 °C cell. The slopes of the previous two expressions deviate by 7.09 % and 8.74 % respectively from that of equation 4.13. This indicates that Beer's law is approximately obeyed for the peak of the absorption line. It is also important to note that the experimental optical density values for the vapour at 800 °C are systematically lower than those for the

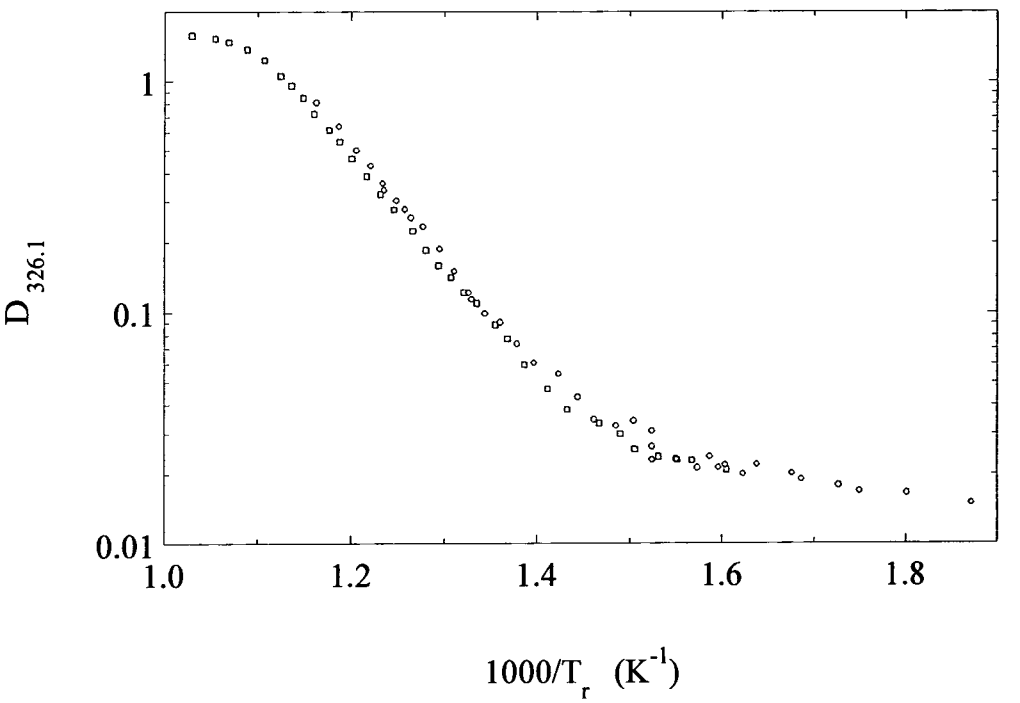

Figure 6. Peak optical densities as a function of reciprocal reservoir temperature for cadmium vapour at 614 °C (O) and 800 °C (□).

vapour at 614 °C. This is in accordance with equations 4.2 or 4.4, since an increase in the vapour temperature has the effect of decreasing the concentration of absorbing atoms, and hence the optical density. This implies that $\varepsilon_{326.1}$ does not vary considerably with vapour temperature. The third feature that can be observed in figure 6 is the gradual change of slope for reservoir temperatures of < 425 °C (~3 mbar). It could be argued that since the measured optical densities are so small , the change in slope might

be due to detection or intensity fluctuations, i.e. an experimental error of the order of the optical density could be expected. However, this does not seem likely to be the case since the determination of the baseline and transmission spectra were done simultaneously, the baseline being extracted from an extrapolation of the non-absorbing wings of the transmission spectrum, as explained earlier. Although a conclusion could not be drawn, it is possible that the departure from linearity is a consequence of insufficient monochromator resolving power, since we are dealing with peak optical densities values, rather than total absorption area [25]. However, when the area under the absorption curve was integrated the results gave a similar behaviour to figure 6. Alternatively, the change in slope may have been due to pressure broadening associated with residual foreign gas present in the cell. The presence of a foreign gas can cause an effective increase in absorption, since the collisions between cadmium and foreign gas particles can reduce the lifetime of the excited state [3,24]. A volume of 0.1 cm^3 at room temperature and atmospheric pressure was confirmed to be present in the cell, which translates to a foreign gas pressure of 4 to 6 mbar in the range 614-800 °C. These pressures are close to the cadmium vapour pressures where the slope starts to change, suggesting that when like-pair collisions start to prevail over unlike-pair collisions, the foreign gas pressure broadening effect fades out. This supports the thesis of foreign gas pressure broadening.

4.3 EXPERIMENTAL APPARATUS FOR VAPOUR PRESSURE MONITORING: DESCRIPTION AND CALIBRATION.

It is obvious that while a monochromator could be used to monitor the vapour pressure of either Cd or Te_2 during CdTe in the growth system in real time, it could not

measure *both* simultaneously and independently. Therefore, on the basis of the absorption spectra described above, a detection system more suitable for use *in situ* in the vapour growth apparatus has been developed. The absorption spectra results show that the use of the 326.1 nm line for cadmium and of any line between 470 and 510 nm for tellurium can be used to obtain their respective partial pressures, since there is negligible overlap between the tellurium and cadmium absorption bands at the pressures of interest in a typical crystal growth experiment.

4.3.1 Light Source and Detection Design.

An Osram cadmium hollow cathode lamp (HCL) was chosen as the light source. The cadmium HCL provides very narrow emission lines, which are necessary when the detector system does not include a monochromator. More importantly, these lines included the 326.1 nm line, three useful lines for Te_2 monitoring, the 467,479 and 508 nm lines, and a line in the red region, the 643.8 nm line.

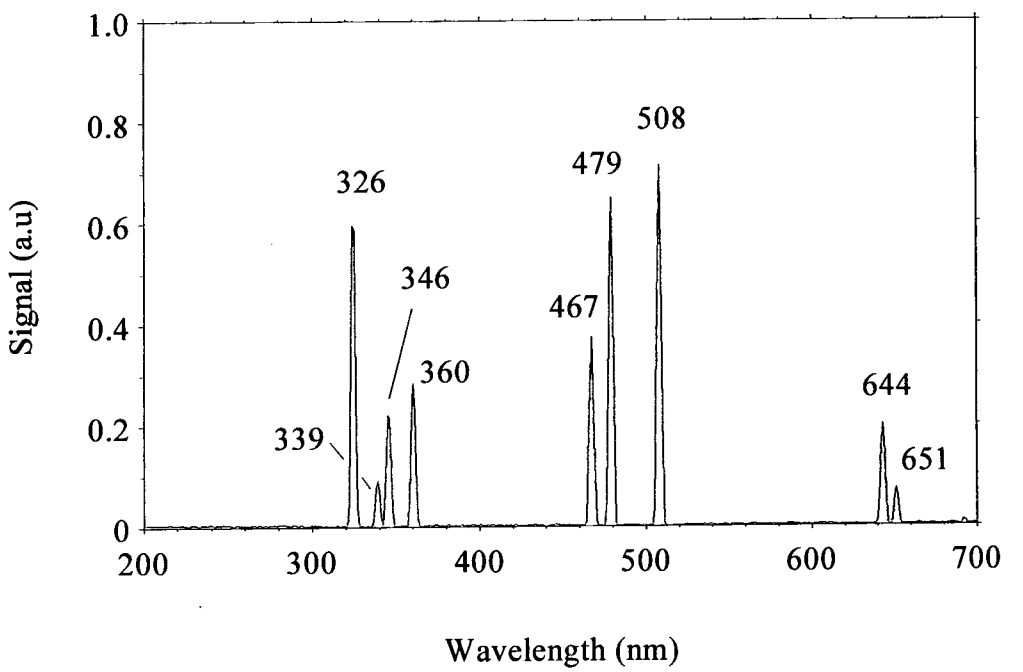

Figure 7. Low resolution spectral output of a cadmium HCL lamp. The lack of the strong 228.8 nm line is due to absorption by the Pyrex glass envelope of the lamp.

The 643.8 nm line was used as a reference line, since at low pressures it is not absorbed by either cadmium or tellurium vapours, allowing changes in the lamp output to be monitored. The spectral output of a typical cadmium lamp is shown in figure 7.

The detection system was designed for monitoring the reference, cadmium and tellurium lines simultaneously. Detection was by silicon photodiodes (Hamamatsu S1336-18BK for the 643.8, 479 and 508 nm lines and S1336-18BQ for the 326.1 nm line) located behind appropriate interference filters allowing each photodiode to monitor just one of the spectral lines. Interference filters centred at wavelengths of 328, 508, 482 and 644 nm, and with FWHM's of approximately 8, 9, 10 and 9 nm respectively were selected. These filters allowed a small (< 1% transmission) contribution to the transmission from neighbouring emission lines, i.e. 339 nm line in the case of the 328 nm filter and 651 nm line in the case of the 644 nm filter. The detector system was duplicated to enable vapour pressures to be measured either side of the flow restrictor in the crossmember of the growth apparatus (figure 8).

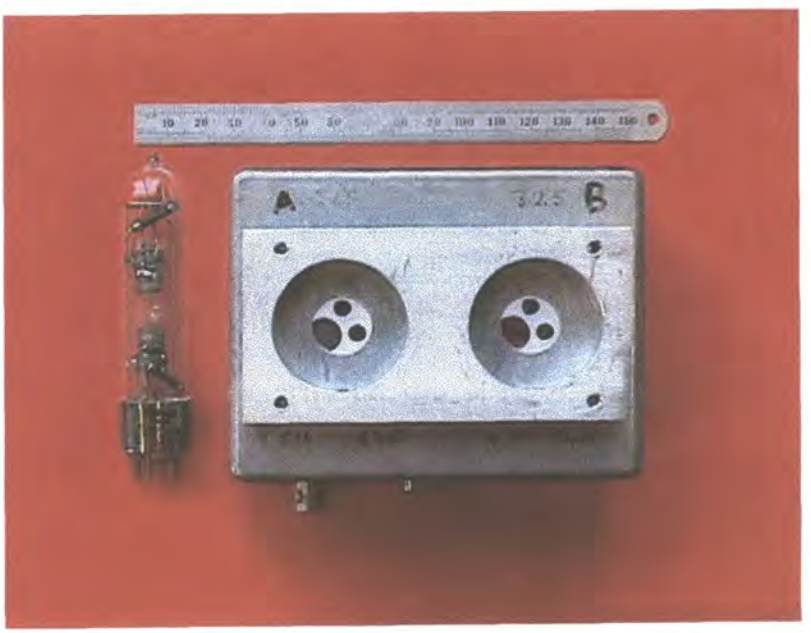

Figure 8. HC Lamp and detection system for *in situ* monitoring of cadmium and tellurium vapour pressures in the CdTe Durham vapour growth apparatus.

The experimental setup to monitor the vapour pressures was similar to figure 1, but without the need for lens 2, since the three diode/filter assemblies (see figure 8) could be illuminated simultaneously by the beam exiting the furnace. The resulting photocurrents were amplified before being multiplexed, detected by the lock-in amplifier and then measured and logged by a digital voltmeter and a microcomputer.

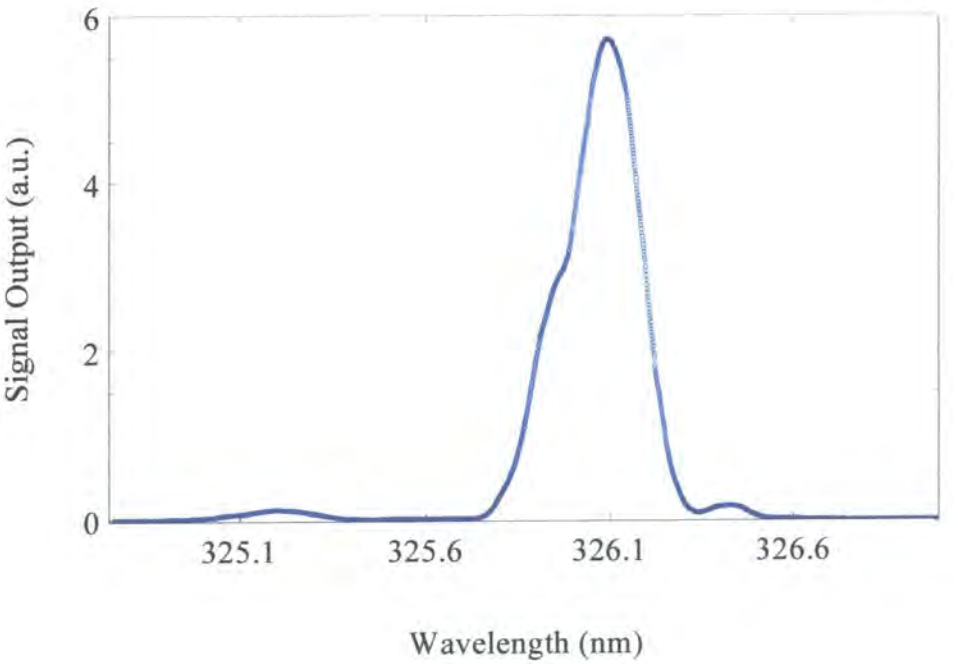

Figure 9. High resolution emission spectrum of the 326.1 nm HCL cadmium lamp. The spectrum was recorded with an H&W Monospek 1000 monochromator, at a scan speed of 0.5 Å/min with slits width < 0.1 mm, giving a resolving power better than 0.8 Å.

It is important to point out at this stage the consequences (particularly for the 326.1 nm Cd absorption line) of using a cadmium HCL and interference filters with relatively broad bandpass. First, the spectral lines emitted by an HCL lamp are known to be extremely narrow [5], and since the temperature and pressure in the lamp are not the same as in the absorption cell, the emission lamp will have in general a different FWHM and centre emission line for the 326.1 nm line (see figure 9). In addition, the 326.1 nm filter admits the whole absorption band. These factors alone are likely to

result in departures from the Beer's law, as discussed previously. This is not expected to be the case for the 479 and 508 nm tellurium monitoring lines, since according to figure 2, the absorption can be considered constant over the FWHM bandpass of the interference filters.

4.4 EXPERIMENTAL CALIBRATION: RESULTS.

In order to test the accuracy of the cadmium lamp – detection system, several absorption experiments were carried out with pure cadmium and tellurium vapours at the 326.1 and 479 and 508 nm wavelengths respectively. The interest here was not only to evaluate the monitoring system but also to obtain optical density versus (pure cadmium and tellurium) vapour pressure calibration curves under identical length path and similar growth temperature conditions to that encountered in the growth apparatus. Once these calibration curves were obtained, several trials of pressure measurement over a CdTe source were carried out to assess the performance of the system under mixed vapour conditions.

4.4.1 Tellurium Vapour Calibration.

The experimental setup used to obtain a calibration curve for the 479 and 508 nm absorption lines was the same as that of figure 1, excepting for lens 2, which was unnecessary since the monitoring detection system was used here. The procedure has been explained earlier, the only difference here being that the 643.8 nm line was used to both monitor the output stability of the lamp and to obtain the baseline. The calibration results for a 50.1 mm absorption cell at a temperature of 784 °C are shown in figure 10. It can be seen that a straight line is obtained for both absorption lines, as expected, due

to the broad absorption band of tellurium vapour. It will also be seen that the slopes of both lines are very close to the slope of the tellurium vapour pressure *1/T* characteristic, indicating that Beer's law is approximately obeyed. The best fits (for $p_{Te_2} > 0.1$ mbar) for the optical densities D_{479} and D_{508} are,

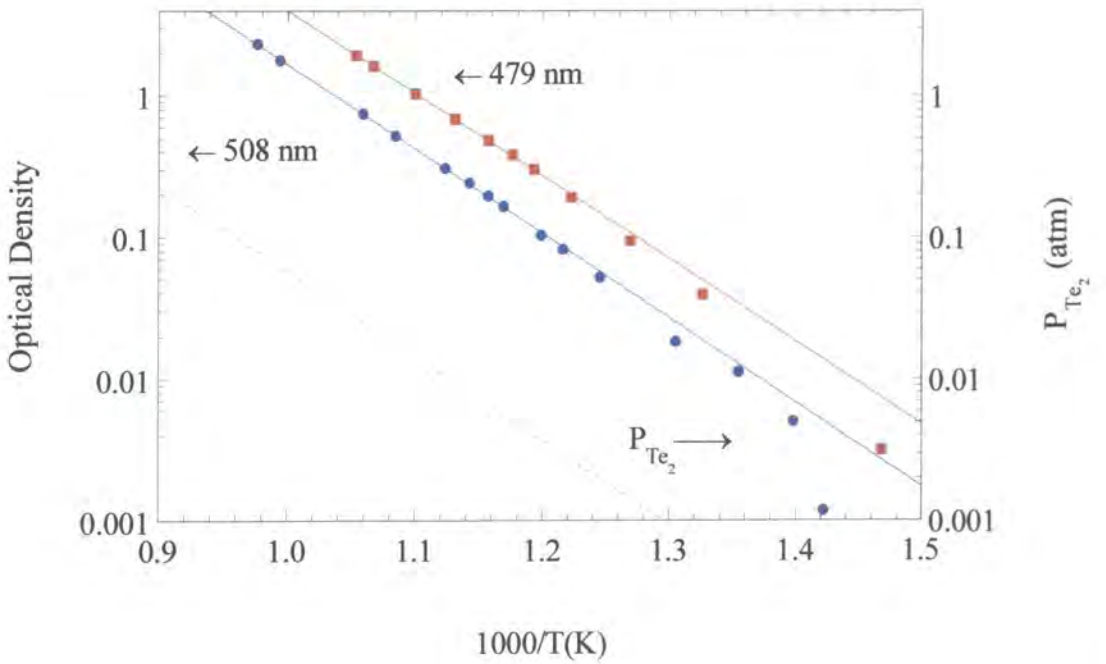

Figure 10. Optical densities D_{479} and D_{508} versus $1000/T_r$ for tellurium vapour. The right axis applies only to the dotted line.

$$\log D_{479} = \frac{-5826}{T_r} + 6.425 \tag{4.16}$$

$$\log D_{508} = \frac{-5956}{T_r} + 6.176 \tag{4.17}$$

The equilibrium vapour pressure (in mbar) of tellurium can be expressed as [26]:

$$\log p_{Te_2} = \frac{-6258.596}{T_r} + 8.074898 \qquad (722.65 - 800K) \tag{4.18}$$

$$\log p_{Te_2} = \frac{-6099.228}{T_r} + 7.875549 \qquad (4.19)$$
$$(800 - 921.6K)$$

$$\log p_{Te_2} = \frac{-5960.2}{T_r} + 7.724709 \qquad (4.20)$$
$$(921.6 - 1142.5K)$$

Equations 4.18 and 4.19 can be put together with a maximum loss of accuracy of 0.01 mbar, giving the expression,

$$\log p_{Te_2} = \frac{-6107.43}{T_r} + 7.88467 \qquad (4.21)$$
$$(722.65 - 921.6K)$$

The best fits of D_{479} and D_{508} have slopes which have a maximum deviation from the slope of equation 4.20 of 2.25 % and 0.06 % respectively, and from that of equation 4.21 of 4.61 % and 2.47 % respectively. The range of tellurium vapour pressures normally encountered in vapour growth is in the range 1-10 mbar, which is covered by 4.21. Correspondingly, use of equation 4.12 when applied to equations 4.16, 4.17 and 4.21 gives the relation between tellurium vapour pressure at 784 °C and its optical density, for a 50.1 mm path length,

$$p_{Te_2} = 14.11 D_{479}^{1.048} \qquad \text{(mbar)} \qquad (4.22)$$

$$p_{Te_2} = 35.60 D_{508}^{1.025} \qquad \text{(mbar)} \qquad (4.23)$$

valid for tellurium vapour pressures around 0.1-18 mbar and a 50.1 mm cell at 784 °C. It is interesting to note that Beer's law is approximately obeyed and that the exponents of the optical densities deviate from the ideal value of one by approximately the same percentage amount as the slopes deviate from that of equation 4.21. The 326.1 nm line optical density was always below 0.01 for tellurium vapour pressures less than approximately 18 mbar, confirming the non-overlap of absorption bands at low pressures. However at Te_2 pressures of approximately 80 mbar, the 326.1 nm optical

density reached a value of 0.48. A correction will therefore be required when monitoring cadmium vapour over CdTe to compensate for absorption by Te_2 for tellurium pressures higher than ~20 mbar, although this situation is highly unlikely to be encountered during vapour growth in a semi-open tube system. In contrast, the 643.8 nm line optical density remained below 0.005 for tellurium vapour pressures below ~60 mbar, reaching a value of 0.08 at ~80 mbar.

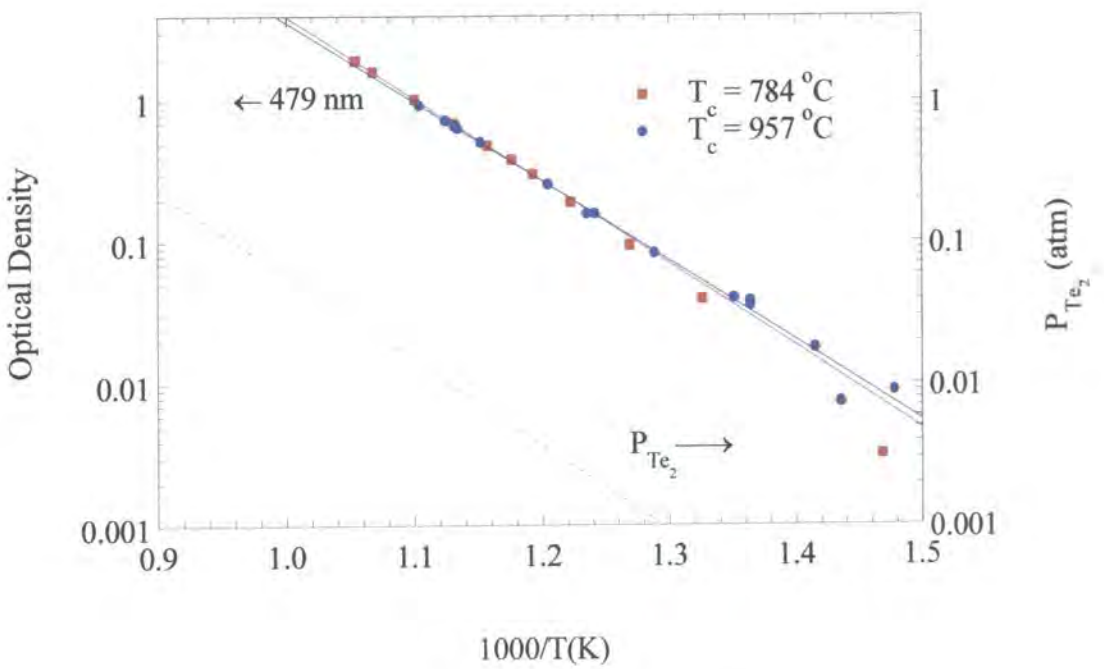

Figure 11. D_{479} for tellurium vapour at 784 °C and 957 °C. Right axis applies only to the dotted line.

It has to be pointed out that the relations 4.22 and 4.23 are only valid for tellurium vapours at 784 °C. For any other temperature, a correction is needed. Since the vapour temperature can influence not only the number of molecules per unit of volume, but the shape of the absorption band, an experiment was carried out to determine the influence of the vapour temperature. Figure 11 shows the optical densities obtained at both 784 °C and 957 °C for the 479 nm line. The later temperature was chosen since all

the growth trials in the Durham crystal growth system are normally done with the crossmember at around this temperature (± 20 °C).

The best fit for the experimental points obtained at 957 °C is

$$\log D_{479} = \frac{-5617}{T_r} + 6.172 \tag{4.24}$$

Comparison of this equation with 4.16 leads to two conclusions. First, the slopes for both vapour temperatures are approximately the same, as expected, since Beer's law is obeyed. Secondly, the *molar extinction coefficient* ε_λ does not remain constant with a change in temperature, since the ratio of their intercepts, according equation 4.4 should be equal to the vapour temperature (in K) ratio. However this is not the case since,

$$\frac{b^{784}}{b^{957}} = \frac{\varepsilon_{479}^{784}}{\varepsilon_{479}^{957}} \times \frac{T_{957}}{T_{784}} = 1.041 \tag{4.25}$$

meanwhile

$$\frac{T_{957}}{T_{784}} = 1.1637 \tag{4.26}$$

which differs from 4.25 by 10.55 %. Combining the two previous equations, we obtain,

$$\frac{\varepsilon_{479}^{789}}{\varepsilon_{479}^{957}} = 0.8948$$

In conclusion, it is important to note that equation 4.4 cannot generally be used to extrapolate the relation between optical density and pressure obtained at one vapour temperature to other vapour temperatures without incorporating some error. This is due to the slight dependency of ε_λ on vapour temperature. Nonetheless, combination of equations 4.21 and 4.24, according to 4.11, gives a calibration expression for the crossmember conditions normally used during growth,

$$p_{Te_2}^{957} = 14.90 D^{1.087} \quad \text{(mbar)} \tag{4.27}$$

for the monitoring of tellurium partial vapour pressures. The above expression is close to 4.22. This is as a consequence of the cancelling effects of ε_λ, (which increases with T_c), and $1/T_c$ in 4.5. It has not been possible to obtain any reference to compare with the values obtained in 4.22, 4.23 and 4.27 for α_λ at λ = 479 and 508 nm; however, for wavelengths (λ = 481.8 nm and 509.4 nm) and vapour temperatures (755, 800 and 860 °C) close to those investigated here, the values ($\alpha_{481.8}$ = 15.06 at 755 °C, $\alpha_{481.8}$ = 14.73 and $\alpha_{509.4}$ = 37.18 at 800 °C and $\alpha_{481.8}$ = 14.99 and $\alpha_{509.4}$ = 35.35 at 860 °C) are in close agreement [19,21].

4.4.2 Cadmium Vapour Calibration.

The experimental setup used here was the same as that used in the previous tellurium calibration. The narrowness of the 326.1 nm *resonance* cadmium line emitted by the lamp is expected to produce non-linearities, since the absorption by cadmium vapours might not be at the same line centre, and will probably be of different width [5]. Since the line is absorbed by cadmium, one would expect strong absorption, and since the bandpass of the filters is, as detailed earlier in section 4.3.1, larger than the absorption line, the Beer's law is not expected to be obeyed. This can be seen in figure 12, where the measured optical density versus $1/T_r$ is plotted for several different lamps. The difference between lamps is expected, since their emission is extremely sensitive to operating temperature, current intensity and gas pressure in the emitting hollow tube, i.e. design and operating characteristics.

It can be observed in the previous graph, that for the same lamp at different temperatures (lamp 1 at 615 and 816 °C), there is no significant difference in the optical values, as one would expect according to 4.4. However, equation 4.4 does not apply in

here, since the whole absorption band is accounted for in the optical density values. In order to make sure that no intensity related saturation phenomena were the cause of the

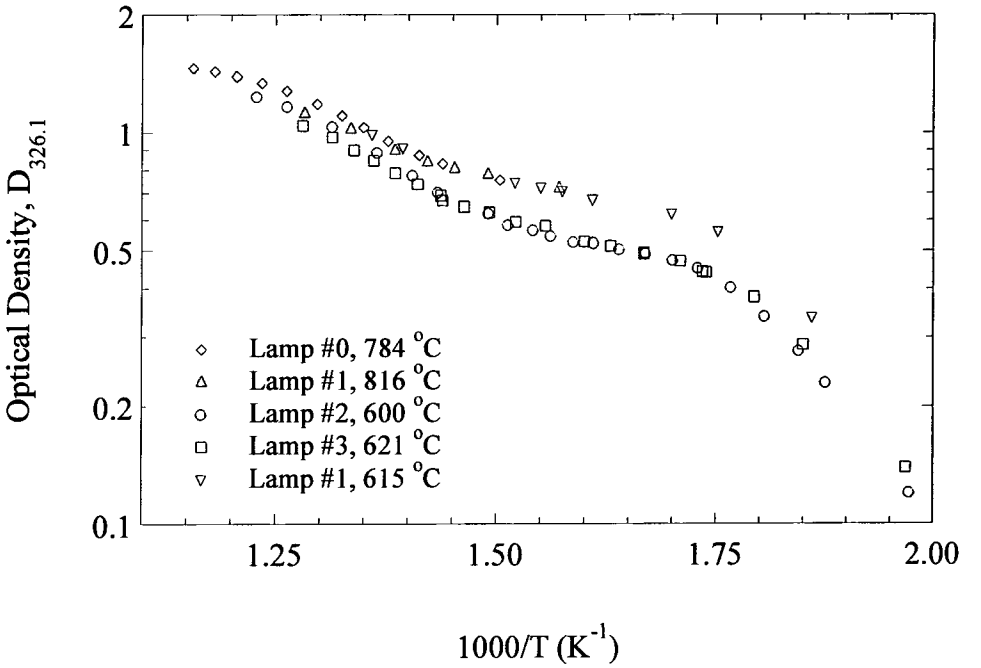

Figure 12. Optical density of the 326.1 nm cadmium absorption line for several cadmium cell temperatures, and different hollow cathode lamps.

shape of the curve, 10 % and 30 % neutral density filters (NDF) were used to diminish the incident light intensity. This was done with lamp #1 under the same reservoir and vapour (both 614 °C and 821 °C) conditions. The optical densities obtained in this manner were, within experimental error, identical to the ones obtained without the NDF filters, indicating no saturation.

Moreover, the characteristic common shape of the slope for all the lamps can be fully explained if one takes into account the different broadening processes that take place at different reservoir temperatures (and hence cadmium vapour pressures), namely natural, Doppler and collision broadening [25,27,28]. The theory will not be developed here, although a qualitative explanation will be given. The characteristic shape of the

curve is normally called *"curve of growth"*, and it is governed by the contribution of the different broadening processes. At high vapour pressures, the centre of the line is fully absorbed, and the absorption process is governed by the wings of the line. As the vapour pressures decrease, the collision broadening becomes less important and the absorption process is governed by the Doppler and natural broadening (although the latter is normally negligible). The point at which this transition takes place depends on the vapour pressure and temperature of the cell, but also on the nature of the line, and is the point where the slope starts to change. Although it is possible to correct for all these factors, this has not been done here, since we are interested primarily in obtaining a calibration curve, rather than undertaking a critical and exhaustive spectroscopic study of the 326.1 nm line.

Only lamps # 2 and #3 were used in different vapour growth experiments. Due to the complicated shape of the curve, no simple expression was obtained to relate optical density and pressure. Rather, the conversion from optical density to vapour pressure was done using the calibration graph in figure 13, constructed using standard expressions to relate reservoir temperature to the cadmium vapour pressure [6,23,29]. It can be seen in the graph of figure 13, that very low vapour pressures can be monitored easily, due to the strong absorption of the resonance 326.1 nm line. Another important feature is the fact that the calibration does not change, within experimental error, for the same lamp and different vapour temperatures. Figure 14 shows a comparison for vapour cell temperatures of 621 and 918 °C. It can be seen that especially in the range of pressures 2-20 mbar, where the calibration curve is linear, the optical densities are in close agreement.

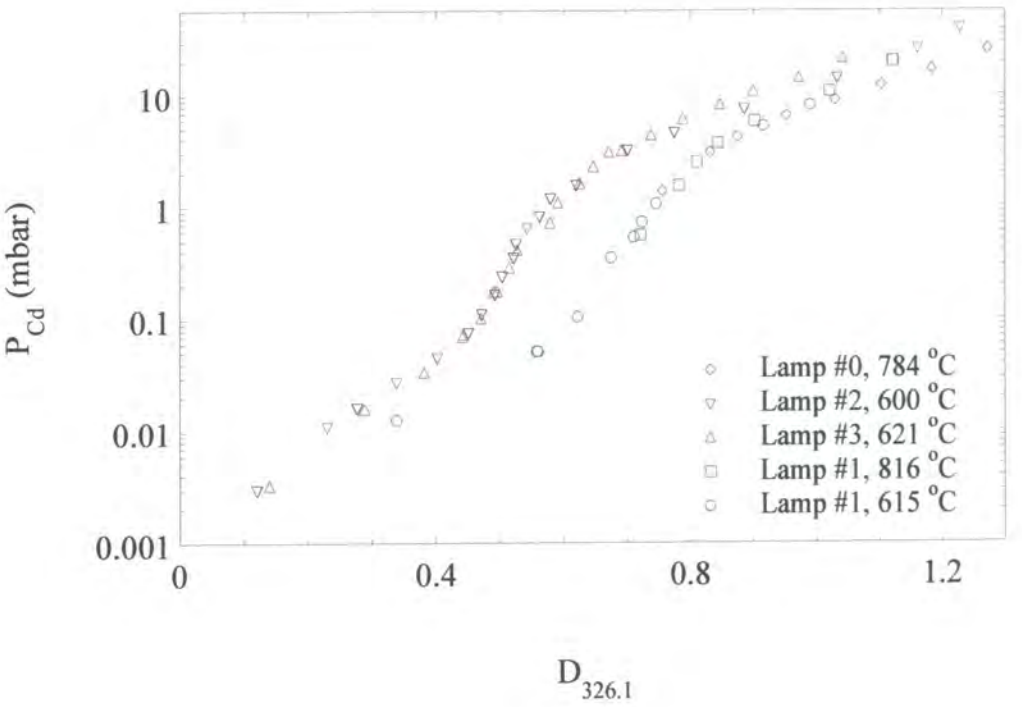

Figure 13. Calibration curves for cadmium vapour pressure monitoring, for different lamps.

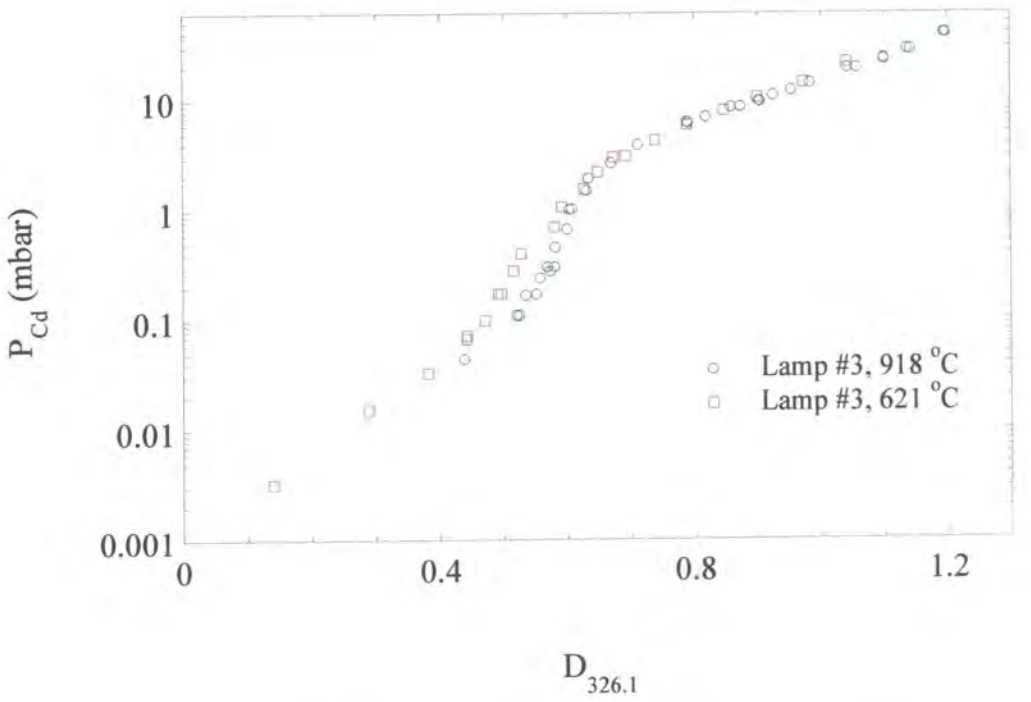

Figure 14. Comparison of calibration curves for two different cell temperatures.

4.4.3 Cadmium Telluride.

To assess the utility of the previous calibration for measuring partial pressures during growth, a trial experiment using the compound as a source was carried out. Pure (99.999%) CdTe was sublimed under dynamic vacuum to obtain a source as stoichiometric as possible. A 50.1 mm optical cell with a CdTe reservoir was set-up in the same way as described previously. The experiment consisted of measuring D_{508} and D_{326} as a function of time, while the source was heated from 422 °C, where the Cd and Te_2 partial pressures are less than 10^{-5} mbar, up to 839 °C. The source achieved the maximum temperature in approximately one hour. Assuming there was no broadening of the 326.1 nm cadmium atomic line by Te_2 molecules, and applying the previous calibrations (lamp #0 was used) to the measured optical densities, it was possible to monitor the variation in partial pressures. The intention was to demonstrate the use of the system in monitoring changes in partial pressures.

Figure 15 shows the variation of the partial pressures with time. Two features are clear: 1) as expected, a sharp rise in partial pressure occurred in the initial stages of heating up, and 2) the ratio $\alpha = p_{Cd} / p_{Te_2}$ quickly reached a value close to 2, characteristic of stoichiometric sources. This result validates the calibrations done previously. The partial pressure of cadmium and tellurium were also in accordance with that expected for the source temperature of 839 °C [30]. This ratio did not, however, stabilise at this value but increased with time. This result may indicate that the stoichiometry of the vapour changed progressively during the course of the experiment, and implies that congruent sublimation was inhibited, possibly due to some initial nonstoichiometry in the source. However, the increase in both tellurium and cadmium pressures with time suggests that the system did not reach equilibrium.

A second CdTe vapour transport experiment was carried out, this time under dynamic vacuum in order to avoid any complication arising from nonstoichiometry of the source, and hopefully enabling a more straightforward evaluation of the calibration. The experimental setup was identical to that of figure 16 in chapter 5, but without a porous silica disc. Although the partial pressure ratio was close to two, with an error percentage of ~ 15 %, the dynamic pumping and rapid transport (< 2 minutes for 0.754 gm) did not allow for the vapour pressure to reach (dynamic) equilibrium.

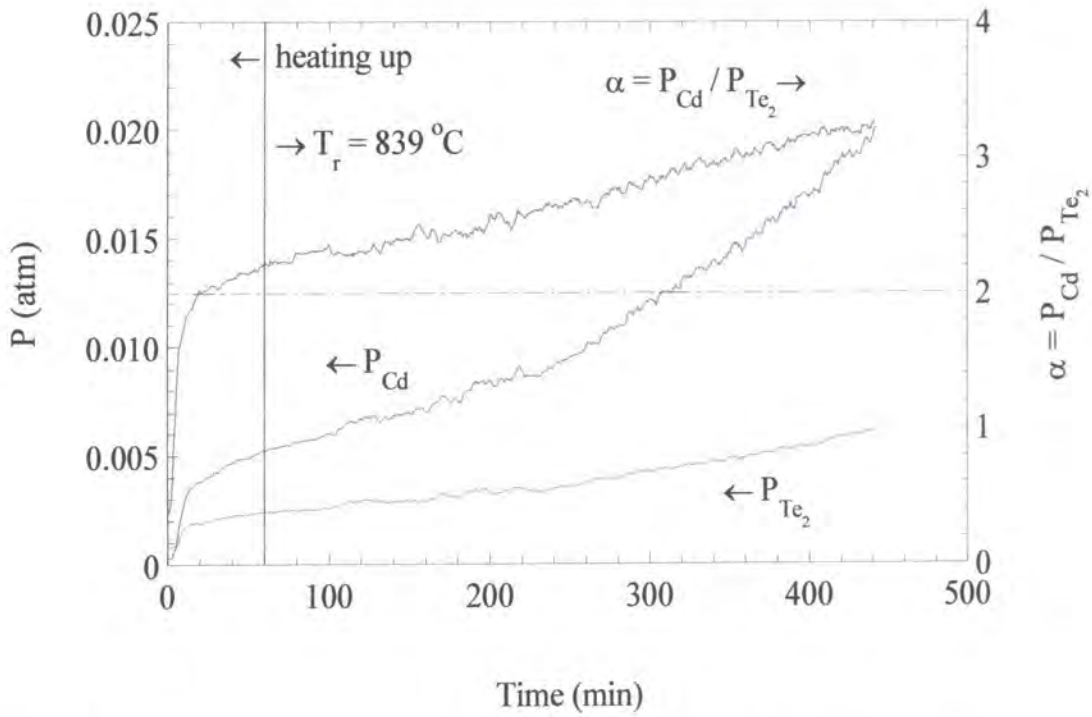

Figure 15. Monitoring of partial pressures of cadmium and tellurium as a function of time during the heating of CdTe from 422 °C to 839 °C in a closed ampoule.

4.5 DISCUSSION AND CONCLUSIONS.

The absorption spectra of tellurium vapour in the range 300-650 nm and the absorption of the 326.1 nm *resonance* line in cadmium vapour have been studied. The spectrum for tellurium shows that is possible to monitor tellurium vapour partial

pressures over CdTe vapour in the range 0.1-18 mbar using any wavelength in the range 470-510 nm, since in this range there is no overlap with any cadmium absorption line. Similarly, the cadmium absorption line at 326.1 nm may be used to measure cadmium partial pressure independently of that of tellurium.

Accordingly, a simple, compact system capable of monitoring partial pressures simultaneously, independently and in real time during growth was designed. A cadmium hollow cathode lamp providing a range of narrow emission lines, was chosen as a light source. The detection system consisting of suitable interference filters and photodiodes was designed to take advantage of the discrete cadmium lamp emission spectrum to monitor partial vapour pressures of Cd and Te_2 over CdTe vapour during growth in the multi-tube vapour growth apparatus. Calibration experiments with pure cadmium and tellurium were carried out in order to obtain a set of expressions to relate vapour pressure to optical density for a fixed length and several vapour temperatures. The calibration curve obtained for the 326.1 nm absorption in cadmium vapour showed that monitoring of the optical density was not independent of the instrumental bandpass, due to the narrowness of the line. In particular, a set of calibration expressions was obtained for the typical vapour temperatures encountered in the crossmember of the apparatus during growth. The calibration expressions and curves obtained allowed reliable measurement of cadmium pressures in the range 0.01-20 mbar and tellurium pressures in the range 0.1-18 mbar.

REFERENCES FOR CHAPTER FOUR

[1] H. H. Perkampus. *Encyclopedia of Spectroscopy*. VCH, New York (1995)

[2] R. E. Dodd. *Chemical Spectroscopy*. Elsevier, Amsterdam (1962).

[3] G. F. Lothian. *Absorption Spectrophotometry*. Hilger & Watts, London (1949).

[4] P. F. Bernath. *Spectra of Atoms and Molecules*. Oxford University Press, New York (1995).

[5] J. D. Ingle and S. R. Crouch. *Spectrochemical Analysis*. Prentice Hall, New Jersey (1988).

[6] D. M Chizhikov. *Cadmium*. Pergamon Press, Oxford (1966).

[7] A. P. Ubelis, in: *Radiation and Collisional Characteristics of Atoms and Molecules of Tellurium –A Collection of Scientific Papers*. Edited by A. P. Ubelis, R. S. Ferber and M. Ya. Tamanis. Latvian SSR Ministry of Public Education, P. Schutka Latvian University, Riga, Latvia (1989) (in Russian). (available in English: NASA TT-20831, 1990).

[8] J. Carles, J. T. Mullins and A. W. Brinkman. *"Partial Pressure Monitoring in Cadmium Telluride Vapour Growth"*. J. Crystal Growth, **174** (1997) 740.

[9] D. M. Chizhikov and V. P. Shchastlivyi. *Tellurium and Tellurides*. Collet's Publishers, London (1970).

[10] R. F. Brebrick and A. J. Strauss. *"Partial Pressures in Equilibrium with Group IV Tellurides. I. Optical Absorption Method and Results for PbTe"*. J. Chem. Phys., **40** (1964) 3230.

[11] R. J. De Young. *"Visible Spectrum Optical Absorption in Te_2 Vapor"*. Appl. Phys. Lett., **64** (1994) 2631.

[12] P. Goldfinger and M. Jeunehomme. *"Mass Spectrometric and Knudsen Cell Vaporization Studies of Group 2B-6B Compounds"*. Trans. Faraday Soc., **59** (1963) 2851.

[13] M. S. Helmi, T. Grycuk and G. D. Roston. *"Interatomic Potentials and the Van der Waals' Coefficient for the Intercombination Cd 326.1 nm Absorption Line Broadened by Cadmium Pressure"*. Spectrochim. Acta B, **51** (1996) 633.

[14] F. W. Byron, M. N. McDermott and R. Novick. *"Self-Broadening of Optical Double Resonance Lines in Cadmium"*. Phys. Rev., **134** (1964) A615.

[15] J. P. A. v. Hengstum. *"Spectral Measurement of Transition Probabilities in the Cadmium Atom"*. Ph. D. Thesis (in Dutch), Drukkerij Gebr. Janssen, Nijmegen (1955).

[16] O. N. Muradova and V. G. Muradov. *"Vapour Pressure of Solid Cadmium"*. Russ. J. Phys. Chem., **46** (1972) 282.

[17] G. Scatchard and R. H. Boyd. *"The Equilibrium of α-Silver-Cadmium Alloys with Cadmium Vapor"*. J. Am. Chem. Soc., **78** (1956) 3889.

[18] G. Scatchard and T. Po Ling. *"The Equilibrium of α-Silver-Zinc-Cadmium Alloys with Zinc and Cadmium Vapor"*. J. Am. Chem. Soc., **84** (1962) 28.

[19] Ching-Hua Su, Pok-Kai Liao and R. F. Brebrick. *"Partial Pressures over the Pseudobinary Solid Solution $Hg_{1-x}Cd_xTe$ (s) for x = 0.70 and 0.95 and over Four Te-rich Ternary Melts"*. J. Electrochem. Soc.: Solid-State Sci. and Tech., **132** (1985) 942.

[20] Ching-Hua Su, Pok-Kai Liao, Y. Huang, S. Liou and R. F. Brebrick. *"Interatomic Potentials for Cd, Zn and Hg from Absorption Spectra"*. J. Chem. Phys., **81** (1984) 11.

[21] J. P. Schwartz, T. Tung and R. F. Brebrick. *"Partial Pressures over HgTe-CdTe Solid Solutions. I. Calibration Experiments and Results for 41.6 Mole Percent CdTe"*. J. Electrochem. Soc.: Solid-State Sci. and Tech., **128** (1981) 438.

[22] R. F. Brebrick. *"Partial Pressures in the Cd-Te and Zn-Te Systems"*. J. Electrochem. Soc.: Solid-State Sci. and Tech., **118** (1971) 2014.

[23] D. R. Stull and G. C. Sinke. *Thermodynamic Properties of the Elements.* American Chemical Society, Washington DC (1956).

[24] A. Bielski, S. Brym, R. Ciurylo, J. Domyslawska, E. Lisicki and R. S. Trawinski. *"Low Pressure broadening and Shift of the Cadmium Intercombination line 326.1 nm (5^1S_o - 5^3P_1) perturbed by He and Ne"*. J. Phys. B: At. Mol. Opt. Phys., **27** (1994) 5863.

[25] A. C. G. Mitchell and M. W. Zemansky. *Radiation and Excited Atoms.* Cambridge University Press, New York (1961).

[26] R. Fang and R. F. Brebrick. *"CdTe I: Solidus Curve and Composition-Temperature – Tellurium Partial Pressure Data for Te-Rich CdTe(s) from Optical Density Measurements"*. J. Phys. Chem. Solids, **57** (1996) 443.

[27] P. A. Rice and D. V. Ragone. *"Simultaneous Determination of f Values and Vapor Pressures from Optical Absorption Measurements."*. J. Chem. Phys., **42** (1965) 701.

[28] S. S. Penner. *Quantitative Molecular Spectroscopy and Gas Emissivities.* Addison-Wesley, London (1959).

[29] *CRC Handbook of Chemistry and Physics.* 70th and 71st edition. CRC Press, New York (1995-7)

[30] K. Zanio. *Cadmium Telluride.* Semiconductors and Semimetals Treatise, Volume 13. Edited by R. K. Willardson and A. C. Beer. Academic Press, London (1978).

Chapter Five

Mass Transport through Porous Silica Discs and Its Application to Vapour Stoichiometry and Mass Flow Control in Vapour Growth

5.0 INTRODUCTION.

As explained in chapter two, a constant vapour pressure ratio is of paramount importance if a sustainable, fluctuation-free growth rate is to be obtained. Since CdTe does not sublime congruently [1], in a closed growth system the vapour is normally non-stoichiometric and the ratio of partial pressures in the vapour during growth depends strongly on the purification and preparation processes that take place before growth. In addition, impurities or foreign gases that might be present in the source or incorporated during the growth process (outgassing from the silica container, contamination from furnace heaters, etc.) can upset the ratio of partial pressures in the vapour, and this can be exacerbated as growth continues. In a closed or semiclosed system, this may cause diffusion barriers near the vapour-crystal interface [2,3] which can not only reduce growth rates but lead to the formation of precipitates and/or inclusions [4] as well as change the electrical properties of the crystal by addition of undesired impurities [5]. Hence, it would be preferable to:

- 1.- Obtain a reliable mass flow control of the species to the crystal surface that does not depend strongly on the source stoichiometry, and to some extent, on the growth temperature. For this it would be necessary to decouple the growth rate from the temperature difference between source and growing crystal.
- 2.- Achieve a certain degree of control over the ratio of partial pressures in the vapour throughout the growth process.

The necessity of controlling the rate of mass transfer has been realised only recently. Rosenberger *et al.* [6] used a circular capillary between source and growth chambers in order to decouple source and growth sides and restrict growth, since their

calculations showed that, for typical ampoule diameters and vapour pressures during growth, predicted transport rates would be too high and consequently grown crystals would be poor in morphological and structural quality due to the (rate limiting) vapour-crystal interface kinetics.

The general idea of controlling the mass flow is relatively simple: if one could control the rate of molecules impinging in the crystal surface, provided sublimation from the source and interfacial kinetics are not rate determining, the growth rate can be studied, in semiopen systems, as a function of fundamental parameters such as vapour stoichiometry, gradient temperature in the crystal neighbourhood (supersaturation) and seed orientation. Besides fundamental studies, there is some degree of interest in understanding the dependency of growth rate in order to maximise it for commercial purposes. It is well known [6] that if growth occurs too rapidly, under non-steady transport fluxes, boules with non-uniform composition will result, and growth reproducibility is not possible. Hence, a full understanding of mass flow mechanisms, their dependency on growth parameters and how to control them is necessary in order to produce high quality binary and ternary semiconductor compounds reliably.

Porous silica discs, made by a sintering process, seem a good candidate to control the flow in the Durham system. They have been previously used in Vapour Levitation Epitaxy (LVE) to produce high uniformity epitaxial films [7] and in CVD to produce laminar flow and allow for mixing of the feed vapours [8]. In the context of bulk vapour growth, they have been used as physical supports for the source material in vertical growth configurations [9,10]. As will be shown in this chapter, they offer the possibility of selecting between transport modes (viscous or Knudsen) and hence can be

used in principle to set the partial pressure ratio in the vapour as well as, in a semiopen system under dynamic vacuum, to produce important pressure differences between the source side and the growth side. This would allow a reduction in the growth temperature, since the gradient difference between growth and source sides is no longer the driving force responsible for transport in a semiopen, dynamically pumped system, the temperature gradient being substituted by a physical device, i.e. the porous disc. Other properties that make porous silica discs suitable are their compatibility with the crucible, the lack of structural changes at high temperatures (up to ~1200 °C), and their availability in different sizes and porosities. An initial drawback is the unknown relation between porosity, specific surface area and dimensions with flow conductivity, and hence each porous disc requires, at least in principle, a calibration experiment. Hence, there is a need to characterise and understand the flow properties of these porous discs, and this chapter is fundamentally a study of the physical structure and flow conductivity of porous silica discs (as a function of pressure, temperature and molecular weight of the gas), and its application to crystal growth from the vapour.

5.1 THEORETICAL BACKGROUND.

5.1.1 Introduction.

In general, the structure of porous media is extremely complicated and irregular, and probably has a fractal nature [11]. It is not surprising therefore, that it has not been possible to date to develop a rigorous mathematical theory that relates important parameters such as porosity, pore size distribution, permeability, etc, to its internal geometrical structure. In fact, since most of the models that describe flow in porous media are based on analogies with capillaries and since models for these in the viscous,

transition and molecular flow regimes are only applicable in specific circumstances (see below), the flow through porous media is necessarily described in a semi-empirical, qualitative manner rather than quantitatively. There have been many attempts to develop a model that relates the structure of a porous medium to the flow of gases and liquids through it [12], mainly motivated by the application, for example, oil extraction, water management, catalysis in chemical engineering [13-15] and growth of nanocrystals [16]. Although some ingenious theories like the dusty-gas model [17,18] have been quite successful in predicting diffusion and flow without making any analogy to flow in capillaries, the reality is that existing models are only semi-empirical in nature and always need one or more adjusting parameters [19]. Although these parameters may, in principle, have a physical meaning (pore cross-section, effective pore length, etc.), they are intrinsic to the porous material type. Hence, besides the need to determine them *ad hoc* for every material type, they are in practice used as adjusting parameters to fit theory to experiment [20]. Since the goal here was to obtain a relationship between gas or vapour flow through porous silica discs and its pore structure in one hand, and to determine the dependence of the flow on temperature, molecular weight and pressure on the other, rather than to fully characterise all the geometrical parameters of their structure, a simple model was used to describe the porous discs.

5.1.2 Flow regimes in capillaries.

Flow through a capillary can be turbulent, viscous, molecular or Knudsen and transition or "slip", depending on the differential pressure range, or more precisely, on the ratio between the mean free path of the gas λ, and the radius of the capillary, r. Turbulent flow will not be considered since the pressures involved do not apply to vapour growth. Viscous flow occurs when $\lambda << r$, i.e. when one may consider that

collisions between the molecules themselves dominate the transport, and collisions with the walls are negligible. Molecular or Knudsen flow occurs when the contrary is true, i.e. $\lambda >> r$. The transition or "slip" flow occurs when both kind of collisions are important, i.e. when $\lambda \sim r$.

Knudsen flow through a capillary of length L is given by the expression [21]:

$$\psi\left(\frac{moles}{t}\right)=\frac{2\pi r^3}{3}\left(\frac{8RT}{\pi M}\right)^{1/2}\frac{\Delta P}{LRT} \tag{5.1}$$

where R is the gas constant, T is the temperature , M is the molecular weight of the gas and ΔP is the pressure difference between the ends of the capillary, $\Delta P = P_f - P_b$. It is strictly valid only for $\lambda >> r$, and for $L >> r$. Viscous flow is given by Poiseuille's equation [21]:

$$\varphi\left(\frac{moles}{t}\right)=\frac{\pi r^4 P_m \Delta P}{8\eta LRT} \tag{5.2}$$

where the mean pressure, $P_m = (P_f + P_b)/2$, and η is the viscosity of the gas. It is valid if i) the gas is incompressible, ii) the flow velocity profile is constant throughout the length (that normally occurs for capillaries where $L >> r$), iii) the flow is not turbulent iv) the flow velocity at the walls is zero and v) $\lambda << r$. A simple quantitative expression for "slip" flow is not available. When $\lambda \sim r$, it is customary to use Poiseuille's formula with an additive correction term, calculated qualitatively assuming that the flow velocity at the walls is not zero, and which accounts for the effects of the "slip" at the walls [21,22]. The expression is:

$$\chi\left(\frac{moles}{t}\right)=\frac{\pi r^4 P_m \Delta P}{8\eta LRT}+\frac{\pi^2 r^3 \Delta P}{(8\pi MRT)^{1/2} L}\left(\frac{2}{f}-1\right) \tag{5.3}$$

where f is a parameter which is interpreted as the fraction of gas molecules diffusely reflected from the capillary walls [23]. It is worth noting that the second term differs from equation (5.1) only in a factor of $3\pi/16$, but has the same pressure, temperature and more importantly, molecular weight dependence. To obtain an idea of the range of pressures at which equations 5.1-5.3 are applicable, table 1 shows some examples of the mean free path of H_2, Cd and Te_2 at several pressures and temperatures calculated using the rigid sphere model [21],

$$\lambda = \frac{K_B T}{\sqrt{2}\pi P \sigma^2} \tag{5.4}$$

where K_B is the Boltzmann's constant, and σ is the molecular diameter. The values of the mean free paths obtained using 5.4 can only be approximate, due to the crudeness of the model, as well as the uncertainty in the molecular diameter [24]. Values for molecular diameters are usually calculated from experimental viscosity data, and although these normally differ from values calculated using data from other experimental variables [25], they are considered to be the most reliable. Where no viscosity data are available, the Van der Waals molecular radius, "which refers to the radius it presents to the world beyond the molecule" [26], is used. In typical vapour growth ampoules (r < 2 cm), for typical sources temperatures (~ 1200 K), and growth pressures (> 1 mbar) one can see that viscous flow is predominant. However, in a porous silica disc where, as will be seen in the characterisation section, the average pore size is in the range 1-10 μm, "slip" and Knudsen flow will be the main transport mechanisms even at relatively high pressures, since the mean free path in a pore must necessarily be of the same order of magnitude as the pore radii, as first realised by Adzumi [27] and later explained by Tokunaga [28].

λ (μm)	1013 (mbar)	10 (mbar)	1 (mbar)	0.1 (mbar)
H_2				
293 K	0.16	15.8	158	1581
1273 K	0.68	68.7	687	6869
Cd				
293 K	0.13	13.4	134	1341
1273 K	0.58	58.2	582	5826
Te_2				
293 K	0.06	5.8	57.9	579
1273 K	0.25	25.1	251	2515

TABLE 1. Mean free paths (in μm) of H_2 (σ = 2.40 Å [26]), Cd (σ = 2.606 [29]) and Te_2 (σ = 3.966 [30]) at several temperatures and pressures relevant to vapour growth.

5.1.3 A capillary model for porous media: the Kozeny-Carman equation.

This model [19,31,32] assumes that the porous body consists of N identical, parallel pores per unit of area, each of the same length L and cross-sectional area a and average radii r, for which the flow expression 5.2 or 5.3 for a circular capillary, can be applied to. To account for the non-circular cross-section of the pores, the so called *hydraulic radius*, m, is used. It is defined as the cross-sectional area of the pore divided by its perimeter l:

$$m = \frac{a}{l} \tag{5.5}$$

Equation 5.3 can then be rewritten as:

$$\chi\left(\frac{moles}{t}\right) = \frac{m^2 a P_m \Delta P}{k_o \eta LRT} + \frac{\pi ma\Delta P}{(2\pi MRT)^{1/2} L}\left(\frac{2}{f} - 1\right) \tag{5.6}$$

where k_o would be 2 for a circular capillary and varies from 1.2 to 3.0 for other geometrical shapes [19]. Since a porous body is mainly characterised by its porosity ε and specific surface area S, and these are easier to measure than a and m, it is necessary to relate the former to the latter. In the capillary model, the porosity, defined as the volume of voids per unit volume of porous body, is given by:

$$\varepsilon = \frac{NaAL}{AL} = Na \tag{5.7}$$

where A is the total cross-sectional area of the porous body. The specific surface area, defined as the surface area per unit volume of solid material can be written as:

$$S = \frac{NAlL}{AL(1-\varepsilon)} = \frac{Nl}{(1-\varepsilon)} \tag{5.8}$$

Combining equations 5.5 and 5.7 we obtain

$$m = \frac{\varepsilon}{Nl} \tag{5.9}$$

and using 5.8 we finally obtain an expression relating ε and S to m:

$$m = \frac{\varepsilon}{S(1-\varepsilon)} \tag{5.10}$$

Putting 5.10 into 5.6, and multiplying both sides by N and A gives us finally the equation of flow through a porous body containing N parallel pores per unit area:

$$F\left(\frac{moles}{t}\right) = \frac{\varepsilon^3 AP_m \Delta P}{(1-\varepsilon)^2 S^2 k_o \eta LRT} + \frac{\pi\varepsilon^2 A\Delta P}{(1-\varepsilon)S(2\pi MRT)^{1/2} L}\left(\frac{2}{f}-1\right) \tag{5.11}$$

Since the pores are never parallel or equal in length and the cross-sectional shape constant is normally difficult to evaluate, two constants, k_t and k_d are introduced to account for these uncertainties, and putting $k_v = k_o \times k_t$ we obtain for the total flow through the porous body,

$$F\left(\frac{moles}{t}\right) = \frac{\varepsilon^3 AP_m \Delta P}{k_v(1-\varepsilon)^2 S^2 \eta LRT} + \frac{\pi\varepsilon^2 A\Delta P}{k_d(1-\varepsilon)S(2\pi MRT)^{1/2} L}\left(\frac{2}{f}-1\right) \tag{5.12}$$

It is more useful to write equation 5.12 in volume units, since one normally measures specific volume flow rates at temperature T_o and atmospheric pressure P_o. If in addition one defines the slip factor Z as

$$Z = \frac{1}{k_d}\left(\frac{2}{f} - 1\right) \tag{5.13}$$

then we finally obtain the Kozeny-Carman equation for the *specific flow* through a porous body,

$$G' = \frac{V}{t \times \Delta P} = \frac{\varepsilon^3 A T_o P_m}{k_v (1-\varepsilon)^2 S^2 \eta L R T P_o} + \frac{\pi \varepsilon^2 A Z R T_o}{(1-\varepsilon) S (2\pi MRT)^{1/2} L P_o} \tag{5.14}$$

where V is the volume of the gas at P_o and T_o. According to 5.14, in order to predict the flow of any gas through a porous samples, it is necessary to obtain the structural parameters ε, S, k_v and Z. Once these are determined, it is possible in principle, and for the same porous sample, to predict the flow of any gas or vapour provided phenomena like adsorption or surface diffusion are negligible. P.C.Carman [19] made an experimental study for a wide variety of porous samples of known specific surface area and porosity and found in all cases a value of k_v = 5.0. The porosity ε can be determined by standard techniques such as Hg porosimetry, or pycnometry and the specific surface area S can be obtained with adsorption isotherm techniques (BET) [33]. However, these techniques are not always suitable, since Hg porosity includes dead ended pores or voids in the material, which do not contribute to the flow [34], and BET techniques have a minimum value (~ 0.01 m^2/gm) of applicability. The slip factor Z is a function of the gas and surface properties, and hence in general is unknown. Therefore it is necessary to obtain these three fundamental parameters directly by passing gases

through a sample and comparing the experimental results with equation 5.14. In principle, a single gas at one temperature and several mean pressures would be enough to obtain S and Z, since in plotting G' against the mean pressure P_m will yield, according to 5.14, a straight line of slope α and intercept β, given by:

$$\alpha = \frac{AT_o}{k_v \eta LTP_o} \times \frac{\varepsilon^3}{(1-\varepsilon)^2 S^2} \tag{5.15}$$

$$\beta = \frac{\pi AZRT_o}{LP_o (2\pi MRT)^{1/2}} \times \frac{\varepsilon^2}{(1-\varepsilon)S} \tag{5.16}$$

and solving these equations simultaneously, we obtain expressions for S and Z in terms of known variables:

$$S = \left(\frac{\varepsilon}{1-\varepsilon}\right) \times \sqrt{\frac{\varepsilon AT_o}{k_v \alpha \eta LTP_o}} \tag{5.17}$$

$$Z = \beta \times \sqrt{\frac{2MLP_o}{k_v \pi \alpha \eta \varepsilon ART_o}} \tag{5.18}$$

However, when very precise data are required, it is necessary to undertake flow experiments for a range of gases and in particular at different temperatures, since vapour growth may take place at a variety of temperatures, and according to 5.14, flow through the porous disc will depend on them. Plotting the slopes α for each temperature and gas against $1/\eta T$ should give a straight line of slope γ,

$$\gamma = \frac{\varepsilon^3 AT_o}{k_v LP_o (1-\varepsilon)^2} \times \frac{1}{S^2} \tag{5.19}$$

which gives us a reliable expression for S assuming that the porosity and dimension related parameters of the sample change little with temperature:

$$S = \left(\frac{\varepsilon}{1-\varepsilon}\right) \times \sqrt{\frac{\varepsilon AT_o}{k_v \gamma LP_o}} \tag{5.20}$$

In an analogous way, plotting the intercepts β for each gas and temperature against $1/(MT)^{1/2}$ should give a straight line assuming that Z is independent of the gas used and of the temperature, the slope of which, δ,

$$\delta = \frac{\pi\, AZRT_o}{LP_o\sqrt{2\pi\, R}} \times \frac{\varepsilon^2}{(1-\varepsilon)S} \tag{5.21}$$

allows us to obtain the slip factor Z by solving simultaneously with 5.20,

$$Z = \delta \times \sqrt{\frac{2LP_o}{k_v \pi\gamma\varepsilon ART_o}} \tag{5.22}$$

If a straight line is not obtained, it would indicate that the slip factor depends on the gas temperature and/or gas nature, and hence in the latter case the structural parameters and flow rates obtained using simple gases would not be applicable to Cd and Te_2 flow.

5.2 STRUCTURAL CHARACTERISATION OF POROUS SILICA DISCS.

In order to obtain the parameters S, Z and ε, several characterisation tests were necessary. As concluded in the last section, gas flow experiments provide a reliable measurement of the specific surface area S and slip factor Z. Accordingly, an experiment was set up to measure G' at several temperatures for a porous silica disc (of the type intended for use in vapour growth) and several gases (He, N_2, Ar, Kr and SF_6) providing a broad range of molecular weights. The porosity ε was also studied since equation 5.14 depends strongly on it, and hence it is necessary to determine its true value if reliable values of S and Z were to be obtained.

5.2.1 Determination of porosity.

Figures 1 and 2 show detailed SEM microphotographs of the fracture surface of a porous silica sample of the same porosity grade as the one used in the gas flow experiments. It can be seen that the pore size range distribution is quite narrow varying from 1 to 10 μm, in agreement with the stated manufacturer average pore size of 4 to 15 μm. The pore size distribution is relatively narrow, as expected since the mode of manufacture is by a sintering process, using as starting material silica particles of very uniform size and narrow size distribution [35].

Although the porosity could be determined directly by analysing SEM photographs, this technique is not very reliable due to the intrinsic statistical fluctuations that appear when relatively small areas of the sample are analysed. Three other techniques were used therefore to analyse the porosity: density method, liquid uptake and Boyle's law.

Since the porous discs were made of pure silica of known density ρ_{silica} = 2.20 gm/cm^3 , it is straightforward to calculate the porosity of the sample by the simple process of measuring its volume V and weight W:

$$\varepsilon_\rho = \frac{V_{pores}}{V_{porous\,disc}} = \frac{V_{porous\,disc} - (W_{porous\,disc} \times \rho_{silica}^{-1})}{V_{porous\,disc}} \tag{5.23}$$

For the sample used in the flow experiments, the above equation gave a value ε_ρ= 0.40. However, since the porosity dependence of equation 5.14 could be important due to quadratic and cubic terms (see figure 3), a Ruska Universal Porosimeter was used to

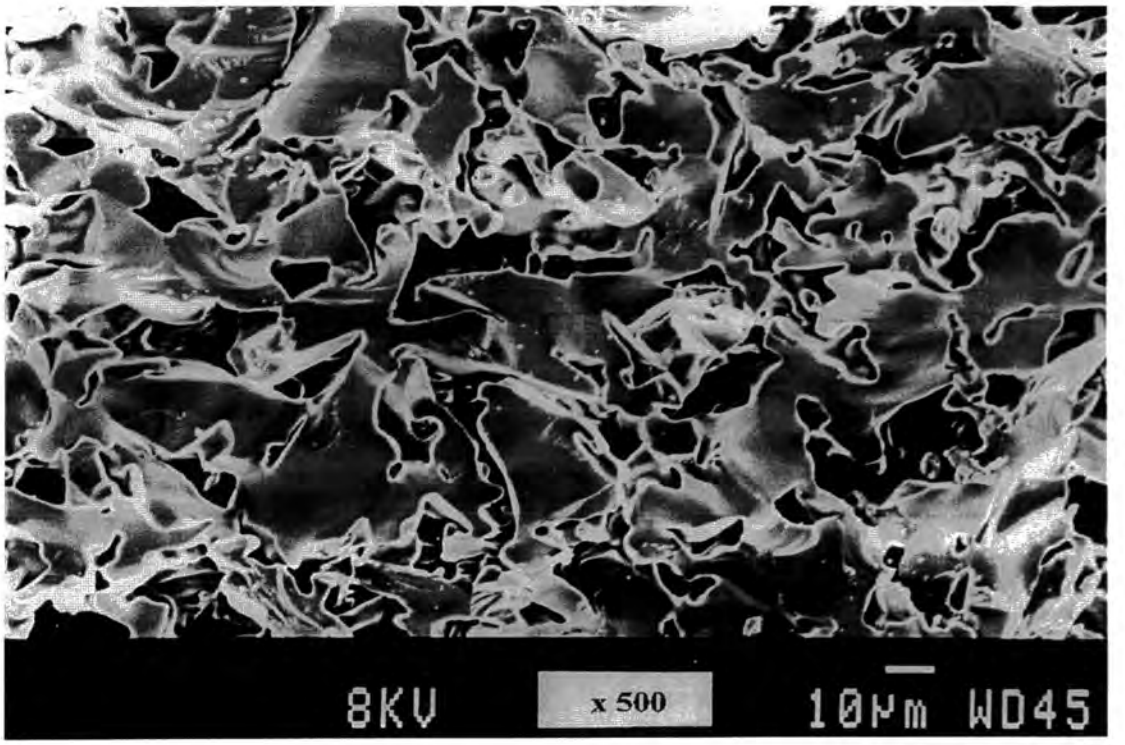

Figure 1. SEM microphotograph of the fracture surface of a porous silica disc of the same porosity grade as the one used in the flow experiments.

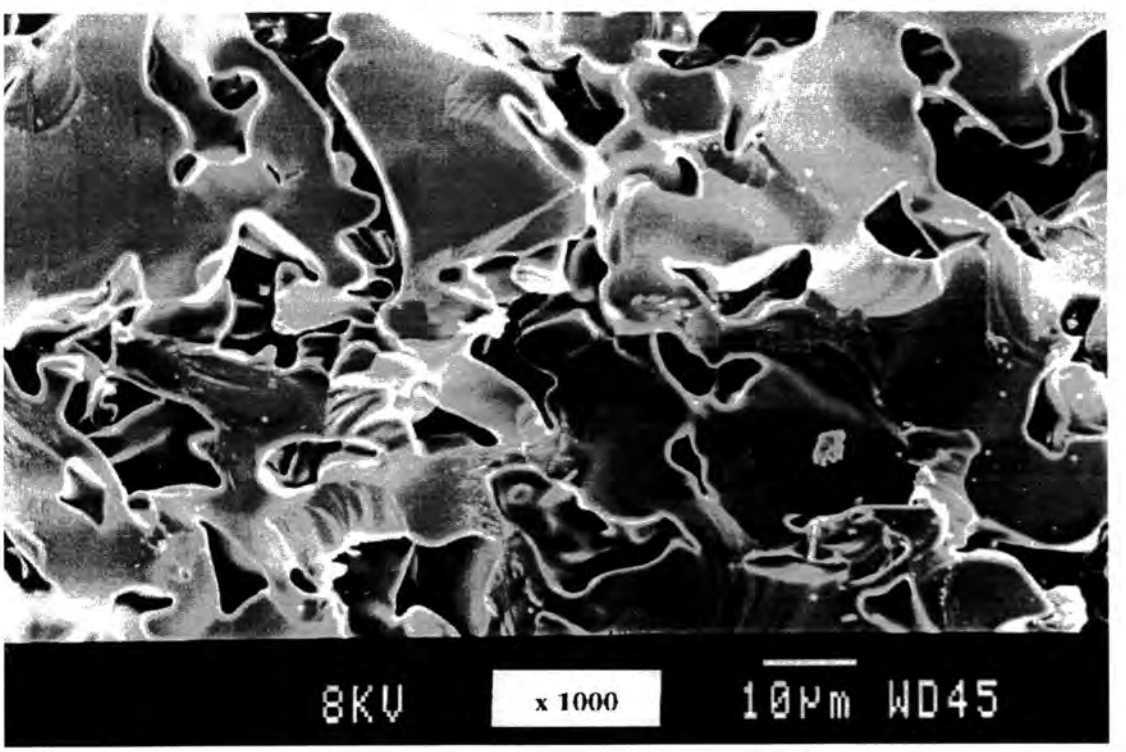

Figure 2. SEM microphotograph showing a detailed view of the pore shape and dimensions. Pore size range is 1-10 microns.

obtain the porosity of the disc with the Kobe or Boyle's Law method, ε_k. The value obtained of $\varepsilon_k = 0.39$ agreed quite well with that from the density method. Since the total porosity accounts for open pores, but also for closed end pores and voids, and although the latter are not expected when using sintering processes for manufacturing, a further experiment was used to evaluate the effective porosity. It consisted of simply measuring the increase of weight when the pores are filled with a liquid (preferably of low molecular weight so that fine pores are filled [14]). Distilled water was used as the liquid and a microbalance was used to measure the water uptake. The porosity measured in this way resulted in a value $\varepsilon_w = 0.39$. Although the accuracy of this method is limited by the difficulty of drying the external surface of the disc without removing water from the largest pores and the fact that some water can be held around the contact points between particles, thus leaving some pores unfilled, it can be concluded that the effective porosity for gas flow is the porosity determined by the water uptake method. In any case, such small variation between the Kobe or density methods and the liquid filling method results in an acceptable uncertainty of the porosity functions of equation 5.14 for porosities in the range 0.2 – 0.8 as can be seen in figure 3.

In order to obtain an idea of the reliability of the porosity value stated by the manufacturer, several samples of the same dimensions and porosity grade as stated by the manufacturer were analysed using the same three different techniques as before. The results are presented in table 2. In all cases, ε_w is smaller than ε_k and ε_ρ, although by a small amount. Although an estimated 10 % experimental error is applicable to the measured values, and hence all three methods give similar values, the consistently smaller values of ε_w for all four samples can be interpreted as a prove that the void porosity is not being measured.

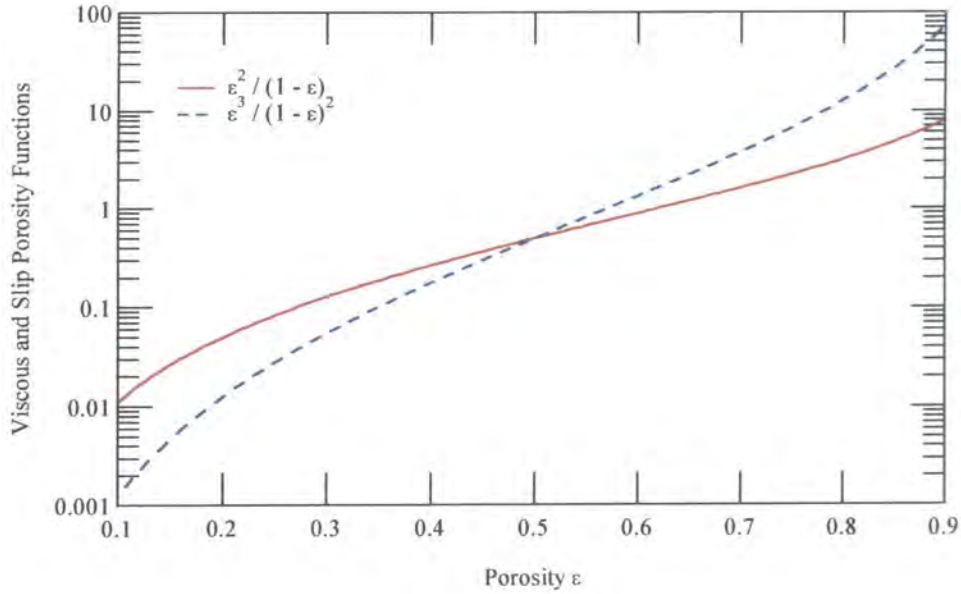

Figure 3. Variation of the porosity functions of equation 5.14 with porosity ε. The small uncertainties in the porosity have a greater effect on the viscous porosity function (dotted) than on the slip one (straight).

Sample	ε_ρ	ε_k	ε_w
# 1	0.42	0.41	0.35
# 2	0.42	0.39	0.32
# 3	0.53	0.49	0.44
# 4	0.50	0.45	0.39

TABLE 2. Comparison of porosity values obtained using three different methods for four porous silica discs (nominally identical to the disc used in the gas flow experiments, i.e. of the same porosity grade)

5.2.2 Determination of *S* and *Z*: Gas Flow Method.

A sketch of the experimental setup (similar to those used by Barrer *et al.* [34] and Kraus *et al.* [36]) used in the gas flow experiments is shown in figure 4. The porous silica disc S (Heraeus, porosity grade 4) of 17 mm diameter and 3 mm length was

carefully mounted by fusing its border in an open ended silica tube. The test gases (purity > 99.8 %) were introduced in one side of the disc through a mass flow controller which was set to a constant flow rate in order to set a constant pressure difference across the porous disc. The gas that passed through the porous disc was continuously removed by a rotary vacuum pump and once dynamic equilibrium was achieved, collected in a calibrated trough, where the volume of the gas at room temperature and pressure was measured. In each flow experiment, special care was taken in order to obtain steady state flow conditions, as determined by measuring the pressures in each side of the porous disc with a pressure gauge (Druck, 1 - 1000 mbar) and valves V2 and V3. Once steady state flow was reached, the disc temperature and the values of the pressure in each side were recorded and the experiment started. The duration of each experiment depended on the flow rate and varied between 3 minutes and 2 hours. By measuring the time and the volume of gas collected in the trough, the flow rate through the porous disc was obtained. A one zone furnace was used to set the porous disc and flowing gases to the desired temperature, and this was monitored with a Pt/13%Rh thermocouple carefully positioned at the base of the porous disc. No thermal gradient existed along 10 cm at either side of the porous disc. Helium, Nitrogen, Argon, Krypton and Sulphur Hexafluoride of molecular weights 4.00, 28.02, 39.95, 83.80 and 146.06 respectively were used as test gases. Experiments were performed at 20, 200, 400, 600, 800 and 1000 °C, with the exception of SF_6, for which significant dissociation takes place at ~750 °C [37]. Such high temperatures were necessary since typical growth temperatures are in the 600 – 1000 °C range. Additional experiments were performed at 100 °C for Helium and SF_6 and at 150 °C for SF_6. The range of mean pressures for each flow experiment varied depending on the temperature and gas, but was always in the range 3–260 mbar.

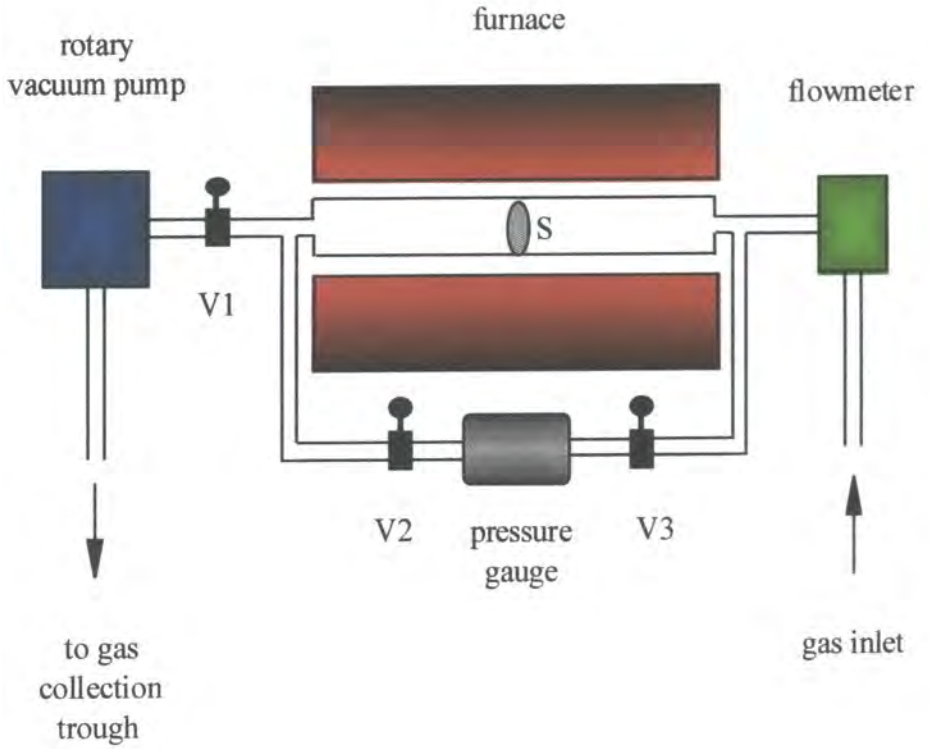

Figure 4. Sketch of the experimental setup used in the flow experiments with test gases.

Plots of the specific flow rate versus mean pressures are shown in figures 5, 6, 7, 8 and 9 for He, N_2, Ar, Kr and SF_6 respectively. Straight lines were obtained at all temperatures for each gas, and the slopes and intercepts decreased with increasing temperature, as predicted by equations 5.15 and 5.16. The solid lines indicate the best fits. Table 3 lists the numerical values of the slope α, intercept β for each gas and temperature.

Figure 10 shows specific flow rates at 600 °C for all five gases. As predicted by equation 5.14 for a given temperature, the slopes of the straight lines decrease with increasing viscosity (see table 4 for values of viscosity) and the intercepts decrease as the molecular weight of the gas increases.

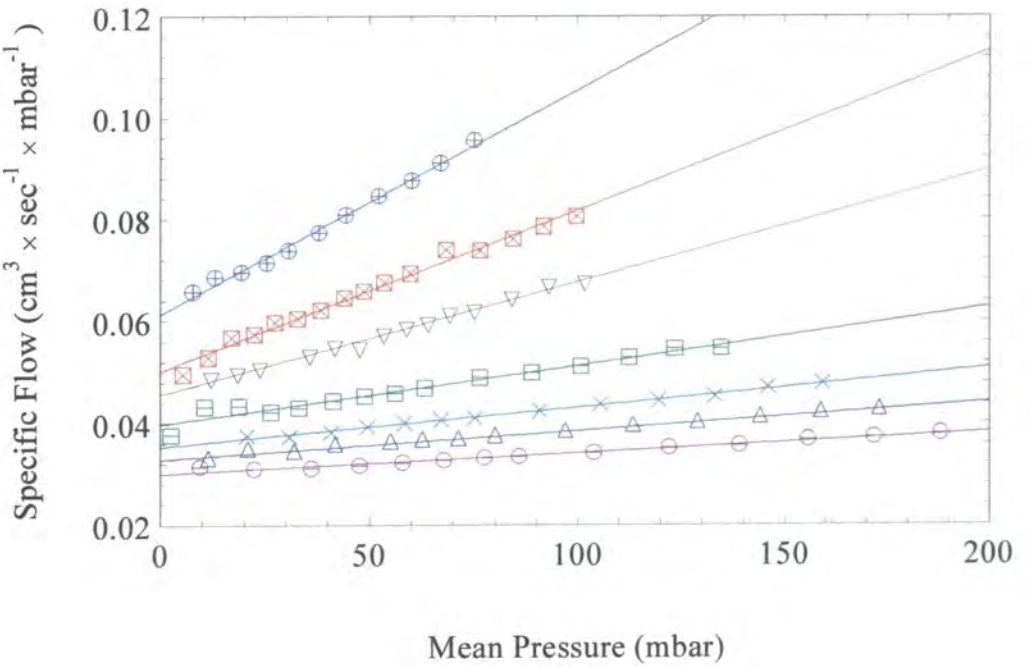

Figure 5. Specific flow rate vs. mean pressure for Helium. From top to bottom: 21, 100, 200, 400, 600, 800 and 1000 °C.

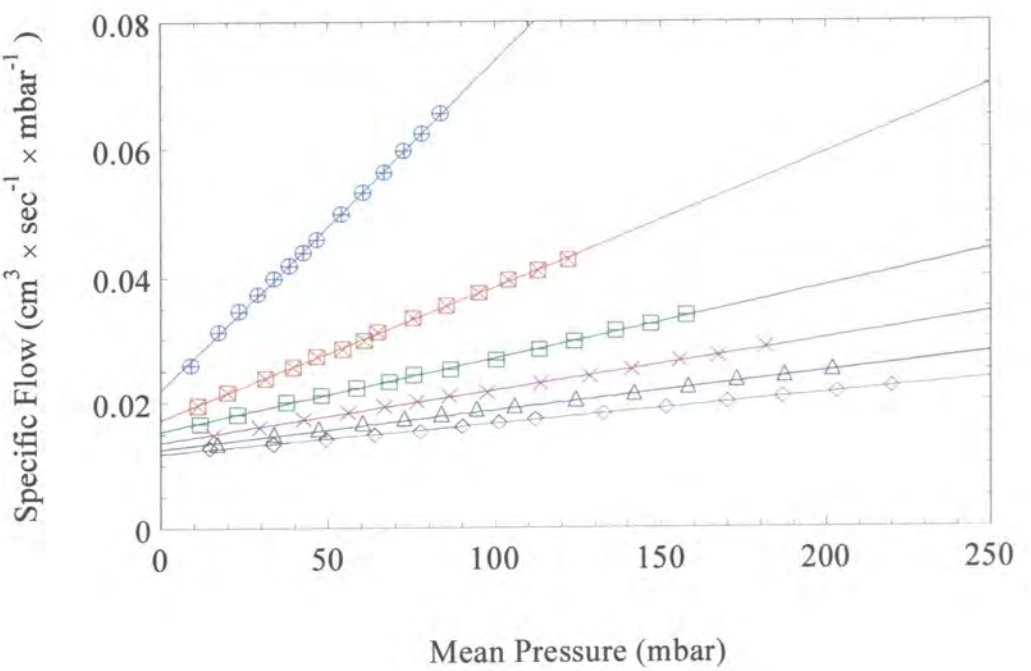

Figure 6. Specific flow rate vs. mean pressure for Nitrogen. From top to bottom: 21, 200, 400, 600, 800 and 1000 °C.

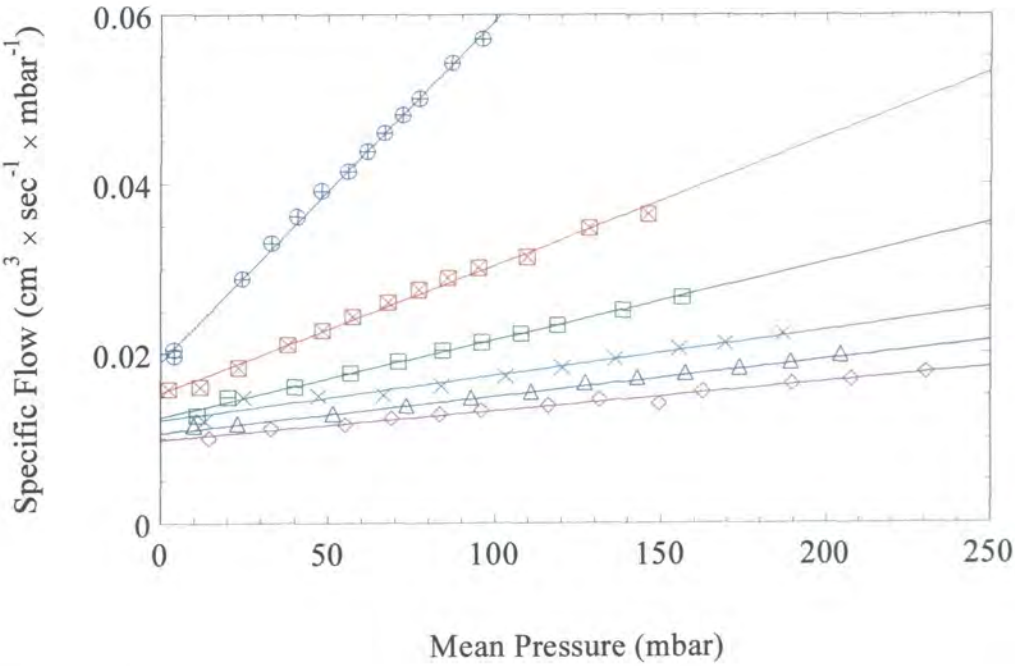

Figure 7. Specific flow rate vs. mean pressure for Argon. From top to bottom: 21, 200, 400, 600, 800 and 1000 °C.

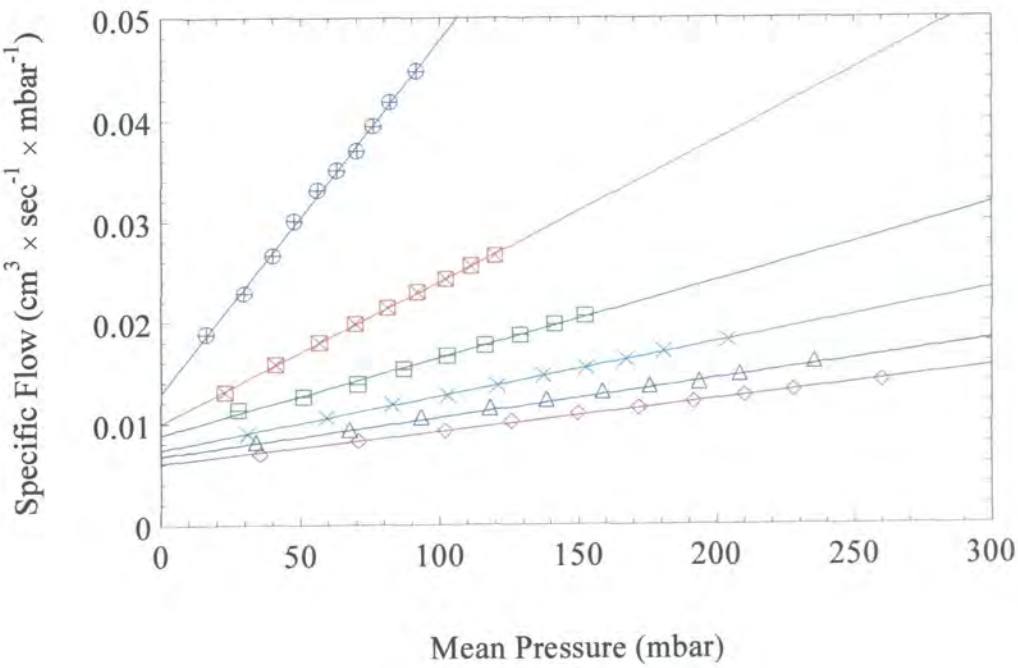

Figure 8. Specific flow rate vs. mean pressure for Krypton. From top to bottom: 22, 200, 400, 600, 800 and 1000 °C.

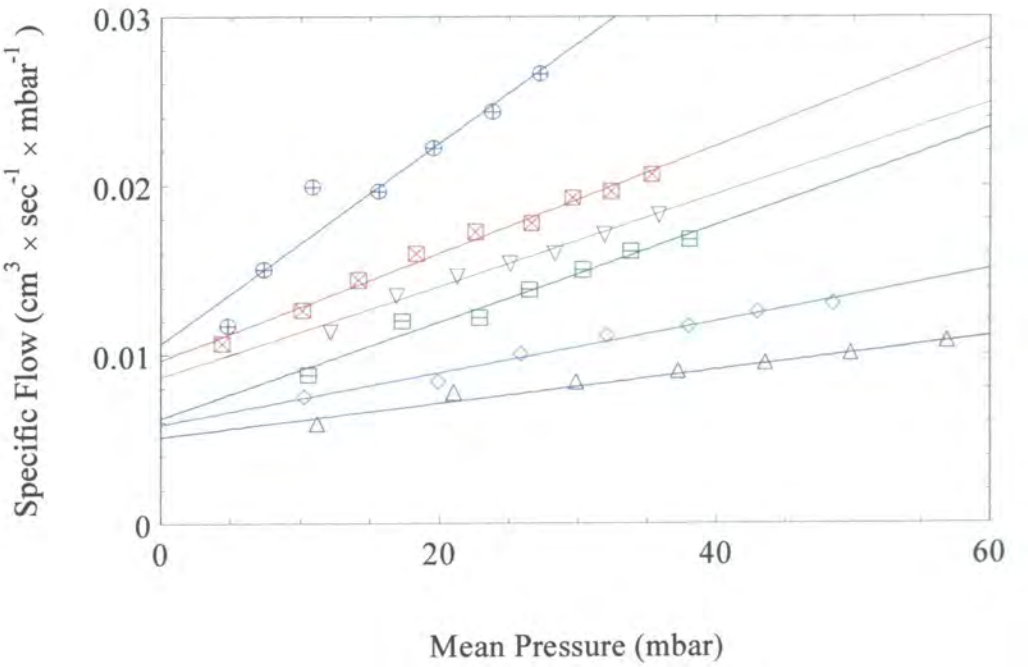

Figure 9. Specific flow rate vs. mean pressure for Sulphur Hexafluoride. From top to bottom: 22, 100, 150, 200, 400 and 600 °C.

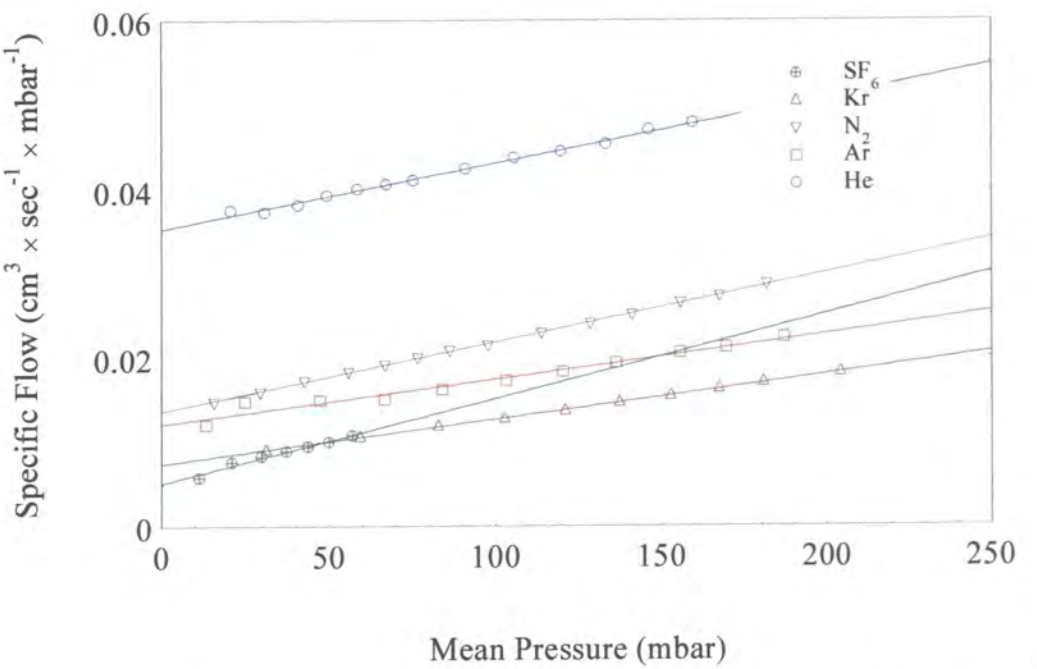

Figure 10. Comparison between the test gases (see legend) at 600 °C. Solid lines are best fits.

Test Gas	Temperature (K)	Slope α ($cm^3 \times s^{-1} \times mbar^{-2}$)	Intercept β ($cm^3 \times s^{-1} \times mbar^{-1}$)
He	294	4.42E-04	0.0613
He	373	3.22E-04	0.0497
He	473	2.20E-04	0.0456
He	673	1.20E-04	0.0393
He	873	7.66E-05	0.0355
He	1073	5.71E-05	0.0328
He	1273	4.01E-05	0.0302
N_2	294	5.20E-04	0.0219
N_2	473	2.11E-04	0.0173
N_2	673	1.16E-04	0.0154
N_2	873	8.22E-05	0.0136
N_2	1073	6.12E-05	0.0125
N_2	1273	4.74E-05	0.0118
Ar	294	4.04E-04	0.0190
Ar	473	1.52E-04	0.0153
Ar	673	9.19E-05	0.0125
Ar	873	5.76E-05	0.0115
Ar	1073	4.37E-05	0.0106
Ar	1273	3.44E-05	0.0098
Kr	294	3.49E-04	0.0130
Kr	473	1.40E-04	0.0100
Kr	673	7.62E-05	0.0089
Kr	873	5.30E-05	0.0074
Kr	1073	3.82E-05	0.0068
Kr	1273	3.16E-05	0.0061
SF_6	296	5.78E-04	0.0107
SF_6	373	3.17E-04	0.0097
SF_6	423	2.70E-04	0.0087
SF_6	473	2.86E-04	0.0062
SF_6	673	1.55E-04	0.0058
SF_6	873	1.00E-04	0.0051

TABLE 3. Numerical values of the slopes α and β for all the test gases and temperatures.

5.3 FLOW PROPERTIES OF POROUS SILICA DISCS

5.3.1 Experimental results: analysis.

As explained in the previous section, experimental data obtained at different temperatures using several gases of a wide range of molecular weights allows us to obtain Z and S reliably. In order to obtain the parameter γ necessary to obtain S, a log-log graph of the slopes α versus $1/\eta T$ has been plotted in figure 11. Experimental viscosity values have been obtained from the literature when possible. In the cases where no experimental data was available, usually at high temperatures (see table 4), an extrapolation from the lower range of temperatures was done, using Sunderland's semi-empirical expression [21], since theoretical expressions for viscosity values at high temperatures deviate significantly from experimental data [21].

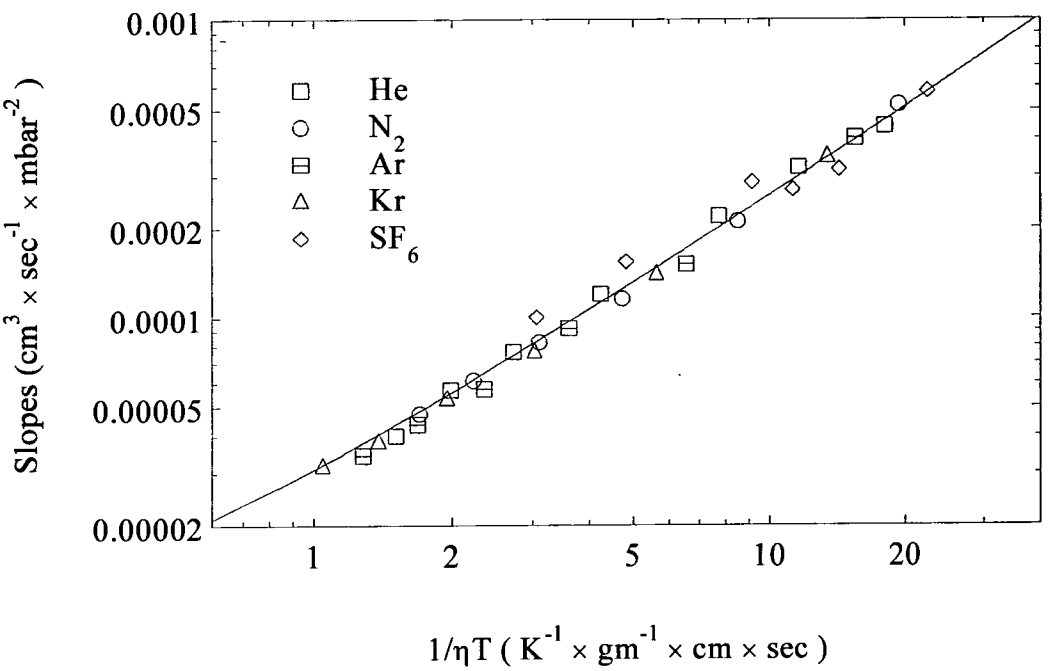

Figure 11. Plot of the slopes α obtained from the flow experiments vs. $1/\eta T$. The solid line is the best fit.

The slope of the best fit obtained gave a value for the parameter γ,

$$\gamma = 2.536\times10^{-5} \quad \left(\frac{\mathrm{cm}^2\times\mathrm{gm}\times\mathrm{K}}{\mathrm{s}^2\times\mathrm{mbar}^2}\right)$$

and putting this value in equation 5.20 together with the values of ε, A and L, a value for the specific surface area S is obtained:

$$S = 2.34\times10^{3} \ \mathrm{cm}^{-1}$$

or in units of area per unit of mass,

$$S = 0.106 \ \mathrm{m}^2\mathrm{gm}^{-1}$$

This is a very low value of the specific surface area S, but is a typical value for sintered glass [31] and typical silica powder [38]. In order to obtain an idea of the accuracy of the method, equation 5.10 can be used to obtain a rough idea of the expected specific surface if one assumes the pores to be cylindrical, in which case $m = r/2$ and hence,

$$r = \frac{2\varepsilon}{(1-\varepsilon)S} = 5.45\mu\mathrm{m}$$

which gives an average pore diameter of about 11 μm, which is consistent with the SEM results presented in section 5.2.1.

η (gm×cm^{-1}×s^{-1})	He [39]	N_2 [40]	Ar [41]	Kr [42]	SF_6 [37]
T (K)	$\eta\times10^7$	$\eta\times10^7$	$\eta\times10^7$	$\eta\times10^7$	$\eta\times10^7$
294	1887	1756	2222	2522	1509
373	2316	-	-	-	1879
423	-	-	-	-	2101
473	2735	2482	3227	3752	2314
673	3504	3135	4120	4897	3080
873	4213	3689	4878	5877	3743
1073	4692*	4177	5547	6744*	-
1273	5203*	4617	6150	7525*	-

TABLE 4. Experimental viscosity values for the test gases for the temperatures of interest. (*) High temperature values extrapolated.

Similarly, a graph of the intercepts β versus $1/(MT)^{1/2}$ was plotted, which should produce a straight line of slope δ. Figure 12 shows that this is the case.

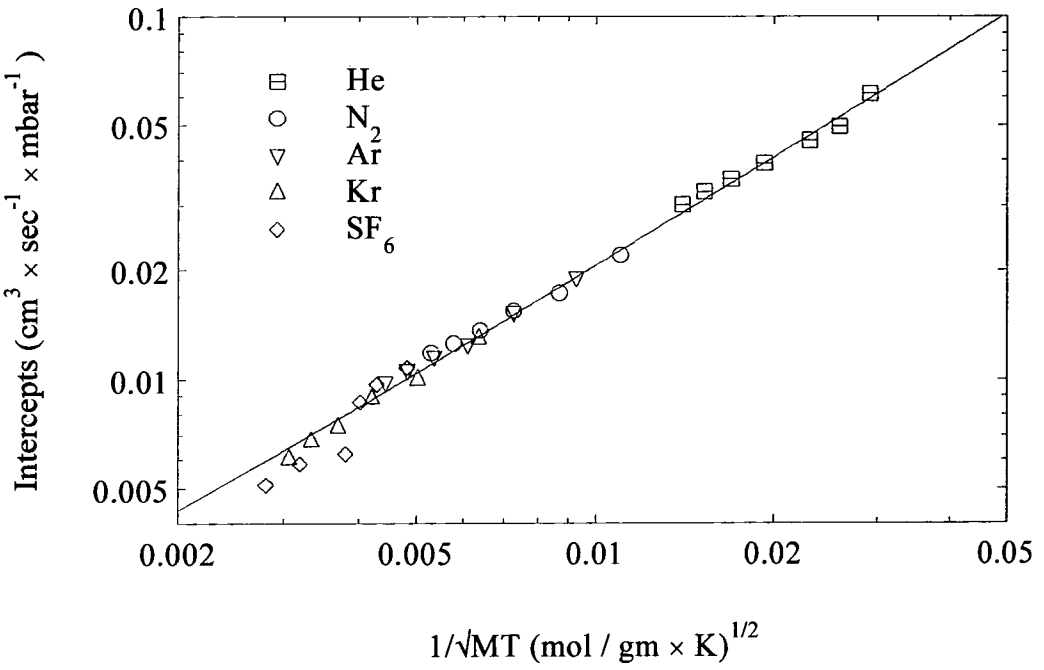

Figure 12. Plot of the intercepts β obtained from the flow experiments vs. $1/(MT)^{1/2}$. The solid line is the best fit.

The slope δ of the best fit was determined, and its value,

$$\delta = 2.028 \quad \left(\frac{\mathrm{cm}^3 \times \mathrm{gm}^{1/2} \times \mathrm{K}^{1/2}}{\mathrm{s} \times \mathrm{mol}^{1/2} \times \mathrm{mbar}} \right)$$

together with values of ε and γ, allows the value for the slip factor Z to be obtained using equation 5.22,

$$Z = 0.611$$

It can be seen from figure 12, that with perhaps the exception of SF_6 at high temperatures, all the other gases have the same behaviour, confirming the hypothesis used to obtain 5.22 that the slip factor does not vary significantly with the nature of the

gas. The behaviour of SF_6 at high temperatures could be explained if the gas started to dissociate, forming a mixture of fluorine and SF_4, in which case the dependency in $1/(MT)^{1/2}$ with $M = 140.06$ would not be valid anymore.

Once the parameters S and Z are determined, it is possible to estimate the flow rates of Cd and Te_2 vapours through the same porous silica disc. Since Cd and Te_2 molecular weights are very different, and according to equation 5.14 mass flow depends on it, a comparison between the experimental values for the mass flow of the test gases has been done. For each temperature, the ratio of the intercept values of say Helium divided by the values of the other gases, should give, according to equation 5.14 a parameter $\Gamma_{\frac{He}{i}}$ dependent only on the molecular weights:

$$\Gamma_{\frac{He}{i}} = \frac{\beta_{He}}{\beta_i} = \sqrt{\frac{M_i}{M_{He}}} \quad \text{for } i = N_2, \text{Ar, Kr, } SF_6 \tag{5.24}$$

if Z, ε and S are independent of the gas nature, as has been experimentally proven. Accordingly, the experimental values of $\Gamma_{\frac{He}{i}}$ have been plotted in figure 13 as a function of temperature. Table 5 shows a comparison between experimental bests fits for each pair and theoretical values.

Gases	Experimental	Theoretical	Variation (%)
He-N_2	2.630	2.645	- 0.56 %
He-Ar	3.104	3.159	- 1.74 %
He-Kr	4.719	4.576	+ 3.12 %
He-SF_6	6.366	6.041	+ 5.38 %

TABLE 5. Experimental best fits and theoretical values of $\Gamma_{\frac{He}{i}}$ for i = N_2, Ar, Kr and SF_6.

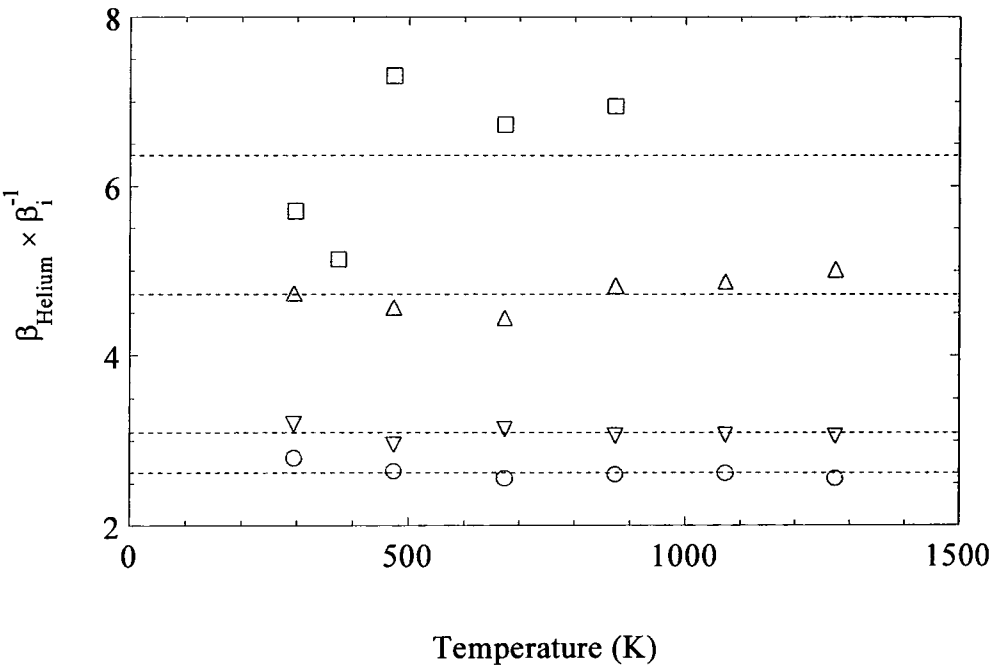

Figure 13. Experimental values of the β_{He}/β_i for SF_6 (□), Kr (Δ), Ar (∇) and N_2 (O) showing. Dotted lines are best fits.

It can be seen from figure 13 and table 5 that equation 5.24 is obeyed. The relative importance of the viscous and slip contributions to flow depends on the mean pressure P_m according to 5.14. It is thus important to quantify the weight of each term in order to understand how different mean pressures, can modify the transport mechanisms, and what the effects will be. Table 6 shows the ratio $\beta / \alpha P_m$ for various mean pressures obtained from the experimental results. The change in the SF_6 values as temperature increases reaffirms the presence of some decomposition. As can be seen, the lower the molecular weight of the gas and the temperature is, the bigger is the importance of the slip term for a given pressure. This is to be expected since according to 5.15 and 5.16, the ratio $\beta / \alpha P_m$ is inversely proportional to $M^{1/2}$. On the other hand, the slip term becomes less important as the pressure increases, again as expected

intuitively, since the mean free path is inversely proportional to the mean pressure. According to the results presented in table 6, in the range of pressures and temperatures encountered in vapour crystal growth, the slip flow contribution will be predominant, and in practice one can neglect the viscous term contribution to flow.

It is also now clear that when slip (or Knudsen) flow is the main transport mechanism, preferential transport (in accordance with equation 5.24) of the lightest gas or vapour species will take place when the gas or vapour flowing through the porous disc is a mixture of two (or more) gases or vapours. This will always occur as long as the mean free path of the species involved is similar to or larger than the mean pore radii. Due to the small pore size, the mean free path of any molecule inside the porous media is of the same order of magnitude of the pore [28]. This intrinsic behaviour of any mixture of vapours or gases could have consequences on the stoichiometry of the vapour over the source and crystal during vapour growth of CdTe. These consequences are analysed in the following section.

5.3.2 Theoretical analysis of Cd and Te_2 vapours flow.

As the previous experimental analysis has shown, at low mean pressures the main transport mechanism is slip or transition flow, and at very low pressures, Knudsen or effusion flow dominates. At low pressures (i.e. $P_m \rightarrow 0$), preferential transport of low molecular weight gases will occur in a gas mixture, as equation 5.24 indicates. This is a direct consequence of the different mean velocities of the gas atoms or molecules, which in turn is related to their different molecular weights. Vapour growth of CdTe normally takes place at a total pressure in the range 1–20 mbar, and hence to a very good approximation it may be assumed that all transport is via slip or transition flow.

	$\beta / \alpha P_m$			
T(K)	Pm = 0.1 mbar	Pm = 1 mbar	Pm = 10 mbar	Pm = 100 mbar
He				
294	1387.71	138.77	13.88	1.39
373	1544.17	154.42	15.44	1.54
473	2066.93	206.69	20.67	2.07
673	3273.42	327.34	32.73	3.27
873	4639.73	463.97	46.40	4.64
1073	5753.69	575.37	57.54	5.75
1273	7543.04	754.30	75.43	7.54
N_2				
294	421.75	42.18	4.22	0.42
473	817.85	81.79	8.18	0.82
673	1331.72	133.17	13.32	1.33
873	1657.82	165.78	16.58	1.66
1073	2048.66	204.87	20.49	2.05
1273	2490.76	249.08	24.91	2.49
Ar				
294	470.85	47.09	4.71	0.47
473	1008.43	100.84	10.08	1.01
673	1355.38	135.54	13.55	1.36
873	2001.98	200.20	20.02	2.00
1073	2423.25	242.32	24.23	2.42
1273	2847.77	284.78	28.48	2.85
Kr				
294	373.04	37.30	3.73	0.37
473	715.43	71.54	7.15	0.72
673	1166.93	116.69	11.67	1.17
873	1395.86	139.59	13.96	1.40
1073	1775.19	177.52	17.75	1.78
1273	1914.04	191.40	19.14	1.91
SF_6				
296	185.85	18.59	1.86	0.19
373	305.79	30.58	3.06	0.31
423	320.60	32.06	3.21	0.32
473	217.63	21.76	2.18	0.22
673	377.74	37.77	3.78	0.38
873	509.26	50.93	5.09	0.51

TABLE 6. Experimental values of $\beta / \alpha P_m$ for the test gases at several representative mean pressures.

It is therefore necessary to analyse the consequences that this will have on the vapour stoichiometry.

The source-vapour-crystal system as represented in figure 14 may be used to obtain the partial pressure ratio on both sides of the porous silica disc. If the temperature of the source is constant, then there would be a constant input flux of Cd and Te_2 vapours, $n^i_{Cd} = C_{Cd}$ and $n^i_{Te_2} = C_{Te_2}$ (mols/s) respectively, with the relation

$$C_{Cd} = 2C_{Te_2} \tag{5.25}$$

for a stoichiometric source. Due to the nature of the porous silica disc, the output flow ratio of vapours will be influenced by equation 5.24. Consider first the case of a single gas flowing into a box at a constant flow rate C, and let $n_{box}(t)$ be the number of mols at any time in the box.

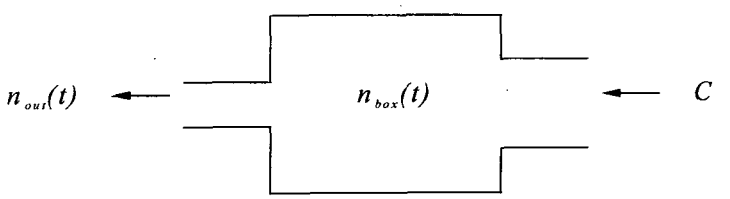

Figure 14. A simplified source-vapour-crystal system with a restrictor.

Assuming slip flow to be dominant (as discussed in the previous section), the flow output will be $n_{out}(t) = \frac{\beta_o}{\sqrt{M_{gas}}}\left(P_{box} - P_{out}\right)$, where β_o is the second term of equation

5.12 divided by ΔP and multiplied by $M^{1/2}$. If the system is being dynamically pumped, then $P_{out} \rightarrow 0$, and requiring mass continuity,

$$\frac{dn_{box}}{dt} = C - n_{out} \tag{5.26}$$

and using the ideal law of gases, the following differential equation is obtained,

$$\frac{V}{RT}\frac{dP_{box}}{dt} = C - \frac{\beta_o}{\sqrt{M}}P_{box} \tag{5.27}$$

which has the solution

$$P_{box} = \frac{C\sqrt{M}}{\beta_o}\left(1 - e^{-\frac{\beta_o RT}{\sqrt{M}V}t}\right) \tag{5.28}$$

assuming the boundary condition that at $t = 0$, $P_{box} = 0$.

Hence the pressure in the inlet side after an initial relaxation period (which depends mainly on the volume of the enclosure and the *conductivity* of the disc) becomes

$$P_{box} = \frac{C\sqrt{M}}{\beta_o} \tag{5.29}$$

Now, in the case of Cd and Te_2 vapours, and since the process of "selection" occurs inside the porous disc, rather than in the enclosure, the partial pressure ratio will be, after a dynamic steady state has been reached,

$$\frac{P_{box}^{Cd}}{P_{box}^{Te_2}} = \frac{C_{Cd}}{C_{Te_2}} \times \frac{\beta_o^{Te_2}}{\beta_o^{Cd}} \times \sqrt{\frac{M_{Cd}}{M_{Te_2}}} \tag{5.30}$$

Using 5.25, assuming that $\beta_o^{Cd} = \beta_o^{Te_2}$ and substituting values for the molecular weights, one finally obtains the relation

$$\frac{P_{box}^{Cd}}{P_{box}^{Te_2}} = 1.327 \tag{5.31}$$

It also follows from mass continuity, that the ratio of molar fluxes in the outlet side has the value

$$\left.\frac{C_{Cd}}{C_{Te_2}}\right|_{out} = 2 \tag{5.32}$$

Hence it is the stoichiometry of the vapour in the enclosure that is altered until a steady state has been reached, such that the outgoing vapour ultimately assumes the stoichiometric composition. This will always occur as long as the subliming CdTe does not alter in composition, so that a third phase is formed, in which case the partial pressures will alter to accommodate the change in phase.

The above derivation has been carried out in a different and general way by Knox and Wyatt for a dissociating compound in a Knudsen cell [43], and their results, when applied to CdTe, are in agreement with equation 5.31. The results of Knox and Wyatt were subsequently verified experimentally [44]. However, although the system in consideration here is effectively an effusion cell as shown in the previous section, some experimental evidence is needed to quantify and justify the assumptions made in the analysis, namely that: i) there is a negligible contribution to flow from the viscous term in 5.14, ii) the source stoichiometry remained constant and there was no formation of a third phase, and iii) the slip *conductivity* (i.e. β_o) of the disc was the same for both the Cd and Te_2 vapours. The latter hypothesis can be considered to apply, as it has been shown to apply to the test gases (see figure 12). ii) can only be proved to be right experimentally. Hypothesis i) may also be assumed at the range of pressures typical for vapour transport, (see table 3). However, since the ratio of the slip to viscous term,

$\beta/\alpha P_m$ depends strongly on the nature of the gas, a simple theoretical analysis has been undertaken to investigate how the partial pressure ratio would be affected if the viscous term in 5.14 becomes non-negligible. In this case, assuming that the outlet side in figure 14 has a negligible vapour pressure, the following differential equation system would apply:

$$\frac{V}{RT}\frac{dP_{box}^{Cd}}{dt} = C_{Cd} - \frac{\beta_o}{\sqrt{M_{Cd}}}P_{box}^{Cd} - \frac{\alpha_o\left(P_{box}^{Cd} + P_{box}^{Te_2}\right)^2}{2}$$

$$\frac{V}{RT}\frac{dP_{box}^{Te_2}}{dt} = C_{Te_2} - \frac{\beta_o}{\sqrt{M_{Te_2}}}P_{box}^{Te_2} - \frac{\alpha_o\left(P_{box}^{Cd} + P_{box}^{Te_2}\right)^2}{2} \qquad (5.33)$$

where α_o is the equivalent to β_o for the viscous term in 5.12. Of course this system of equations is really only valid for $\beta_o > \alpha_o$, since otherwise there would not be any selective transport, and the analogy used to derive them would not be valid. This is the case since it is the strong restriction to the output flow that allows the concept of pressure in the enclosure to be applied here. Besides these factors, the evaporation rate constants, $n_{Cd}^i = C_{Cd}$ and $n_{Te_2}^i = C_{Te_2}$ are ultimately set by the constants α_o and β_o, and hence it is ultimately not possible to solve the system analytically since the relation between the C_i constants, and α and β is unknown. The system has been solved by the Runge-Kutta method, and the results are analysed graphically for the case $C_{Cd} = 2C_{Te_2}$ (5.24) and for several values of β_o/α_o. Figure 15 shows the resulting partial pressures ratio: clearly, when slip and viscous regimes both contribute to the flow, the partial pressure ratio can adopt any value between 1.327 and 2. The relaxation times do not represent the real values, since the parameters α_o, β_o, C_i and V/RT were set to comply only with 5.24, and $\beta_o > \alpha_o$ according to the previous results.

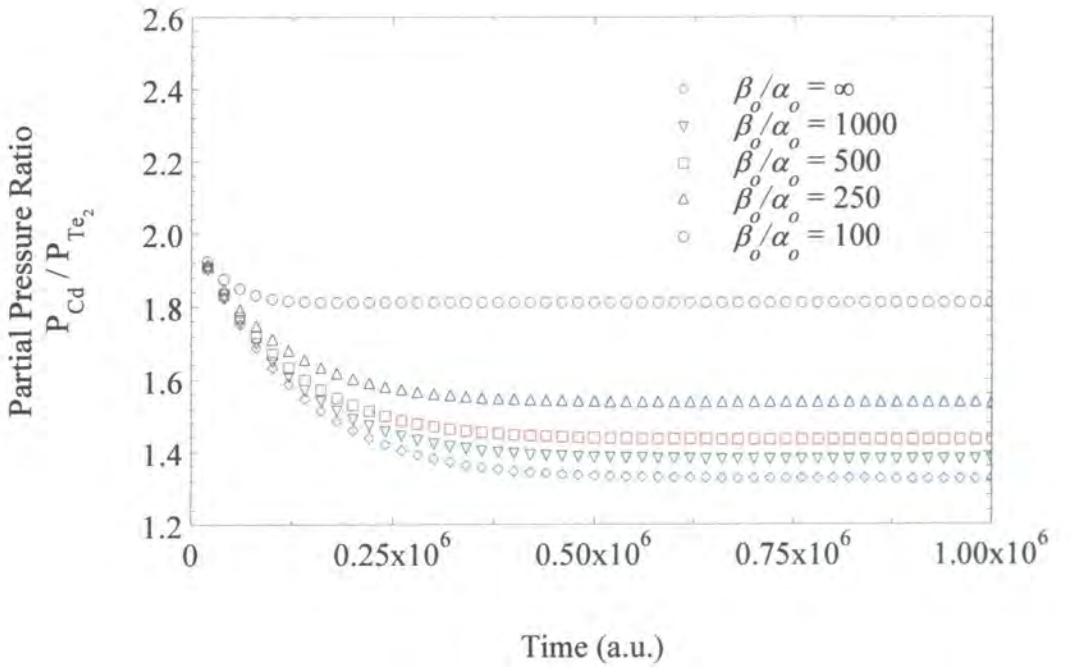

Figure 15. The effect of the ratio of slip to viscous flow on the partial pressure ratio of the vapour over the source.

5.3.3 Transport of CdTe using porous discs as restrictors: experiments and results.

Several transport experiments were carried out in order to test the predictions of the last sections concerning both theoretical transport rates and the consequences of preferential transport on vapour stoichiometry. Figure 16 shows a sketch of the experimental setup. A 50 mm length silica optical cell with flat windows and two opposite arms was used to monitor the partial pressures of Cd and Te_2 independently using the optical monitoring technique [45] developed specifically for the Durham crystal growth system and described previously in detail in chapter four. Here, it is sufficient to say that partial pressures were determined by measuring the absorbance or optical density of Cd and Te_2 vapours at selected wavelengths during the whole

transport process. Previous calibration allows the absorbance or optical density of each species to be related to their partial pressures in the cell. A known weight (~ 1 gm) of CdTe (previously sublimed in vacuum in order to adjust its stoichiometry) was loaded into one end of the first arm, meanwhile the second arm was connected to a rotary pump. Two Pt/Rh thermocouples were used for accurate reading of the CdTe temperature throughout the runs. The whole ampoule was inserted in a two zone furnace, where the temperatures of the cell and porous disc could be set independently of the source temperature. Between the cell and the CdTe charge a silica porous disc, of the same mean pore size as the one previously studied was inserted.

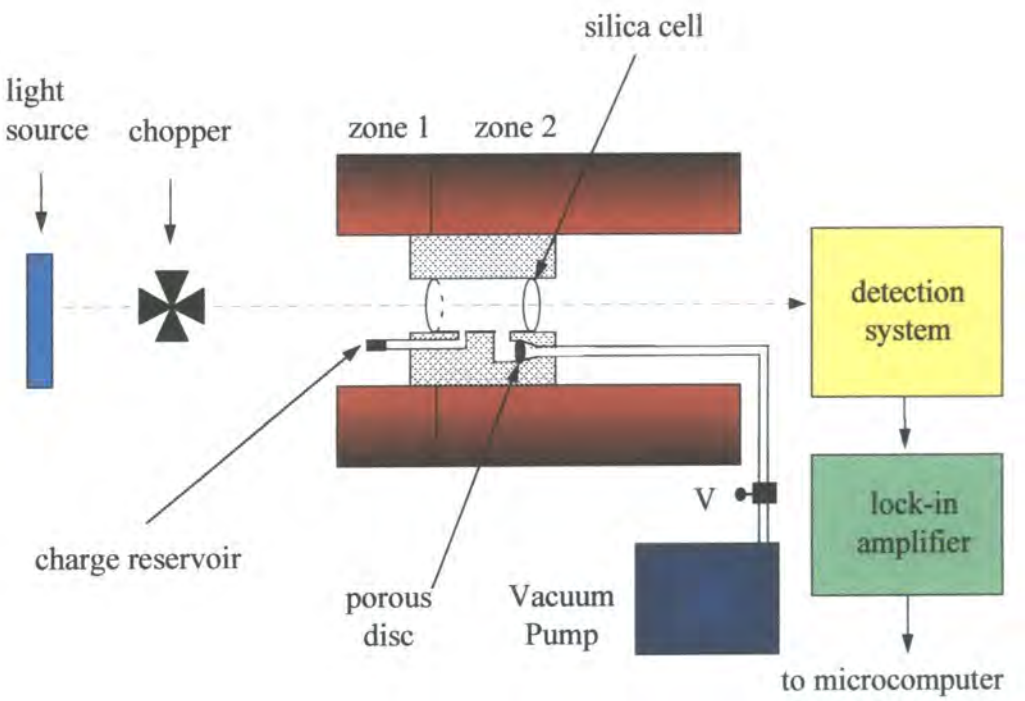

Figure 16. Experimental setup used in the CdTe transport and vapour stoichiometry control experiments.

All the experiments but one were done under dynamic vacuum. This is the case since the porous silica disc alone cannot produce any differential pressure which is totally independent of the temperature gradient in a sealed system, i.e. cannot control

the mass flow rate. In one case, a test experiment was undertaken with the second arm sealed off and the partial pressures at the outlet side monitored. As expected, a pressure build up of one vapour component took place (in this case, cadmium) and transport did not proceed.

In another experiment, the vapour between the source and the disc was monitored. The sintered disc was placed in the outlet, dynamically pumped tube but immediately next to the cell. The source consisted of small chunks 1-4 mm in size of CdTe, weighing 0.527 gm and contained in a length of the tube of about 3 cm. The cell was brought to 960 °C, and once the temperature was stabilised, the temperature of the source was rapidly raised from 608 °C, where the partial pressures of CdTe are negligible, to a mean temperature of 869 °C (886 °C at one end of the source, and 852 °C at the other), where the equilibrium vapour pressure of CdTe in a closed enclosure is expected to be 14.5 mbar. As the experiment proceeded, deposition of the transported material took place initially at the end edge of the outlet tube, which was at room temperature, but progressively moved in the direction of the cell. At any time, the maximum temperature of the deposited CdTe was 595 °C, and hence the residual vapour pressure was totally negligible. Figure 17 shows the partial pressure ratio for the vapour over the source. Once all the material had been transported, the vapour pressures both dropped simultaneously to a value approaching zero mbar. This shows that the stoichiometry of the source did not change during the course of the sublimation experiment. Also, it can be seen that although the temperature of the charge effectively changed slowly as it was being sublimated, due to the thermal gradient, the partial pressure ratio remained approximately constant, its mean value during the transport process over the source being 1.302. This result is in excellent agreement with the

value of 1.327, predicted in equation 5.31, for the case of no viscous flow present. Hence one can conclude that the main transport mechanism was that due to transition or slip flow, as expected. This result cannot be overemphasised, since it clearly implies that in a typical crystal growth experiment in the Durham system, the vapour pressure over the CdTe source will not be stoichiometric when a porous disc is used as a restrictor. It also demonstrates that a third phase is not formed in the source, and it justifies the use of the slip term alone in 5.14, which greatly simplifies any calculation of mass flow through the porous disc. It also illustrates that the porous disc is an excellent restrictor for vapour transport of CdTe. If the same amount of material was to be transported under the same conditions except for the presence of the disc, the charge would have been transported in a matter of several minutes rather than several hours.

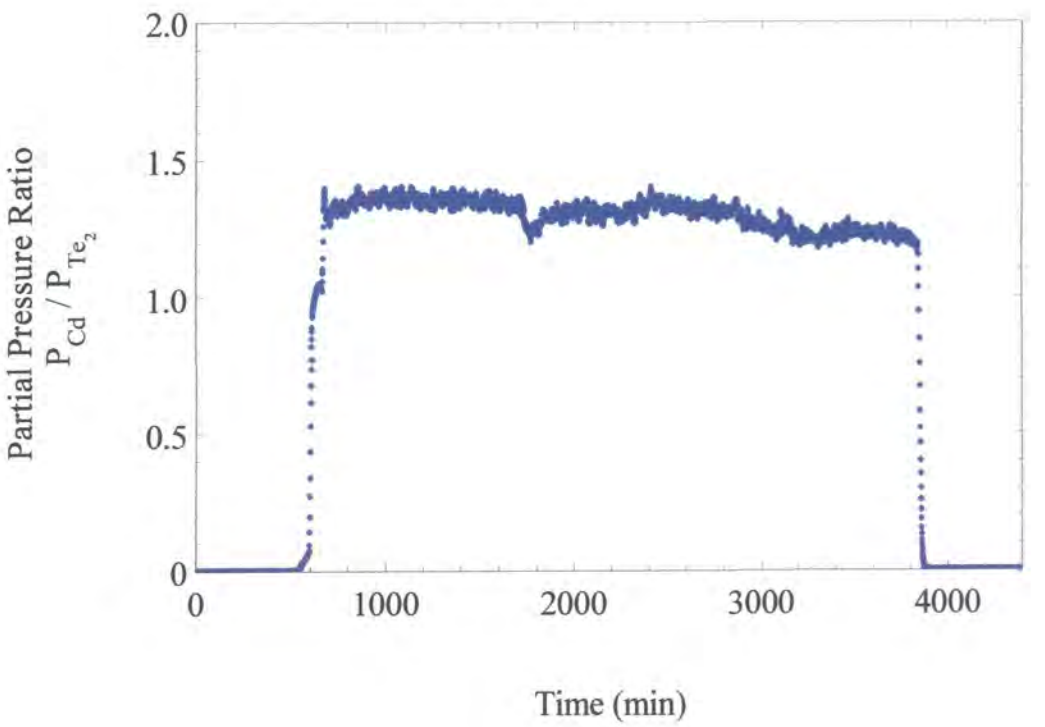

Figure 17. Partial pressure ratio of the vapour over the source during transport through the porous disc.

5.4 APPLICATION TO CdTe VAPOUR GROWTH.

5.4.1 Calculation of the optimum porous disc parameters for CdTe crystal growth.

If one assumes that the growth rate is only dependent on the mass transfer rate, i.e. the sublimation and interfacial kinetic mechanisms are not the rate determining processes, it is possible to model the porous silica disc restrictor necessary to obtain the desired transport rate for optimum CdTe crystal growth. From equation 5.12, we see that there are two kinds of parameters that influence transport rates directly: the intrinsic parameters of the silica disc, namely the porosity ε, the specific surface area S, the slip factor Z and the thickness and area, L and A respectively. The extrinsic parameters are the temperature of the disc and vapours, T, and the mean and differential pressures, P_m and ΔP. All three extrinsic parameters are dependent on both the source and seed temperatures, since the first determines the minimum temperature of the crossmember, which is in turn the temperature of the disc, meanwhile P_m and ΔP are determined by the temperature of the source when the seed temperature is comparatively low, and by both when source and seed temperatures are close. The whole flow dynamics and its consequences for the growth chamber will be discussed extensively in a later chapter.

The intrinsic parameters are not mutually independent, and hence modelling of each of them as a function of the rest is not possible. The thickness and area of the disc are set by the manufacturing process, and given the diameter, the thickness cannot be chosen. In a similar way, given the porosity of the porous disc, the specific surface area cannot be arbitrarily chosen, since these two parameters are intimately linked. Schwertz [31] performed several flow experiments with porous Pyrex discs of different but close

porosities and showed that small increases of as much as 15 % in ε increased the specific surface area S by a factor of 6. Also, the slip factor Z increased by 62 %, and appeared to increase linearly with the reciprocal of the specific surface area. However, the discs had different mean particle size, a case that does not apply here since it is possible to obtain discs which are made using the same mean particle size as the ones used in all the previous experiments. Therefore, the estimation of mass transport rates can only be done graphically as a function of each pair of parameters.

Three parameters will be set from previous experimental results. The intrinsic parameters k_v and Z, are taken from the bibliography and previous experiments in this work respectively. To make Z a constant parameter is reasonable since for a porous disc of a given ε and S, Z is unique. The viscosity η, is calculated from standard expressions obtained from the kinetic theory of gases or from the literature [46]. For the sake of clarity, it is assumed that at any time, the composition of the vapour in the inlet side is stoichiometric, but in any case it is well known [24, 47] that small changes in the composition of a mixture of gases results in only a small variation of the viscosity, and also it has been shown already that the viscous contribution to transport is nearly negligible in the range of vapour pressures of interest for CdTe transport. It is also important to point out that all the calculations were made assuming a gas formed by CdTe molecules, with $M = 240$ gm/mole.

Figure 18 shows the variation of the transport rate as a function of the length of the porous disc for several diameters of the disc. The plot was obtained assuming that all the other variables had the values of table 7, typical of vapour growth experiments. In particular, the values of ε, S and Z were taken from the tested disc.

$\varepsilon = 0.39$
$\Delta P = 20$ mbar
$P_m = 10$ mbar
$S = 2340$ cm^{-1}
$\eta = 9 \times 10^{-4}$ gm.cm^{-1}.s^{-1}
$T = 1223$ K
$Z = 0.611$

TABLE 7. Values used in the mass transport calculations through a disc.

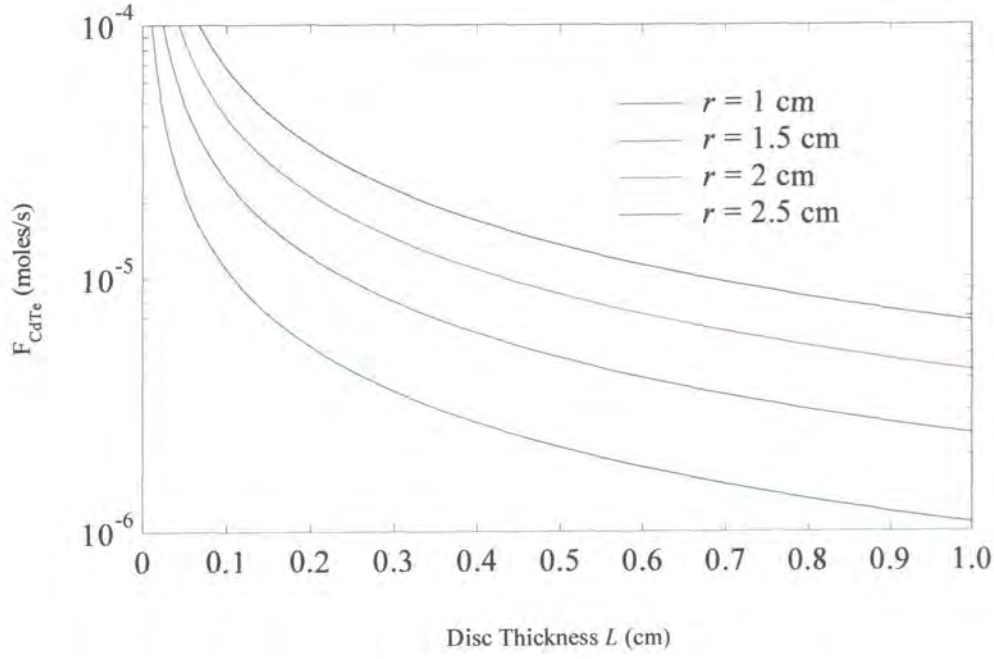

Figure 18. Variation of transport rate with disc length for several disc radii.

The range of thickness available is between 0.3 and 0.5 cm for the diameters considered here. Transport rate can be increased or decreased by an order of magnitude simply by increasing or decreasing the diameter from 2 to 5 cm.

The variation of transport rate with porosity and specific surface is even more marked. Figure 19 shows the variation of transport rate with specific surface areas in the range of porosities of interest. The values of S used in the upper and lower cases can be considered as the minimum and maximum values than one could encounter for a given mean particle size. Since the surface area cannot be obtained before doing the flow experiments for each particular sample, figure 19 is of particular relevance, since it gives an estimation of the transport rates in the best and worst cases, allowing the extrinsic parameters to be modelled.

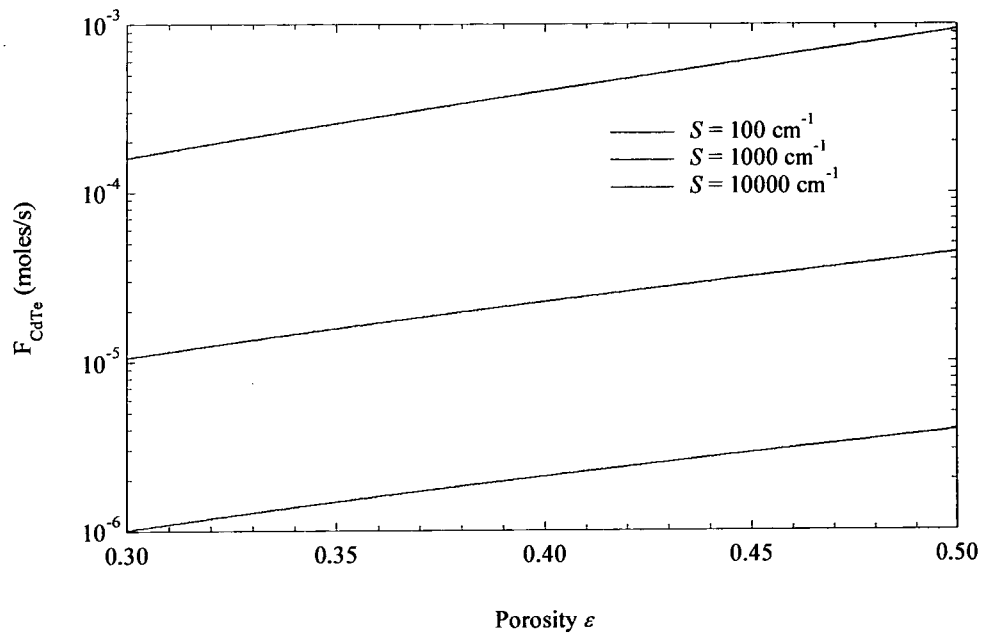

Figure 19. Dependence of the transport rate on the porosity for several possible specific surface areas. Curves are calculated with values from table 7 and $L = 0.5$ and $r = 2$ cm.

The extrinsic parameters are probably the most important in modelling transport rate, since once the intrinsic parameters have been chosen, the temperature T of the disc and gas and the mean and differential pressures can still dictate the transport rate. Of the

three, the temperature of the disc T is the one that exercises the least influence on the transport rate. This can be seen in figure 20.

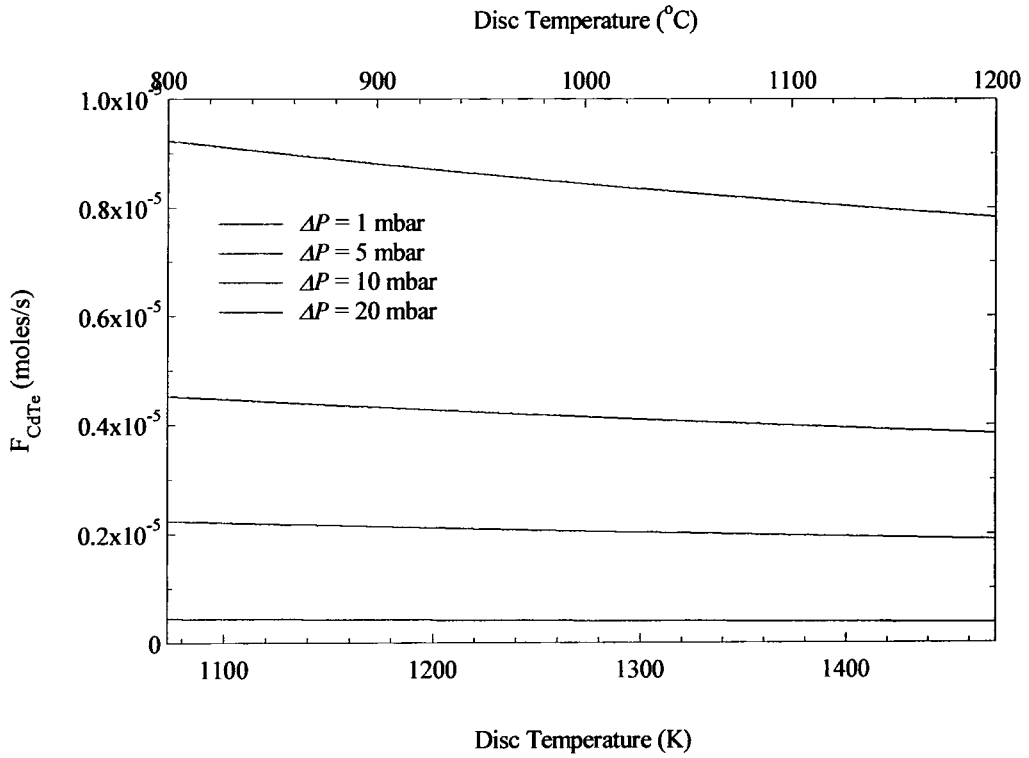

Figure 20. Variation of the transport rate with disc temperature for various ΔP. Calculated curves using table 7, L = 0.5 cm, r = 2 cm and assuming $P_m = \Delta P/2$ in all cases.

Since during growth, and assuming that the growing crystal is near equilibrium, the vapour pressure in the growth side could be set not only by the pump and porous disc, but also by the temperature of the crystal itself, it is necessary to study the transport rate in cases where $\Delta P \neq 2P_m$. In this case, it is necessary to model the flow rate as a function of the pressure in the outlet (growth side), for several typical inlet (source side) pressures, since both the mean pressure and the differential pressure depend on them. The result of the modelling, using the values of table 7, is shown in figure 21.

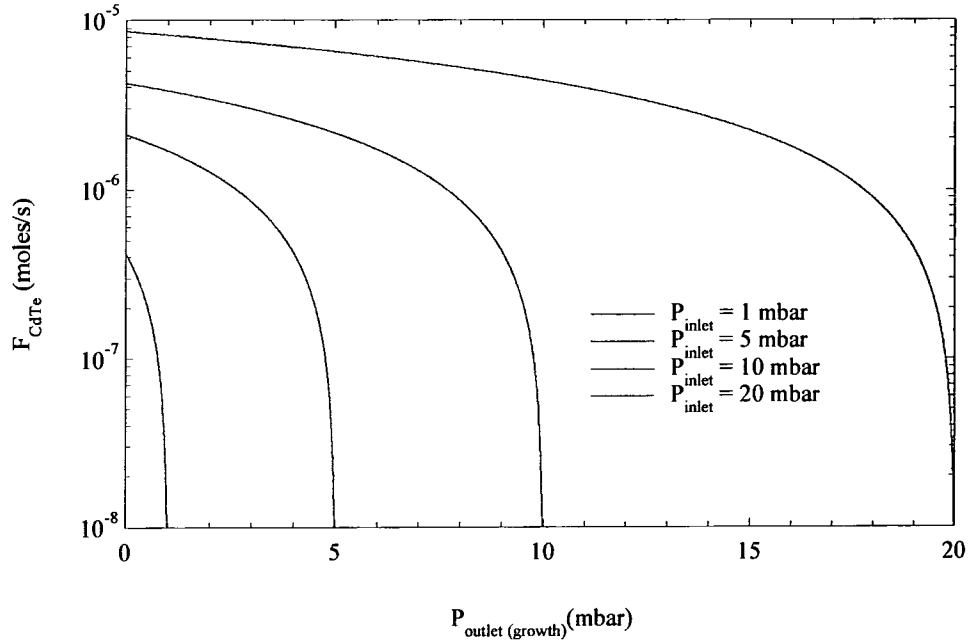

Figure 21. The influence of the pressure in the growth side on the transport rate for several typical source pressures, using the values of table 7.

Two main conclusions can be drawn from the above figure. First, the transport rate is highly dependent on both source and growth temperature, as expected. Second, and more important, to obtain constant, stable transport it is necessary to maintain the source at a constant temperature through the growth run. The growth temperature is not so important when small (and inevitable as the crystal grows) temperature shifts or fluctuations occur, since the transport rate is more strongly dependent on the source temperature than on the growth temperature.

5.4.2 Characterisation of the porous disc used in the Durham system.

In order to obtain the intrinsic parameters that determine the transport behaviour of the porous disc used in the crystal growth system, several *in situ* gas flow experiments were carried out in the same way as done previously with the test disc.

Figure 22 shows a plot of the specific gas flow as a function of mean pressure for four test gases. The results are similar to those encountered before, as expected. Using the same methodology of section 5.3, and the known dimensions of the disc, which was chosen arbitrarily and according to design requirements, one can obtain the parameters Z and S. The values found were:

$$S = 1038 \text{ cm}^2 / \text{cm}^3$$

$$Z = 0.346$$

The porosity of the porous disc was measured as before with three different methods, giving $\varepsilon_\rho = 0.28$, $\varepsilon_k = 0.29$ and $\varepsilon_w = 0.17$. This last figure is unexpected and extremely low when compared to other discs of the same porosity grade, and means that there are domains or regions with closed pores in the porous disc that will make no contribution to the flow. The length and effective area of the disc were 0.47 cm and 4.90 cm^2 respectively.

Using the values of the intrinsic parameters, it is possible to obtain accurate predictions of CdTe mass transport rates. This is shown in figure 23. In all the curves, the temperature of the disc was assumed to be 950 °C and accordingly a viscosity η_{CdTe} $= 9.0 \times 10^{-4}$ $\text{gm.cm}^{-1}.\text{s}^{-1}$ [46]. It can be seen that in the best of the cases, the growth rate corresponding to a 5 cm diameter crystal is about 0.2 cm per day. But it is also clear that the source temperature that produces the pressure in the inlet side is of paramount importance, since a few tens of degrees increase can cause an increase of the transport rate by an order of magnitude. It is clear in here that the porous disc chosen was too restrictive for transport. Indeed, this was the case, since trial experiments using CdTe showed little transport, in agreement with the order of magnitude that figure 23 shows.

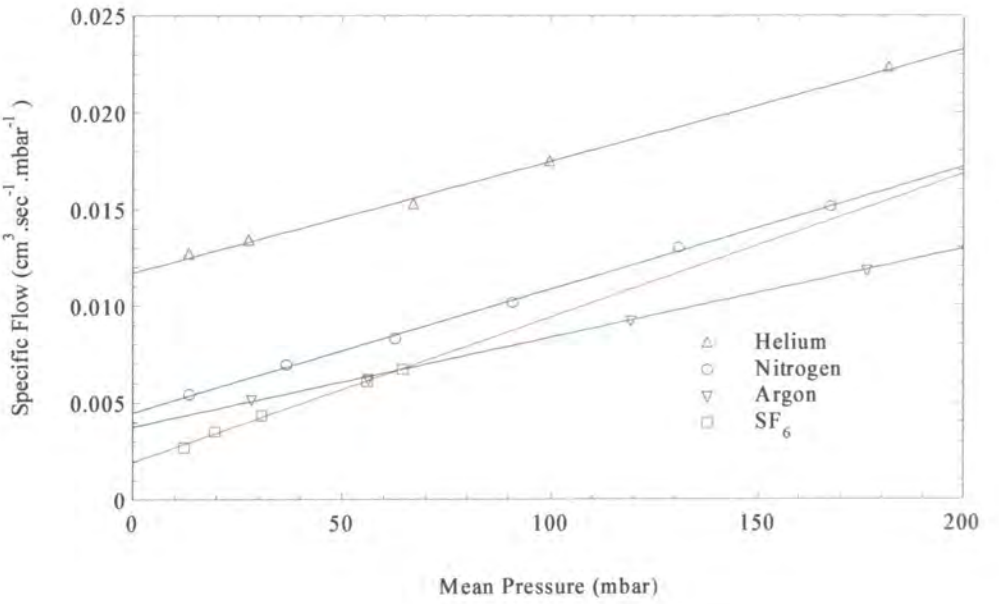

Figure 22. Flow of He, N_2, Ar and SF_6 at room temperature as a function of mean pressure. Measurements were done in-situ in the Durham crystal growth system.

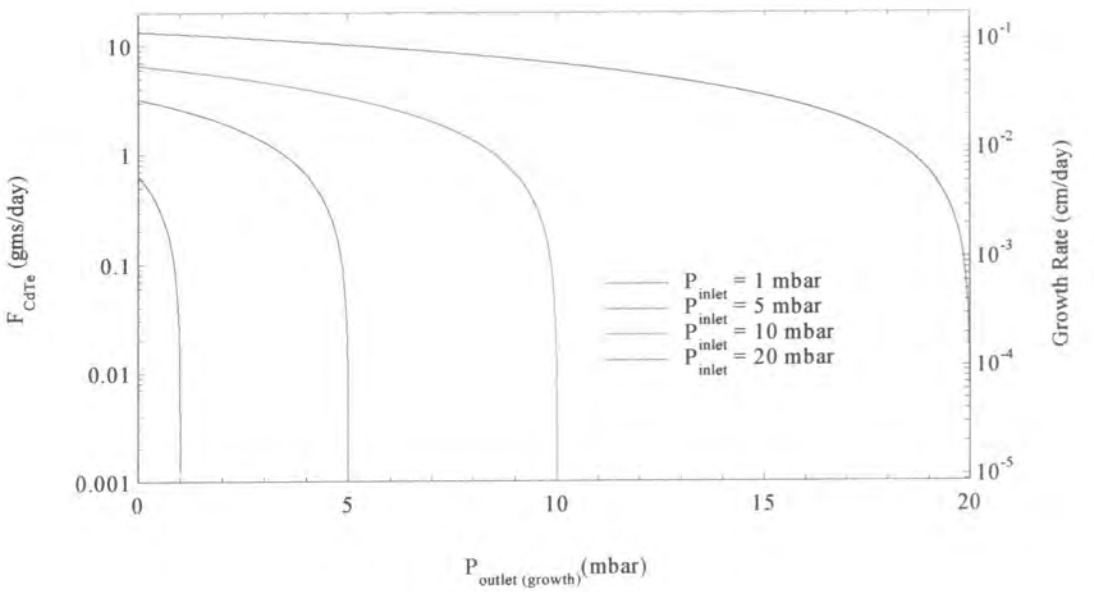

Figure 23. Mass transport through the characterised porous disc used in the Durham growth system. Calculated rates for a 5 cm diameter and 0.2 length disc at 950 °C.

5.5 DISCUSSION AND CONCLUSIONS.

The structure and the gas flow *conductivity* of porous silica disc restrictors for use in mass flow control of Cd and Te_2 vapours during vapour crystal growth have been studied in detail. The porous silica discs studied here have very low flow *conductivity*, and hence when used as flow restrictors during dynamic vacuum, the mass transport can be reduced and controlled when the extrinsic and intrinsic parameters of the vapour and porous disc respectively are chosen adequately. The consequences of flow restriction during dynamic pumping cannot be overstressed: the driving force for crystal growth is not anymore the differential pressure between source and crystal produced by a temperature gradient, but a physical device, the porous disc. This allows in principle the decoupling of source and growth temperatures, i.e. the growth temperature is not constrained by the source temperature. In particular, it has been shown that the Kozeny-Carman equation (5.14) for flow of gases through porous silica discs can be used to quantify the gas or vapour flow regimes. It also has been shown that for typical temperatures and vapour pressures encountered during vapour growth of CdTe, the flow regime through the restrictor can be considered to be of the slip type only. This has several consequences: i) it greatly simplifies the modelling of the extrinsic and intrinsic parameters of the porous disc in order to obtain the desired mass transport rate during growth and ii) the stoichiometry of the vapour over the source will be upset during growth, the partial pressure ratio P_{Cd} / P_{Te_2} being not congruent anymore, but having a value close to 1.32. This important result has been both predicted theoretically and experimentally verified. Mass continuity requires a stoichiometric vapour over the crystal, and hence the upset of vapour composition over the source should not have any consequences on the growth process.

Finally, it has been shown that a very simple modelling of the porous silica disc parameters using typical CdTe vapour growth conditions can be carried out in order to both choose and estimate the mass transport through the restrictor. This allows in principle the option to choose the growth rate and conditions (growth temperature, temperature gradient and supersaturation) as well as its study.

REFERENCES FOR CHAPTER FIVE

[1] N. Yellin and S. Szapiro. *"Vapor Transport of Nonstoichiometric CdTe in Closed Ampoules"*. J. Crystal Growth, **69** (1984) 555.

[2] M. M. Faktor and I. Garret. *Growth of Crystals from the Vapour*. Chapman and Hall, London (1974).

[3] M. M. Faktor, R. Heckingbottom and I. Garret. *"Growth of Crystals from the Gas Phase Part 1. Diffusional Limitations and Interfacial Stability in Crystal Growth by Dissociative Sublimation"*. J. Chem. Soc. **A**, (1970) 2657.

[4] F. Rosenberger. *Fundamentals of Crystal Growth I: Macroscopic Equilibrium and Transport Concepts.* Springer Series in Solid State Sciences. Edited by M. Cardona, P. Fulde and H. J. Queisser. Springer-Verlag, Berlin (1979).

[5] K. Zanio. *Cadmium Telluride.* Semiconductors and Semimetals Treatise, Volume 13. Edited by R. K. Willardson and A. C. Beer. Academic Press, London (1978).

[6] F. Rosenberger, M. Banish and M. B. Duval. *Vapour Crystal Growth Technology Development – Application to Cadmium Telluride.* NASA Technical Memorandum 103786 (1991).

[7] H. M. Cox, S. G. Hummel and V. G. Keramidas. *"Vapor Levitation Epitaxy: System Design and Performance"*. J. Crystal Growth, **79** (1986) 900.

[8] P. N. Gadgil. *"Capillary plug flow distributor for stagnation point flow APCVD reactor"*. Materials Letters, **20** (1994) 351.

[9] M. Laasch, T. Kunz, C. Eiche, M. Fierderle, W. Joerger, G. Kloess and K. W. Benz. *"Growth of Twin-free CdTe Single Crystals in a Semi-closed Vapour Phase System"*. J. Crystal Growth, **174** (1997) 696.

[10] Y. V. Korostelin, V. I. Kozlovsky, A. S. Nasivov and P. V. Shapkin. *"Vapour Growth of II-VI Solid Solution Single Crystals"*. J. Crystal Growth, **159** (1996)181.

[11] A. Y. Fadeev, O.R. Borisova and G.V. Lisichkin. *"Fractality of Porous Silicas: A Comparison of Adsorption and Porosimetry Data"*. J. Colloid Interface Sci., **183** (1996) 1.

[12] F. A. L. Dullien. *Porous Media, Fluid Transport and Pore Structure.* Academic Press, London (1979).

[13] R. Jackson. *Transport in Porous Catalysts.* Elsevier, Amsterdam (1977).

[14] C. N. Satterfield. *Mass Transfer in Heterogeneous Catalysis.* MIT Press, Cambridge, MA (1970).

[15] C. N. Satterfield. *Heterogeneous Catalysis in Practice.* Chemical Engineering Series. McGraw-Hill, New York (1980).

[16] M. C. Robert and F. Lefaucheux. *"Crystal Growth in Gels: Principle and Applications".* J. Crystal Growth, **90** (1988) 358.

[17] R. B. Evans III, G. M. Watson and E. A. Mason. *"Gaseous Diffusion in Porous Media. II. Effect of Pressure Gradients".* J. Chem. Phys., **36** (1962) 1894.

[18] E. A. Mason and A. P. Malinauskas. *Gas Transport in Porous Media: The Dusty-Gas Model.* Elsevier, Amsterdam (1983).

[19] P. C. Carman. *Flow of Gases Through Porous Media.* Butterworths, London (1956).

[20] *Sixth State-of-the-Art Symposium on Flow Through Porous Media.* Washington, D.C. June 9-11 (1969). Chaired by R. J. Nunge. Reprinted from Industrial And Engineering Chemistry. American Chemical Society Publications, Washington D.C. (1970).

[21] R. D. Present. *Kinetic Theory of Gases.* McGraw-Hill, New York (1958).

[22] W. G. Pollard and R. D. Present. *"On Gaseous Self-Diffusion in Long Capillary Tubes".* Phys. Rev., **73** (1948) 762.

[23] G. P. Brown, A. DiNardo, G. K. Cheng and T. K. Sherwood. *"The Flow of Gases in Pipes at Low Pressures".* J. Appl. Phys., **17** (1946) 802.

[24] J. Jeans. *An Introduction to the Kinetic Theory of Gases.* Cambridge University Press, London (1940).

[25] S. Dushman and J. M. Lafferty. *Scientific Foundations of Vacuum Technique.* 2nd ed. John Wiley & Sons, New York (1962).

[26] J. Emsley. *The Elements.* 2nd ed. Clarendon Press, Oxford (1991).

[27] H. Adzumi. Bull. Chem. Soc. Japan, **12** (1937) 304. Cited by P. C. Carman in [19].

[28] T. K. Tokunaga. *"Porous Media Gas Diffusivity from a Free Path Distribution Model".* J. Chem. Phys., **82** (1985) 5289.

[29] R. A. Svehla. NASA Technical Report R-132 (1962).

[30] W. Palosz and H. Wiedemeier. *"Physical Vapor Transport of Cadmium Telluride in Closed Ampoules".* J. Crystal Growth, **129** (1993) 653.

[31] F. A. Schwertz. *"The Structure of Porous Materials from Gas Penetration Rates"*. J. Appl. Phys., **20** (1949) 1070.

[32] P. C. Carman. *"Diffusion and Flow of Gases and Vapours Through Micropores I. Slip Flow and Molecular Streaming"*. Proc. Roy. Soc. London A, **203** (1950) 55.

[33] S. J. Gregg and K. S. W. Sing. *Adsorption, Surface Area and Porosity.* Academic Press, London (1967).

[34] R. M. Barrer and D. M. Grove. *"Flow of Gases and Vapours in a Porous Medium and Its Bearing on Adsorption Problems. Part I: The Steady State Flow"*. Trans. Faraday Soc., **47** (1951) 826.

[35] H. Kozuka and S. Sakka. *"Formation of Silica Gels Composed of Micrometer Sized Particles by the Sol-Gel Method"*, in *The Colloid Chemistry of Silica.* Advances in Chemistry Series, volume 234. American Chemical Society, Washington D.C. (1994).

[36] G. Kraus, J. W. Ross and L. A. Girifalco. *"Surface Area Analysis by Means of Gas Flow Methods I. Steady State Flow in Porous Media."*. J. Phys. Chem., **57** (1953) 330.

[37] C. P. Ellis and C. J. G. Raw. *"High Temperature Gas Viscosities. II. Nitrogen, Nitric Oxide, Boron Trifluoride, Silicon Tetrafluoride and Sulfur Hexafluoride"*. J. Chem. Phys., **30** (1959) 574.

[38] R. E. Collins. *Flow of Fluids Through Porous Materials.* Chapman & Hall, London (1961).

[39] Data recompiled from: J. Kestin, S. T. Ro and W. A. Wakeham. *"Viscosity of Noble Gases in the Temperature Range 25-700 °C"*. J. Chem. Phys., **56** (1972) 4119, and Landolt-Bornstein Handbook, II Band, 5 Teil, Bandteil a, Transportphanomenae I, Springer-Verlag, Berlin (1969).

[40] Data recompiled from: V. Vasilesco. Annal. Physique, **20** (1945) 137, 292, and reference [42] of this chapter.

[41] Data recompiled from: V. Vasilesco. Annal. Physique, **20** (1945) 137, 292, and reference [21] of this chapter.

[42] M. Rigby and E. B. Smith. *"Viscosities of the Inert Gases"*. Trans. Faraday Soc., **62** (1966) 54. See also reference [47] of this chapter.

[43] J. H. Knox and P. A. Wyatt. *"Calculation of Vapour Pressures from Effusion Measurements for Dissociated Vapours"*. J. Chem. Soc., Faraday Trans. I. (1973) 1961.

[44] R. F. C. Farrow, G. M. Williams, P. W. Sullivan, G. R. Jones, D. G. Coates and J. T. M. Wotherspoon. *"The Vaporisation of $Hg_{1-x}Cd_xTe$ and Its Binary End Member Compounds"*. Extended Abstracts of the 2nd BACG Meeting on the Crystal Growth and Characterisation of II-VI Compounds. Chaired by J. B. Mullin. University of Lancaster (1980).

[45] J. Carles, J. T. Mullins and A. W. Brinkman. *"Partial Pressure Monitoring in Cadmium Telluride Vapour Growth"*. J. Crystal Growth, **174** (1997)740.

[46] R. Schwarz. *"Dotierte, massive CdTe – Einkristalle aus der Gasphase"*. Ph. D. Dissertation, Albert-Ludwigs-Universität Freiburg, Germany (1995).

[47] *Handbook of Physical Quantities*. Edited by I. S. Grigoriev and E. Z. Meilikhov. CRC Press, New York (1997).

Chapter Six

Flow Modelling in the Multi-tube PVT Growth Apparatus

6.0 INTRODUCTION.

In this chapter, a model to describe the flow of vapours in the growth apparatus is presented. The fact that growth takes place in a semiopen system will have some consequences for both the transport rates (the presence of diffusion barriers will be limited), due to different flow regimes, and more importantly, on the partial pressure ratio of the vapour (both over the source and crystal). It is unclear what effects the semi-open nature of the ampoule might have on the crystal quality. The innovative design of the growth apparatus provides for a unique opportunity to obtain the partial pressures during growth. As will be seen later, the partial pressure ratio $\alpha = p_{Cd} / p_{Te_2}$ is not two, as might be expected. A model is provided to account for this unexpected behaviour, based on the premise that the partial pressure ratio depends on the *conductivities* of the different elements that form the growth ampoule, namely the capillary or porous silica disc that restrict the mass transport rate, the annular section where the crystal sits and leaks in the glass joints. The model also provides an estimate for the transport rates of CdTe, and once the conductivities of the different glassware elements are quantified theoretically, the growth rate can be obtained as a function of the partial pressures.

6.1 VAPOUR FLOW CHARACTERISTICS OF THE GROWTH APPARATUS ELEMENTS.

In this section the flow conductivities of the crossmember capillary (the case of a porous silica disc was extensively studied in chapter four) and that of the annular section in the growth pedestal are studied from a theoretical point of view for several possible flow regimes.

6.1.1 Flow Through the Glass Joints in the Crossmember.

Since the total pressure during growth in the vacuum jacket that encloses the growth glassware is better than 10^{-5} mbar, the source and growth total pressures are in the range 1-20 mbar and the glass joints are not perfectly tight, some material will be transported through the annular cones that form the joints into the vacuum chamber. Although the material loss may be negligible, its effect on the vapour stoichiometry in both source and growth sides can be important. Indeed, as shown in chapter 4, if the flow through the annular cone gap is molecular or Knudsen type, or has a slip component, the presence of these "leaks" will influence to some extent the partial pressure ratio of the vapour.

Given the dimensions of the annular cone shaped gap, and the range of pressures encountered in the source and growth tubes, it is possible to assess whether the flow will be molecular or not. The length of the cone was determined to be $l_{lg} = 46.5 \pm 0.1$ mm. It was not possible to measure accurately the thickness of the gap, but it was estimated to be $r_{lg} \sim 1$ μm. Since according to table 1, the mean free path during typical growth temperatures and pressures is at least one order of magnitude larger than the size of the gap, it may be concluded that the flow will be mainly of molecular type during growth. Clearly, if the conductivity of the annular shaped glass joints is much larger than that of the capillary or porous disc and annulus, the partial pressure ratio $\alpha = p_{Cd} / p_{Te_2}$ will, after a relaxation period, adopt a value close to 1.327, since the situation here is analogous to that encountered for a porous silica disc in chapter 4. Intuitively however, one would expect the flow conductivity of the glass joints to be several orders of magnitude smaller than that of the other components, and hence a ratio $1.327 < \alpha < 2$ can be expected in both source and growth sides of the crossmember. Therefore, it is

important, in any analysis of the mass transport in the growth apparatus, to quantitatively take into account the flow that takes place through leaks in the glass joints. The importance of such leaks in closed vapour crystal growth systems was realised earlier by Faktor *et al.* [1,2], who used calibrated leak holes to control the stoichiometry of the vapour near the crystal during growth as well as to eliminate the accumulation of volatile impurities in the vapour.

6.1.2 Flow Through the Restrictor in the Crossmember.

In this section, the flow through the capillary in the crossmember is analysed. The importance of understanding the flow mechanisms through the particular capillary is vital, since they can influence mass transport rates and hence the growth rates. More importantly, it allows growth parameters to be selected and the growth process to be studied as a function of them. Several flow regimes that might take place in the capillary of the crossmember will be described here (turbulent or compressible flow will not be considered here, since for the low pressures and flow rates of interest, the Reynolds number, which determines whether flow will be turbulent or not, is too low [3]. These regimes are the viscous regime, the molecular or Knudsen regime and the slip or transition regime. There are no clear boundaries between them, but the *Knudsen* number, defined as $K_d = \lambda / r$ where λ is the mean free path of the gas, and r is the radius of the capillary, gives an indication of the type of flow [4]:

Molecular flow	$K_d > 3$
Transition or slip flow	$3 > K_d > 0.01$
Viscous flow	$K_d < 0.01$

Viscous flow in a capillary has been discussed in chapter 5. Given that the conditions for its validity are obeyed, the expression is:

$$\varphi_c\left(\frac{moles}{t}\right)=\frac{\pi r^4 p_m \Delta p}{8\eta LRT} \tag{6.1}$$

For the particular capillary in use here, L = 11.7 ± 0.1 mm and r = 0.61 ± 0.1 mm, there are two important consequences that should be emphasised. First, although the range of mean free paths for the range of temperatures and pressures encountered during growth is very wide (table 1), given the radius of the capillary, it can be seen that only for source vapour pressures of 20 mbar, when K_d ~ 0.01, can the flow be considered to be fully viscous. Hence one would expect 6.1 not to hold strictly.

λ (μm)	T (K)	20 mbar	15 mbar	10 mbar	5 mbar	1 mbar	0.5 mbar	0.1 mbar
Cd	1073	24.6	32.7	49.1	98.2	491	982	4911
	1123	25.7	34.3	51.4	103	514	1028	5140
	1173	26.8	35.8	53.7	107	537	1074	5369
	1223	28.0	37.3	56.0	112	560	1120	5598
	1273	29.1	38.8	58.3	117	583	1165	5827
Te_2	1073	10.6	14.1	21.2	42.4	212	424	2120
	1123	11.1	14.8	22.2	44.4	222	444	2219
	1173	11.6	15.5	23.2	46.4	232	464	2318
	1223	12.1	16.1	24.2	48.3	242	483	2417
	1273	12.6	16.8	25.2	50.3	252	503	2516

TABLE 1. Calculated mean free paths (in mm) of Cd and Te_2 for several possible growth conditions.

Secondly, the aspect ratio L / r = *19.2* is relatively small, hence viscous flow may not be fully developed. According to Dushman, this results in a lower flow rate for a given pressure difference, or, alternately, an increase in the pressure drop for a

required flow rate. It has been shown [5] that the flow will become fully developed in a distance l_d from the entrance of the capillary given by,

$$l_d = 0.227 r \mathrm{R} \qquad \text{(cm)} \tag{6.2}$$

where R is the Reynolds number. From the definition of the Reynolds number,

$$l_d = \frac{0.227 MF\Delta p}{\pi \eta RT} \qquad \text{(cm)} \tag{6.3}$$

where F is the volumetric flow rate. For T = 950 °C and $\eta = 9.0 \times 10^{-4}$ poises, and for Δp = 20 mbar, the transition length is

$$l_d = 3.8 \times 10^{-3} F \qquad \text{(cm)} \tag{6.4}$$

Hence, for flow rates smaller than ~ 10 cm^3/s, it can be assumed that viscous flow is fully established.

Since both features have the effect of lowering the flow rate [5], equation 6.1 can still be very useful to obtain an upper limit of the flow rate through the capillary. In particular, for the capillary dimensions used here, and a crossmember temperature T_c = 950 °C and $\eta = 9.0 \times 10^{-4}$ poises, the flow rate would be:

$$\varphi_c \left(\frac{moles}{t} \right) = 5.078 \times 10^{-8} p_m \Delta p \tag{6.5}$$

with p_m and Δp in mbar, or in terms of the source and growth pressures,

$$\varphi_c \left(\frac{moles}{t} \right) = 2.539 \times 10^{-8} \left(p_s^2 - p_g^2 \right) \tag{6.6}$$

with p_s and p_g in mbar. The results of this equation can only be interpreted as an upper limit to the mass transport rate, not just as a consequence of the specific dimensions of the capillary, and the crossmember temperature, but also of the dependence of viscosity on temperature and vapour composition. The viscosity variation as a function of vapour

mixture composition is, by no means easy to calculate, since it is a complicated function of the composition and unknown parameters [6]. Figure 1 shows several examples of transport rates of CdTe through the capillary for several typical source vapour pressures and assuming a stoichiometric vapour mixture.

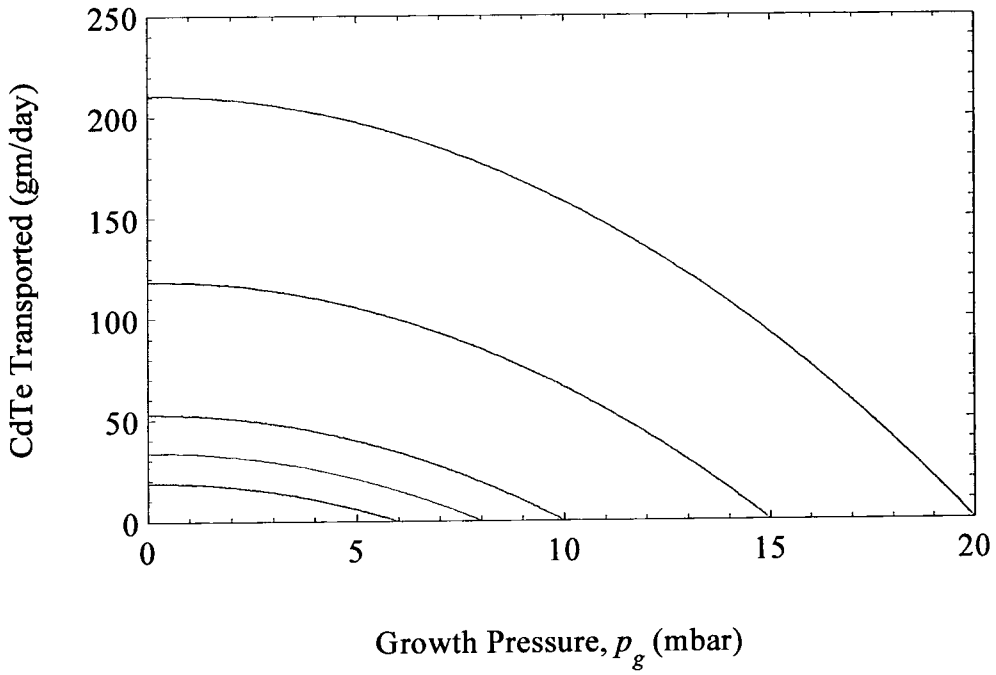

Figure 1. Examples of estimated maximum CdTe transport rates through the capillary used in the Multi-tube growth apparatus assuming that the flow regime is viscous, for a crossmember temperature of 950 °C. From top to bottom: p_s = 20, 15, 10, 8 and 6 mbar.

In the cases where the mean free path is much bigger than the radius of the capillary (which in this case applies for total vapour pressures < 0.5 mbar; according to table 1, $K_d \sim 0.7$ - 1.6 at 0.5 mbar), the flow is of molecular type. Source pressures < 0.5 mbar are not normally used during growth, as the growth rate becomes too low; however, for completeness, the expression for molecular flow in a capillary, as shown in chapter five, will be developed for the particular case here,

$$\psi_c\left(\frac{moles}{t}\right) = \frac{2\pi r^3}{3}\left(\frac{8RT}{\pi M}\right)^{1/2}\frac{\Delta P}{LRT} \qquad (6.7)$$

where it is important to note the absence of a mean pressure term and a smaller power dependence of the radius. If the flow is molecular, Cd and Te_2 particles flow independently, and hence the total flow through the capillary can be expressed as,

$$\psi_c\left(\frac{moles}{t}\right)=\frac{2\pi r^3}{3LRT}\left(\frac{8RT}{\pi}\right)^{1/2}\times\left(\frac{\Delta p_{Cd}}{\sqrt{M_{Cd}}}+\frac{\Delta p_{Te_2}}{\sqrt{M_{Te_2}}}\right) \tag{6.8}$$

and since in our particular case, this expression can be valid only for pressures < 0.5 mbar, we can assume that $p_g \sim 0$, and hence, once dynamic equilibrium is reached and substituting for M_{Cd} and M_{Te_2},

$$\Delta p_{Cd} = 1.327\Delta p_{Te_2} \tag{6.9}$$

(this boundary condition would also occur if there was another restrictor downstream that produced preferential transport; it will be seen that the annular gap around the crystal holder together with the crystal itself can produce preferential transport). Substituting 6.9 into 6.8, and using the values for the molecular weights gives,

$$\psi_c\left(\frac{moles}{t}\right)=0.125\times\frac{\pi r^3}{LRT}\left(\frac{8RT}{\pi}\right)^{1/2}\Delta p_{Te_2} \tag{6.10}$$

in cgs units. Inserting the values of r, L, R and, for example, a temperature of $T_c = 950\ ^{\circ}C$,

$$\psi_c\left(\frac{moles}{t}\right)=3.818\times10^{-7}\Delta p_{Te_2} \tag{6.11}$$

with Δp_{Te_2} in mbar. Since Δp_{Te_2} can only be < 0.5 mbar, it can be seen that the mass transport rate in the best of the cases during growth is ~ 4 gm/day.

In normal operation conditions, it can be seen from table 1 that the flow regime encountered during growth in the capillary will be slip or transition flow. Scott and Dullien [7,8], recently obtained a rigorous expression for slip flow for a long capillary,

$$\chi_c\left(\frac{moles}{t}\right)=\left(1-e^{-\sinh^{-1}\left(\frac{2r}{\lambda}\right)}\right)\times\left(\frac{\pi r^4 p_m \Delta p}{8\eta LRT}+\frac{4\pi^{3/2} r^3 \Delta p}{3(8MRT)^{1/2} L}\right) + e^{-\sinh^{-1}\left(\frac{2r}{\lambda}\right)}\times\left(\frac{16 r^3 \pi^{1/2} \Delta p}{3(8MRT)^{1/2}}\right) \tag{6.12}$$

The above expression reproduces accurately the experimentally found minimum in the specific flow rate - mean pressure curve for high aspect ratio circular capillaries. The expression is reduced to 6.1 for $r >> \lambda$ but not to the slip expression 5.3 of chapter five for $L >> r$, since the latter is an approximation for capillaries. For $L >> r$, the expression reduces to an empirical relation proposed by Knudsen that reproduces the experimentally found minimum. The existence of a minimum in the specific flow rate versus mean pressure curve occurs at mean pressures < 1 mbar. Also, since the purpose here is to obtain an approximate mass flow rate and the existence of a minimum will not affect the analysis for pressures > 1 mbar, the simple expression, previously used in chapter five,

$$\chi_c\left(\frac{moles}{t}\right)=\frac{\pi r^4 P_m \Delta P}{8\eta LRT}+\frac{\pi^2 r^3 \Delta P}{(8\pi MRT)^{1/2} L}\left(\frac{2}{f}-1\right) \tag{6.13}$$

will give an upper limit to the transport rate under slip conditions. For the present case ($T_c = 950$ °C and $\eta = 9.0\times10^{-4}$ poises, and using $f = 1$),

$$\chi_c\left(\frac{moles}{t}\right)=2.539\times10^{-8}(p_s^2-p_g^2) + 1.130\times10^{-7}(p_s^{Cd}-p_g^{Cd}) + 7.498\times10^{-8}(p_s^{Te_2}-p_g^{Te_2}) \tag{6.14}$$

The above expression implies that even under slip flow conditions, preferential transport will take place. Hence, once dynamic equilibrium has been established, the partial pressure ratio $\alpha = p_{Cd} / p_{Te_2}$ in the source side will have a value between 1.327 and 2.0.

6.1.3 Flow Through the Annular Section in the Growth Pedestal.

The *conductivity* of the annular gap that exists between the crystal holder and container wall is studied in this section. The importance of investigating the flow regimes here are not only related to the stoichiometry of the vapour near the crystal, but also to the yield of the growth process, since it is clear that if the gap is too large, most of the CdTe will be transported through the gap due to the lower temperature and pressure at the end of the growth tube.

The dimensions of the seed support or pedestal used in most growth experiments were 49.28 mm ± 0.01 mm for the diameter d, 10.22 mm ± 0.01 mm for the length l_a, and 0.045 mm ± 0.005 mm for the gap, r_a. Given the latter dimension, and p_g = 10 mbar as an estimate for the maximum vapour pressure encountered during growth, it can be seen from table 1, that the Knudsen number has a minimum value $K_d^{\min} \sim 0.5$, and hence it can be considered that flow through the annular gap will be of molecular or Knudsen type. As before, the vapour stoichiometry will change after a relaxation period, until the partial pressure ratio reaches a value of ~ 1.327. However, it is not clear if the vapour pressure in the growth tube will be set by the temperature of the growing crystal (when growth would proceed near equilibrium conditions) or by the *conductivities* of the different glassware elements (when the crystal would grow under nonequilibrium conditions). This important information can only be obtained using the partial pressure monitoring system described in chapter four and with a precise knowledge of the crystal surface temperature. For completeness, for the viscous flow regime, the general expression for flow in an annulus with high aspect ratio is [4]:

$$\varphi_a\left(\frac{moles}{s}\right)=\frac{\pi}{8\eta LRT}\times\left(R_o^4-R_i^4-\frac{\left(R_o^2-R_i^2\right)^2}{\ln\left(R_o/R_i\right)}\right)\times p_m\Delta p \qquad (6.15)$$

and for typical growth conditions (T_c = 850 °C, η = 9.0×10^{-4} poises) and previous dimensions,

$$\varphi_a\left(\frac{moles}{s}\right)=6.870\times10^{-10}(p_g^2-p_{g'}^2) \tag{6.16}$$

where $p_{g'}$ is the pressure downstream of the crystal pedestal, and can be considered zero.

The *conductivity* for the molecular flow regime in an annulus of length L, and inner and outer diameters R_i and R_o respectively cannot be calculated analytically for the case $L \sim R_i$ [4]. Montecarlo techniques [9] and variational methods [10,11] have been used in the past to obtain empirical equations for several annulus dimensions, using a transmission probability technique that calculates a transmission probability W for a specific set of dimensions. Data for the specific dimensions here is not available, but an extrapolation of the results obtained by Berman [11] for small aspect ratio dimensions has been calculated, with the result $W \approx 0.0419$. According to [4], then,

$$\psi_a\left(\frac{moles}{t}\right)=W\times\left(R_o^2-R_i^2\right)\times\left(\frac{\pi}{2RT}\right)^{1/2}\times\left(\frac{\Delta p_{Cd}}{\sqrt{M_{Cd}}}+\frac{\Delta p_{Te_2}}{\sqrt{M_{Te_2}}}\right) \tag{6.17}$$

and hence in the present case, for a growth temperature of 850 °C,

$$\psi_a\left(\frac{moles}{t}\right)=3.815\times10^{-6}\,\delta\times\Delta p_{Te_2} \tag{6.18}$$

with Δp_{Te_2} in mbar, and where $\delta = 0.188$ for $\Delta p_{Cd} / \Delta p_{Te_2} = 1.327$ and $\delta = 0.251$ for the now clearly unlikely case that $\Delta p_{Cd} / \Delta p_{Te_2} = 2$. In general the approximation $\Delta p_{Te_2} \sim p_{Te_2}$ can be used since $p_{g'} << p_g$.

6.2 GENERAL EQUATIONS FOR QUANTIFYING VAPOUR TRANSPORT.

Using mass continuity arguments and the *conductivity* results obtained above, it is possible to obtain a relation between the partial pressures in both source and growth tubes and the *conductivities* of the different elements. In some cases, it is also possible to determine the growth rate once the partial pressures are known.

The existence of diffusion will be neglected. This is justified since the system is semiopen, and hence no build-up of cadmium or tellurium vapour excess will take place. Also, it can be shown that the diffusion contribution, which is significant at low flow rates, vanishes as the flow rate is increase [12]. For the flow rates encountered in typical growth conditions, advection (Stefan flow) will dominate over diffusion.

6.2.0 General Description.

Figure 2 presents a sketch of the glassware used in the growth apparatus described extensively in chapter three. Here, it is assumed that both the sublimation and condensation (growth) of CdTe take place at a constant rate, $n_s = C_1$ (moles/s) and $n_g = C_2$ (moles/s) respectively. The number of moles per unit of time passing through the capillary, $n_c(t)$, through the annular section, $n_a(t)$, and through the glass joints of the crossmember in the source and growth sides, $n_{ls}(t)$ and $n_{lg}(t)$ respectively, can be described in terms of the pressures in the source and growth tube, $p_s(t)$ and $p_g(t)$ and the respective *conductivities* of each conduit or restrictor and will be investigated in detail. The *conductivities* depend on the nature of the different flow regimes that can be encountered. As previously explained, these flow regimes are dictated directly by the

relation between the mean free path of the vapour atoms or molecules and the characteristic dimension of the restrictor, typically the radius, as detailed previously.

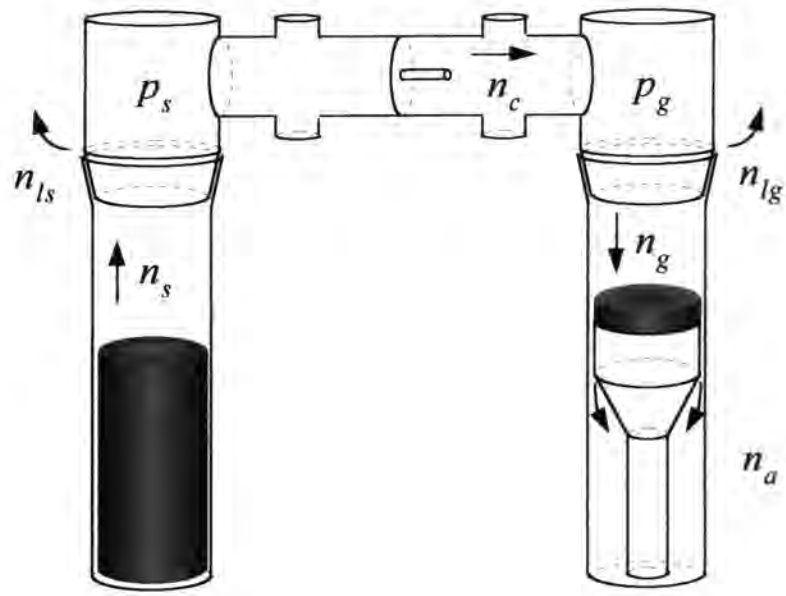

Figure 2. Schematic diagram of the glassware in the growth system used to illustrate the different mass flows.

6.2.1 Viscous Regime.

As discussed above, viscous flow in the two main restrictors of the growth apparatus does not take place at normal operating temperatures and pressures. However, it is interesting to analyse it since the growth apparatus design provides for a way of introducing a constant flow rate of a carrier gas. If this flow of gas was set to produce a total vapour pressure of approximately ~100 mbar or higher, the flow would enter the viscous regime, and equations 6.1 and 6.15 would apply (although the viscosity of a three component mixture would have to be approximated).

Using the sketch in figure 2, and assuming that i) there are no leaks that can produce any upset in the partial pressure ratio and ii) the transport proceeds in the viscous regime in both the annular and crossmember sections, the following system of differential equations can be obtained:

$$\begin{aligned}\frac{V_s}{RT_s}\frac{dp_s}{dt} &= C_1 - a_v\left(p_s^2 - p_g^2\right)\\ \frac{V_g}{RT_g}\frac{dp_g}{dt} &= a_v\left(p_s^2 - p_g^2\right) - b_v p_g^2 - C_2\end{aligned} \tag{6.19}$$

where mass continuity and the ideal gas law have been used, V_s and V_g are the volumes of the source and growth chambers respectively, and T_s and T_g are the temperatures of source and growth respectively. According to equations 6.6 and 6.16, a_v = 2.539×10^{-8} $mbar^{-2}\times mols\times s^{-1}$ and b_v = 6.870×10^{-10} $mbar^{-2}\times mols\times s^{-1}$ when the pressure is measured in mbar, for a stoichiometric vapour mixture consisting of Cd and Te_2 at a source and growth temperature of 950 °C and 850 °C respectively. Once dynamic equilibrium is reached,

$$\begin{aligned}C_1 - a_v\left(p_s^2 - p_g^2\right) &= 0\\ a_v\left(p_s^2 - p_g^2\right) - b_v p_g^2 - C_2 &= 0\end{aligned} \tag{6.20}$$

and hence, rearranging, the source and growth pressures are obtained,

$$\begin{aligned}p_g &= \sqrt{\frac{C_1 - C_2}{b_v}}\\ p_s &= \sqrt{\frac{C_1}{a_v} + \frac{C_1 - C_2}{b_v}}\end{aligned} \tag{6.21}$$

which is equivalent to the relation

$$p_s^2 - p_g^2 = \frac{C_1}{a_v} \tag{6.22}$$

An expression for the effective transport rate (which can be considered the growth rate if no interfacial or surface kinetics processes play a rate-limiting role in the growth process), can be obtained from the second expression in 6.20,

$$C_2 = a_v p_s^2 - (a_v + b_v) p_g^2 \tag{6.23}$$

and using 6.6 and 6.16,

$$C_2 = 2.539 \times 10^{-8} p_s^2 - 2.608 \times 10^{-8} p_g^2 \tag{6.24}$$

where p_s and p_g are in mbar. Subject to the constraint due on the validity of equations 6.6 and 6.16, equation 6.24 should give a good approximation to the growth rate when viscous flow dominates transport throughout the Multi-tube glassware. The growth rate for several source pressures can be seen in figure 3.

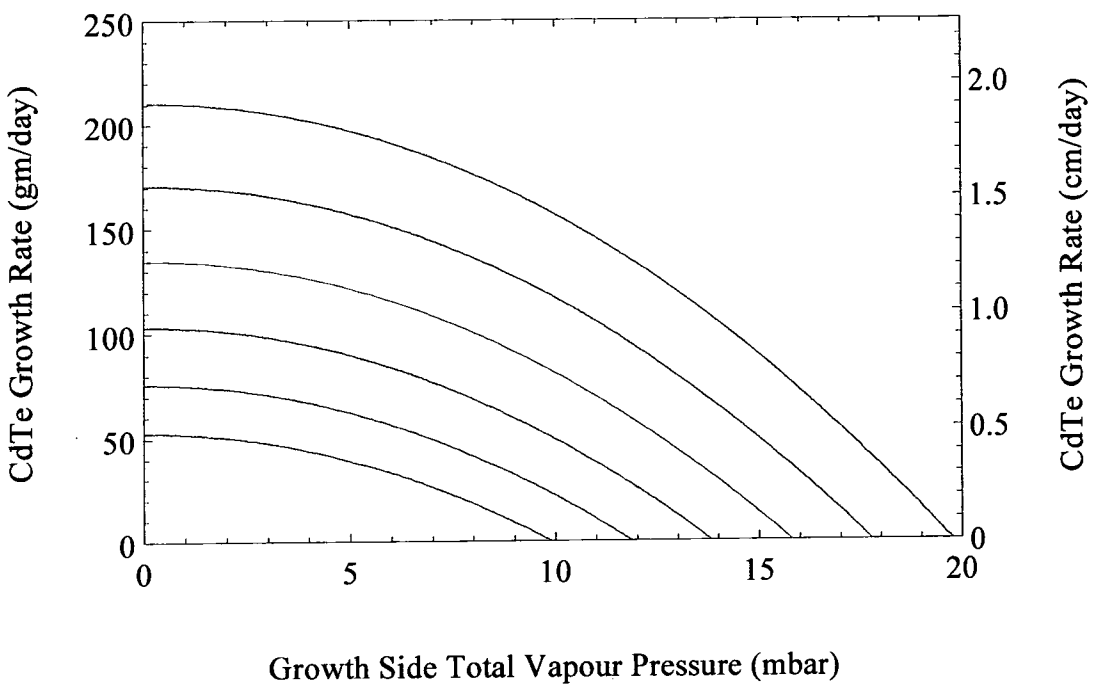

Figure 3. Growth rate of CdTe as a function of growth pressure for various source pressures: from top to bottom, p_s = 20,18, 16, 14, 12 and 10 mbar in the apparatus assuming viscous flow in both capillary and annulus, a crossmember temperature of 950 °C and a growth temperature of 850 °C (right axis valid for growth on a 49 mm wafer seed).

In the case where leaks through the glass joints occur, the growth rate will still be governed by an equation similar to 6.24, since only the partial pressure ratio will change and given the dimensions of the annular cone shaped glass joints the loss of material will be negligible. The only modification that will have to be taken into account would be the change in the viscosity, as mentioned earlier, since the viscosity of a multicomponent vapour depends on the molar ratio of the vapours.

6.2.2 Molecular Regime.

Molecular flow cannot take place in the capillary if reasonable growth rates are to be obtained. However, as seen in chapter five, this is the flow regime that would occur if a porous silica disc is used, and hence it is interesting to analyse molecular mass transport. In the molecular regime, each component of the vapour mixture has to be treated differently. Assuming i) the presence of no leaks, ii) a molecular regime in both capillary and annulus, and using equations 6.7 and 6.17 and figure 2,

$$\begin{aligned} \frac{V_s}{RT_s}\frac{dp_s}{dt} &= C_1 - a_m\left(p_s - p_g\right) \\ \frac{V_g}{RT_g}\frac{dp_g}{dt} &= a_m\left(p_s - p_g\right) - b_m p_g - C_2 \end{aligned} \tag{6.25}$$

for a single vapour, and where a_m and b_m are the proportionality *conductance* constants that relate the partial differential pressure to the molar mass flow (see 6.7 and 6.17). It is assumed that the pressure past the annulus can be considered zero. In dynamic equilibrium,

$$\begin{aligned} C_1 - a_m\left(p_s - p_g\right) &= 0 \\ a_m\left(p_s - p_g\right) - b_m p_g - C_2 &= 0 \end{aligned} \tag{6.26}$$

and rearranging, the relation between *conductivities*, evaporation rate, growth rate and vapour pressure can be obtained,

$$p_g = \frac{C_1 - C_2}{b_m}$$
$$p_s = \frac{C_1}{a_m} + \frac{C_1 - C_2}{b_m} \tag{6.27}$$

which is equivalent to the relation (or from 6.26 directly),

$$p_s - p_g = \frac{C_1}{a_m} \tag{6.28}$$

It is interesting to compare 6.28 with 6.22, the equivalent relation in the case of viscous flow, which depends on the difference of the pressures squared. A relation for net transport rate (growth rate), can be obtained from the second expression in 6.26,

$$C_2 = a_m p_s - (a_m + b_m) p_g \tag{6.29}$$

which is superficially similar to the viscous case. Assuming that

$$C_1^{Cd} = 2C_1^{Te_2} \text{ and } C_2^{Cd} = 2C_2^{Te_2} \tag{6.30}$$

i.e. that CdTe sublimes and grows congruently, and realising from 6.7 that

$$a_m^{Cd} = \sqrt{\frac{M_{Te_2}}{M_{Cd}}} a_m^{Te_2}, \qquad b_m^{Cd} = \sqrt{\frac{M_{Te_2}}{M_{Cd}}} b_m^{Te_2} \tag{6.31}$$

it can be shown using 6.27 that the partial ratio in both growth and source sides is 1.327. The growth rate, according to 6.29, 6.30 and 6.31 can be expressed as

$$C_{CdTe} = C_2^{Cd} + C_2^{Te_2} = 3a_m^{Te_2} p_s^{Te_2} - 3(a_m^{Te_2} + b_m^{Te_2}) p_g^{Te_2} \tag{6.32}$$

and hence, using 6.7 and 6.17 for tellurium vapour only, and for crossmember and growth temperatures of 850 °C and 950 °C respectively

$$C_{CdTe} = 3.819 \times 10^{-7} p_s^{Te_2} - 7.164 \times 10^{-7} p_g^{Te_2} \tag{6.33}$$

Figure 4 shows a graph of the growth rates given by the expression above for several source pressures (for pressures higher than 1-2 mbar, the molecular flow expression does not apply for the capillary).

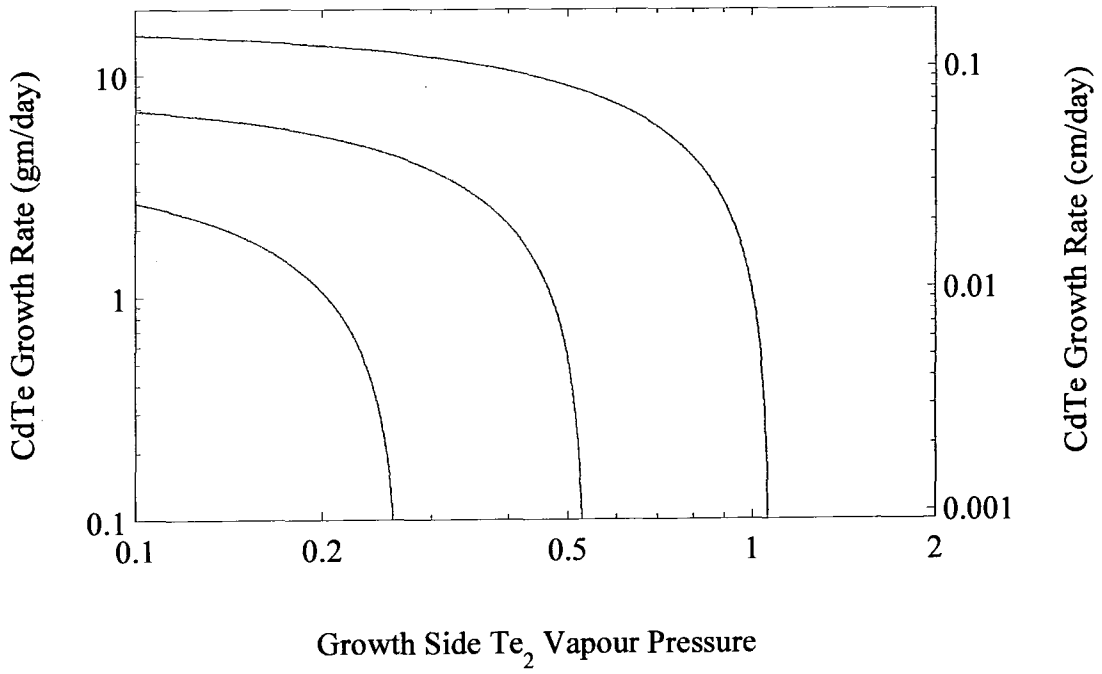

Figure 4. Growth rate of CdTe as a function of growth pressure for various source pressures: from top to bottom, p_s = 2, 1 and 0.5 mbar in the apparatus assuming molecular flow takes place in both capillary and annulus, a crossmember temperature of 950 °C and a growth temperature of 850 °C (right axis valid for growth in a 49 mm wafer seed).

The apparently lower growth rates are merely a consequence of the lower pressures applicable for molecular flow.

In the case where leaks are present, and assuming a conductance d_m through the annular cone shaped leaks, defined by equation 6.17 (for a single component), it is possible to proceed as above. The resulting partial pressures for dynamic equilibrium are then,

$$p_g = \frac{-d_m C_2 + a_m (C_1 - C_2)}{(d_m + a_m)(b_m + d_m) + a_m d_m}$$
$$p_s = \frac{C_1 (b + d) + a(C_1 - C_2)}{(d_m + a_m)(b_m + d_m) + a_m d_m} \qquad (6.34)$$

where it can be seen that for $d_m \rightarrow 0$, p_s and p_g reduce to 6.27, as expected. Combining the expressions for p_g and p_s,

$$p_s - p_g = \frac{d_m C_2 + (b_m + d_m) C_1}{(d_m + a_m)(b_m + d_m) + a_m d_m} \tag{6.35}$$

The partial pressure ratio α will not be further affected. The only effect of the leaks in the molecular flow regime is some very small loss of material, since typically, $d << a$ and $d << b$. This can be seen by substituting the data for the annular cone shaped gap of section 6.1.1 in equation 6.17. According to Berman [11], in this case $W \sim 5\times10^{-5}$, and hence

$$d_m \approx 3.5 \times 10^{-12} \Delta p_{Te_2} \tag{6.36}$$

with Δp_{Te_2} in mbar, which is several orders of magnitude smaller a_m or b_m in 6.33.

6.2.3 Slip Regime.

The slip or transition regime is the most important here, since as seen previously, the combination of the length and radii of the ampoule components, the range of vapour pressures and temperatures during growth and the mean free path under these conditions for Cd and Te_2 particles allow for slip flow to take place. Again, we will consider the case where both annulus and capillary are in the transition regime, assuming no glass joints leaks take place. Again, using mass continuity and the ideal gas law, together with 6.13, the set of equations governing flow in the system is,

$$\begin{aligned} \frac{V_s}{RT_s}\frac{dp_s}{dt} &= C_1 - a_v\left(p_s^2 - p_g^2\right) - b_s\left(p_s - p_g\right) \\ \frac{V_g}{RT_g}\frac{dp_g}{dt} &= a_v\left(p_s^2 - p_g^2\right) - b_s\left(p_s - p_g\right) - C_2 - c_v p_g^2 - d_s p_g \end{aligned} \tag{6.37}$$

where a_v and b_s are the conductances for the capillary and c_v and d_s, the ones for the annulus. Once dynamic equilibrium has been established,

$$\begin{aligned} C_1 - a_v\left(p_s^2 - p_g^2\right) - b_s\left(p_s - p_g\right) &= 0 \\ a_v\left(p_s^2 - p_g^2\right) - b_s\left(p_s - p_g\right) - C_2 - c_v p_g^2 - d_s p_g &= 0 \end{aligned} \tag{6.38}$$

and rearranging, and solving a second degree equation, and rejecting the negative solution (negative pressures are not physically possible),

$$p_g = \frac{-d_s + \sqrt{d_s^2 - 4c_v(C_2 - C_1)}}{2c_v}$$

$$p_s = \frac{1}{2a_v} \times \left(-b_s + \left(b_s^2 - 4a_v \left[-a_v \left(\frac{-d_s + \sqrt{d_s^2 - 4c_v(C_2 - C_1)}}{2c_v} \right)^2 - b_s \left(\frac{-d_s + \sqrt{d_s^2 - 4c_v(C_2 - C_1)}}{2c_v} \right) - C_1 \right] \right)^{1/2} \right) \quad (6.39)$$

The partial pressure ratio α in both the source and growth sides *cannot be calculated* (as was done with the molecular flow case) using the above expressions since it is not physically correct to assume independent flow of Cd and Te_2 molecules in the viscous regime.

In conclusion, when slip or transition flow occurs in both the capillary and the annulus, the partial pressure ratio depends on the *conductivity* of both elements, and can take any partial ratio in both source and growth sides between 1.327 (entirely molecular) and 2.0 (entirely viscous).

6.2.4 Combined Slip and Molecular Regimes.

In the previous sections the flow for three specific regimes has been evaluated. Here, the particular case for the flow conditions that occur during typical growth conditions (namely, slip flow in the capillary and molecular flow in the annulus) will be evaluated. As seen in section 6.1, flow through the annulus can be considered molecular during typical CdTe growth conditions; also, the flow through the capillary is, under

practical growth conditions, of slip type. Using the previously derived expressions, the flow equations are:

$$\begin{aligned}\frac{V_s}{RT_s}\frac{dp_s}{dt} &= C_1 - a_v\left(p_s^2 - p_g^2\right) - b_s\left(p_s - p_g\right)\\ \frac{V_g}{RT_g}\frac{dp_g}{dt} &= a_v\left(p_s^2 - p_g^2\right) - b_s\left(p_s - p_g\right) - C_2 - c_m p_g\end{aligned} \tag{6.40}$$

where a_v and b_v are given by 6.13 and c_m by 6.17. Once dynamic equilibrium conditions are reached,

$$\begin{aligned}C_1 - a_v\left(p_s^2 - p_g^2\right) - b_s\left(p_s - p_g\right) &= 0\\ a_v\left(p_s^2 - p_g^2\right) - b_s\left(p_s - p_g\right) - C_2 - c_m p_g &= 0\end{aligned} \tag{6.41}$$

and solving,

$$\begin{aligned}p_g &= \frac{C_1 - C_2}{c_m}\\ p_s &= -\frac{b_s}{2a_v} + \sqrt{\frac{b_s^2}{4a_v^2} + \left[\frac{C_1 - C_2}{c_m}\right]^2 + \frac{b_s}{a_v}\left[\frac{C_1 - C_2}{c_m}\right] + \frac{C_1}{a_v}}\end{aligned} \tag{6.42}$$

and the partial ratio for Cd and Te_2 molecules is, using 6.30 and 6.31, 1.327 in the growth side. Again, the partial pressure ratio can vary between 1.327 and 2 in the source side, depending on the capillary dimensions and pressures.

6.3 DISCUSSION OF THE CONSEQUENCES OF THE PARTIAL VAPOUR PRESSURE RATIO ON GROWTH RATE AND CRYSTAL QUALITY.

It can be seen from 6.42 that growth will take place from a noncongruent vapour. There is evidence that this can affect the quality or the growth rate of the crystal in a closed growth system, but no experimental data is available from the literature for semiopen systems. As has been seen in chapter 2, previous studies attributed low

growth rates to departures from stoichiometry, and maximum growth rates to congruent vapour. However, this only applies for closed ampoules, where diffusion mechanisms dominate the mass transport. Since the feed vapour is tellurium rich, and the range of existence of CdTe is shifted towards the tellurium (see figure 2, chapter 2), this might have some consequences on tellurium incorporation during growth and the formation of a second phase or precipitates during cooling down. It also can have consequences for the electrical properties of the crystal: according to 6.42, all CdTe crystals should be *p*-type assuming there is no significant incorporation of unwanted foreign atoms that compensate for the Cd vacancies.

This growth system hence provides a unique opportunity to investigate the occurrence of precipitates, and in principle can allow, since partial vapour pressures are known, and after characterisation, elucidation of the mechanism of formation of tellurium incorporation. The effect of the tellurium rich vapour on the growth rate is not clear. Until now, it has been assumed that no interfacial kinetic barriers were present in the crystal surface during growth. However, since the crystal should grow congruently, tellurium excess might produce growth rate limiting conditions, and it is possible that the growth is controlled by diffusion at the interface, since a depletion layer might occur. Although previous studies have concluded that the dissociation of Te_2 molecules is not the step limiting the growth rate, the diffusion of Cd atoms through any such depletion layer to the interface might well be limiting.

The above mass transport modelling clearly shows that the vapour partial pressure of each component above the growing crystal depends on the flow regimes that take place during transport. However, it has been assumed that the growing crystal does

not fix the total partial pressure above the crystal. In closed vapour growth systems, the temperature gradient between source and crystal determines the pressure gradient, and hence the pressure is a dependent variable. With semiopen vapour growth systems it is clear that the pressure is no longer dependent anymore, and can be set independently of the temperature gradient. Moreover, in this system the temperature gradient does not constitute the driving force for mass transport. The consequences of this on constitutional supercooling and hence growth and interface morphological stability should be discussed. Reed *et al.* [13] and Paorici *et al.* [14] showed that only when $p < p_o$ (where p is the pressure over the crystal and p_o is the saturated vapour pressure of the crystal) is the interface stable. They also showed that growth is stable if

$$\frac{dp_o}{dx} \geq \frac{dp}{dx} \tag{6.43}$$

and that there is a maximum growth rate for which the above expression is obeyed. This expression also assumes local equilibrium, so that interfacial kinetics do not play a rate limiting role and is valid for a single vapour component. For dissociative sublimation, the equivalent condition is [1],

$$\frac{d}{dx}\left(\frac{p_{Cd}\, p_{Te_2}^{1/2}}{K_{CdTe}}\right)_{x=0} \leq 0 \tag{6.44}$$

where K_{CdTe} is the equilibrium constant for the sublimation of CdTe. The left-hand side of the above expression is a function of the kinetics of the transport process and of the axial temperature gradient.

Clearly, an equation similar to 6.44 should also apply to the present system if the total pressure of the vapour close to the crystal is fixed by the crystal itself, rather than by the dynamic pumping taking place. It could be argued that for growth to take place,

the vapour pressure over the crystal should be at least equal to the equilibrium saturated vapour pressure. This is not necessarily the case, since it is possible to establish dynamic equilibrium (between the flux of molecules impinging into the crystal surface and that of the molecules leaving the surface), which allows net transport and also a different vapour pressure than that corresponding to the crystal temperature. Again, this can only be tested using the partial pressure monitoring system, and some experimental results will be shown in next chapter.

6.4 CONCLUSIONS.

The mass transport of Cd and Te_2 vapours in the Multi-tube growth apparatus used currently in Durham has been studied. The influence of total vapour pressure on both source and crystal sides under several possible flow regimes has been analysed for a specific set of dimensions of the flow restrictor and pedestal annulus. It has been shown that the flow regime that dominates the transport is mainly slip flow, under typical growth conditions. This can have a direct impact on the partial pressure ratio α of the constituents of the vapour, since under this regime, there is preferential transport of the lighter component of the vapour, i.e. cadmium atoms. After an initial relaxation period, which is proportional to the volume of the source and crystal chambers, the partial pressures in the source side will not be in the stoichiometric ratio, but in a range of values between 1.327 and 2.0. This will depend on both the temperature of the crossmember and the total pressure of the vapour over the source. In the same way, it has been shown that assuming that if the crystal is growing under dynamic equilibrium, the partial pressure ratio of the vapour over the growing crystal will be close to 1.327. The limitations of the arguments used to obtain these results have been outlined

previously: diffusion, thermal diffusion and the existence of thermal gradients near the crystal have been neglected. Experiments performed in the crystal growth system to confirm the previous predictions are necessary and some preliminary results will be presented in the following chapter.

REFERENCES FOR CHAPTER SIX

[1] M. M. Faktor and I. Garret. *Growth of Crystals from the Vapour*. Chapman and Hall, London (1974).

[2] E. Schonherr. "*The Growth of Large Crystals from the Vapor Phase*", in *Crystals: Growth, Properties and Applications*. Volume 2. Springer, Berlin (1980).

[3] G. H. Westphal. *"Convective Transport in Vapor Growth Systems"*. J. Crystal Growth, **65** (1983) 105.

[4] L. Holland, W. Steckelmacher and J. Yarwood. *Vacuum Manual*. E. & F. N. Spon, London (1974).

[5] S. Dushman and J. M. Lafferty. *Scientific Foundations of Vacuum Technique*. 2nd edition. John Wiley & Sons, New York (1962).

[6] S. Chapman and T. G. Cowling. *The Mathematical Theory of Non-Uniform Gases*. Cambridge Press, London (1939).

[7] D. S. Scott and F. A. L. Dullien. *"The Flow of Rarefied Gases"*. A. I. Ch. E. Journal, **8** (1962) 293.

[8] F. A. L. Dullien. *Porous Media, Fluid Transport and Pore Structure*. Academic Press, London (1979).

[9] D. H. Davis. "*Monte Carlo Calculation of Molecular Flow Rates through a Cylindrical Elbow and Pipes of Other Shapes*". J. Appl. Phys., **31** (1960) 1169.

[10] A. S. Berman. *"Free Molecule Transmission Probabilities"*. J. Appl. Phys., **36** (1965) 3356.

[11] A. S. Berman. *"Free Molecule Flow in an Annulus"*. J. Appl. Phys., **40** (1969) 4991.

[12] U. Merten and W. E. Bell. *"The Transpiration Method"* in *The Characterisation of High-Temperature Vapors*. Edited by J. L. Margrave. John Wiley & Sons, New York (1967).

[13] T. B. Reed and W. J. LaFleur. *"Constitutional Supercooling in Iodine Vapor Growth"*. Appl. Phys. Lett., **5** (1964) 191.

[14] C. Paorici, M. Zha, L. Zanotti, L. Carotenuto and T. Tiberti. *"Growth Stability in Semiopen Physical Vapour Transport"*. J. Physique IV, **5** (1995) 1053.

Chapter Seven

Vapour Pressure Monitoring in the Multi-tube PVT System

7.0 INTRODUCTION.

In this chapter, the application of the vapour pressure monitoring system introduced in chapter four to the *in situ* measurement of Cd and Te_2 partial pressures during the growth of CdTe in the MPVT system is presented.

7.1 VAPOUR PRESSURE OPTICAL ABSORPTION MONITORING.

7.1.1 Preliminary Results.

In order to test the vapour pressure optical monitoring system in the Multi-tube growth apparatus, a preliminary experiment was carried out by Dr J. T. Mullins prior to growth trials. This experiment consisted of ramping up the temperature of the source and crossmember zones (the input power of the three growth zones was kept to zero, hence also demonstrating the extent to which the temperatures of the crossmember and growth tubes could be decoupled) of the furnace until sublimation temperatures had been reached. To investigate the sensitivity of the optical monitoring system, the CdTe source temperature was then cycled through several temperatures, as shown in figure 1. Only the source side vapour pressures were monitored.

Figure 2 shows the raw signals as recorded from the detectors in the source side. Two main features are visible. First, after each cycle was completed, all three signals drop to levels below the original values before the start of the heating cycle. This was due to condensation of CdTe on the monitoring windows of the crossmember, as verified after the experiment. Intuitively this might have been expected, as care was not taken to maintain the crossmember always at a higher temperature than the other heater

zones. Since the crossmember has a smaller heat capacity than the rest of the furnace, it cools more rapidly, hence allowing condensation of CdTe within it. As long as the windows are clean before each growth is started, so that a reference baseline can be established for each of the signals, the final value will not be significantly misleading.

Secondly, the 644 nm (not absorbed by Cd or Te_2) line used to monitor the output of the lamp did not remain stable, but oscillated in a well defined pattern. As the crossmember temperature was increased, the 644 nm signal also increased, reaching a maximum as the crossmember reached its set point temperature. While the crossmember temperature remained constant, the 644 nm signal started to decrease, until the crossmember temperature was reduced, when the 644 nm signal again began to increases, though to a smaller peak value after which it started to decrease again returning to its baseline value as the crossmember temperature continued to decrease. The lack of a simple correlation between the 644 nm signal and the heating process of the crossmember (temperature up, signal up; temperature down, signal down) eliminated the possibility that parasitic radiation from the heating QHL's was not being filtered out by the lock-in amplifier.

The correspondence between the heating and cooling down cycle and the increase and decrease respectively of the 479 nm tellurium and 326 nm cadmium monitoring lines is, nonetheless, clearly visible. A closer examination of, for example, the second heating cycle reveals that a dip in the source top zone temperature, correlates directly with a temporary dip in the 479 nm signal, as expected.

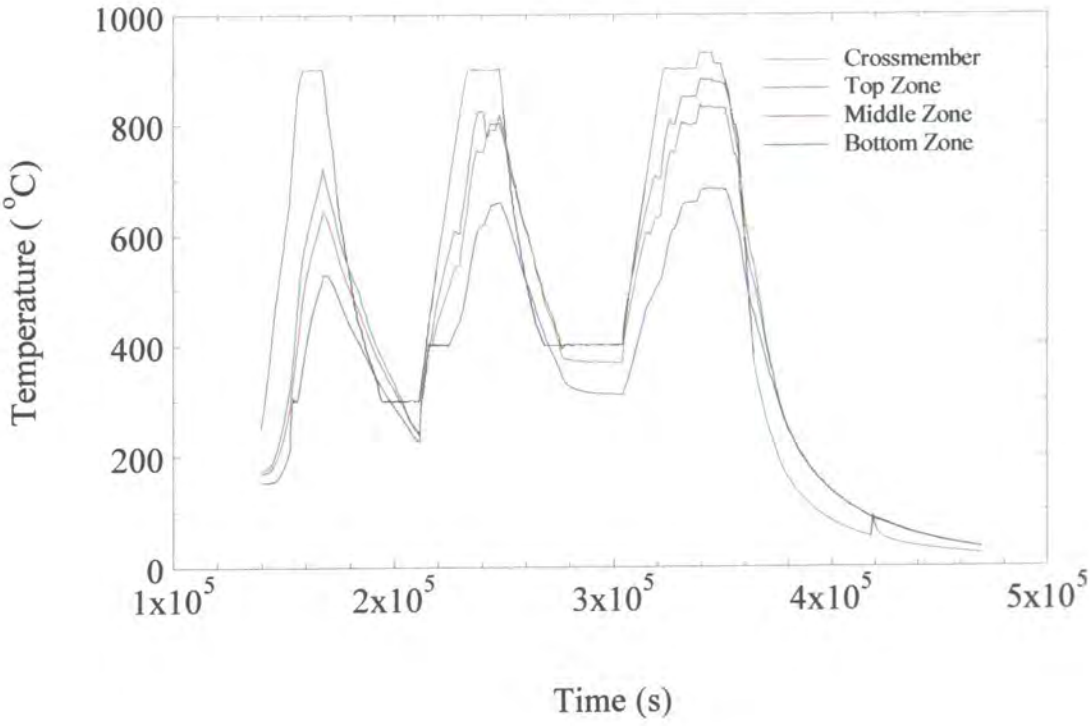

Figure 1. Source zones and crossmember temperatures during the cycling experiment.

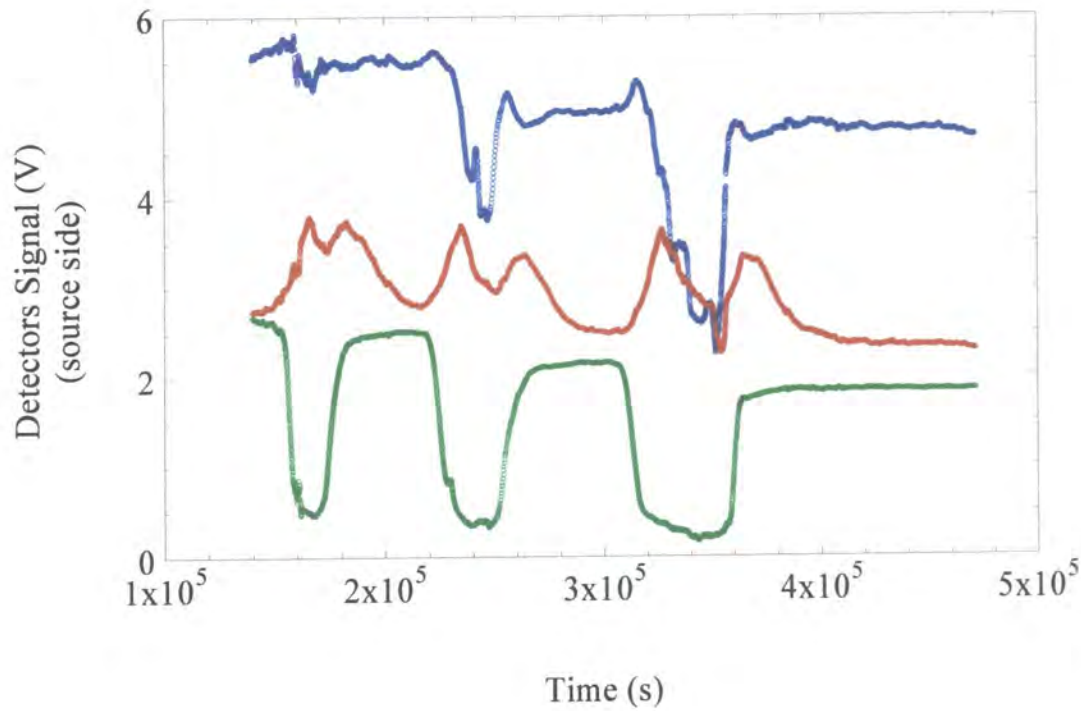

Figure 2. Voltage signal for the 479 nm (top) tellurium line, 644 nm (middle) reference line and 326 nm (bottom) cadmium line.

A similar behaviour for the 326 nm line is not visible in figure two, due to the strong absorbance of the line (see figures 13 and 14 of chapter four) and its non-linear dependence on the Cd vapour pressure. However, the behaviour is clearly visible in figure four.

Since the CdTe absorption coefficient varies little between 326 and 644 nm [1], it is still possible to obtain the optical density of the 479 nm and 326 nm lines by using the 644 nm line. Figure 3 shows the optical density of the tellurium 479 nm line as calculated from: a) the initial baseline value before heating took place solely,

$$D_{479} = \log\left(\frac{I^{o}_{479}}{I_{479}}\right) \tag{7.1}$$

and b) a combination of the initial 644 and 479 nm lines values,

$$D_{479} = \log\left(\frac{I^{o}_{479}}{I_{479}} \times \frac{I_{644}}{I^{o}_{644}}\right) \tag{7.2}$$

which is equivalent to 7.1 when the 644 nm line remains at a constant value. As demonstrated in figure 3, the optical density as calculated from 7.1 gives a constant though non-zero value at low temperatures (figure 1), when necessarily there was no tellurium vapour. When, the tellurium optical density is calculated with 7.2 the density maintains a near zero optical density value at low temperatures, as it should, although this procedure creates some *artificial* bumps during the cooling down process. Hence, it may be concluded that although the coating of the ampoule monitoring windows during the cooling process is responsible for changes in the constant optical density values between the cycling, movement of the heaters/crossmember ampoule is the cause of the oscillations in the 644 nm line. Since each line is detected by a different (positioned) detector, and taking into account the size of the detectors, and the distance between

detectors (and hence the field of view) it is possible that movement of the heaters/crossmember only affected the 644 nm line. A similar behaviour is observed when the optical density of the cadmium 326 nm line is calculated using 7.1 and 7.2.

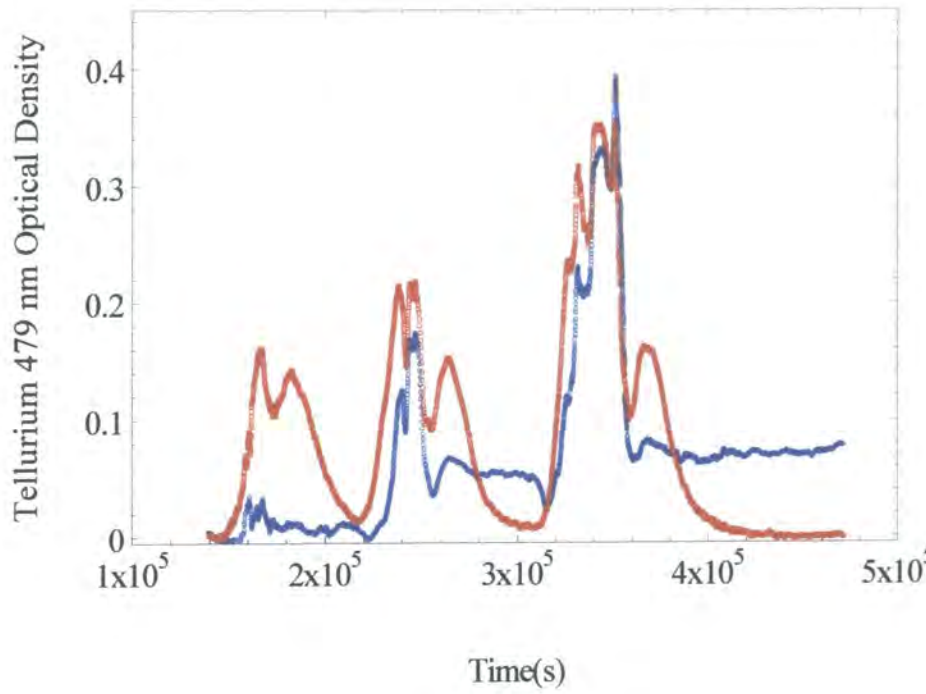

Figure 3. Optical densities of the 479 nm line as calculated with 7.1 (blue circles) and 7.2 (red squares).

The calculated partial vapour pressures of Cd and Te_2 using the calibrations given in chapter four are shown in figures 4b and 4c. As expected the partial vapour pressure of both components increase as the source temperature is increased. Unfortunately, accurate knowledge of the sublimation temperature is not available, since the source material occupied all three source heater zones. However, taking the maximum temperature of the top source zone, 820 °C during the second cycle and using the expressions in 2.5, one obtains, a maximum vapour pressure of ~3.2 mbar for Cd and ~ 1.6 for Te_2, in good agreement with the values in figure 4b and 4c of 3-5 mbar

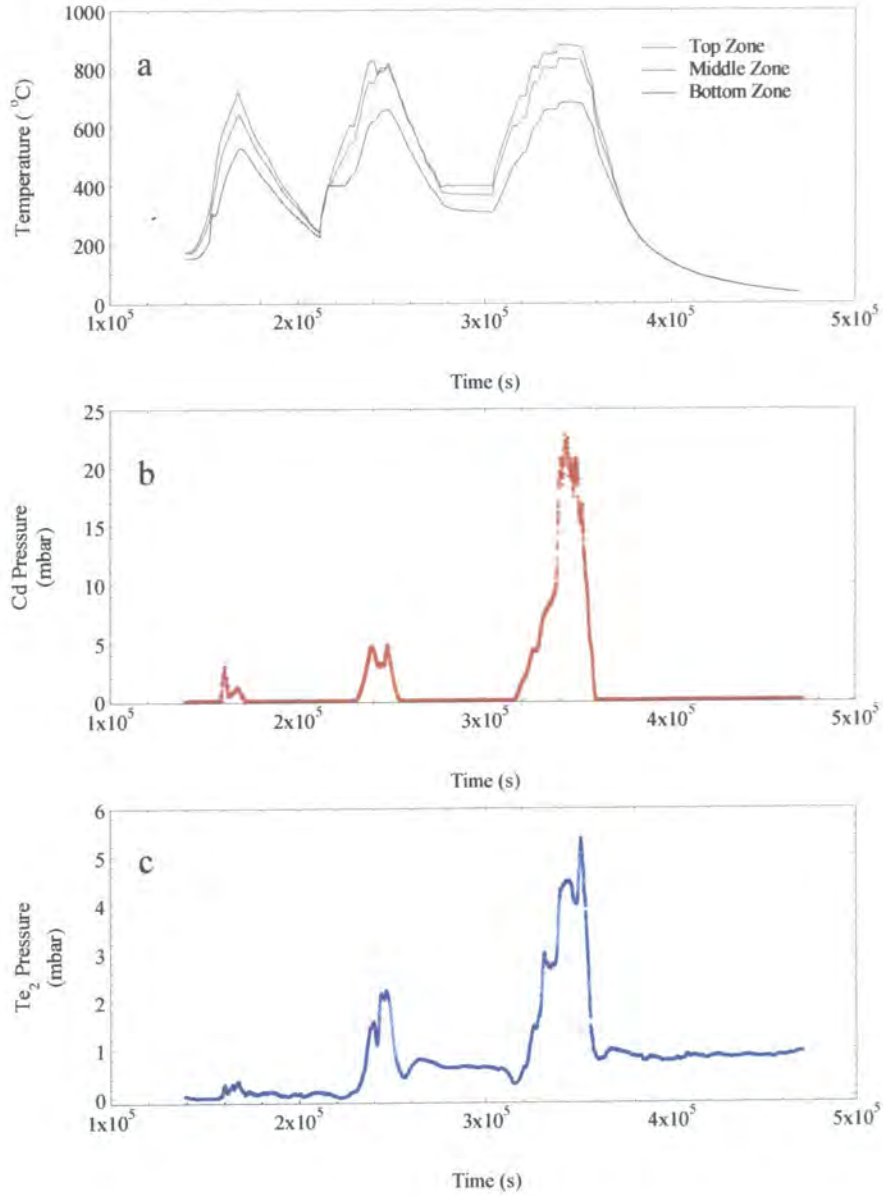

Figure 4. a) plot of the three source zones temperatures as a function of time, b) Cd partial pressure and c) Te_2 partial pressure during the temperature cycles in a).

for Cd and 1.6-2.2 mbar for Te_2. For the third cycle, the expected values at the top temperature of 880 °C according to equation 2.5 would be ~9.5 mbar and 4.8 mbar for Cd and Te_2 respectively. There is good agreement with the Te_2 values in 4c, of 4.5-5 mbar. However, the experimental Cd values appear to be about twice the expected

value. This may be due to preferential cadmium sublimation resulting from the fact that the temperature cycling did not allow the proper establishment of equilibrium, and hence the values predicted by 2.5 would not be expected to hold. The experimental partial pressure ratios as calculated from figures 4b and 4c give a range of values of 2-4 for the first cycle, 2-4 for the second and 2-7 for the third, and show the utility of the optical monitoring technique.

7.1.2 Results during CdTe Growth.

Several growth experiments were carried out in the MPVT apparatus, mainly by Dr. J. T. Mullins. An example of a typical vapour pressure monitoring experiment in the source side is shown in figures 5a and 5b for seeded growth on a 49 mm substrate (run 25/26). Figure 5a shows the temperature profiles, with the partial vapour pressures as calculated according to the calibration plots and expressions given in chapter 4 are shown in figure 5b. In this run the top zone of the source was kept at a higher temperature (925 °C) than the crossmember (900 °C), in order to avoid condensation in the glass joints and in the (colder) optical source access window.

As the source and crossmember temperatures were increased, there was a sharp increase in the cadmium and tellurium vapour pressures, which peaked at 8 and 4.4 mbar respectively, before relaxing to stable levels of ~7.2 and ~3.8 mbar respectively. No corresponding peak occurred in the source temperatures which could explain this transient effect. It is possible that the transient is due to the condensation of a layer of CdTe in areas close to the top zone during previous runs. This is, of course, hotter than the main bulk of the source, giving a higher vapour pressure. However, once the layer has been evaporated, then the pressures reduce to those determined by the main part of

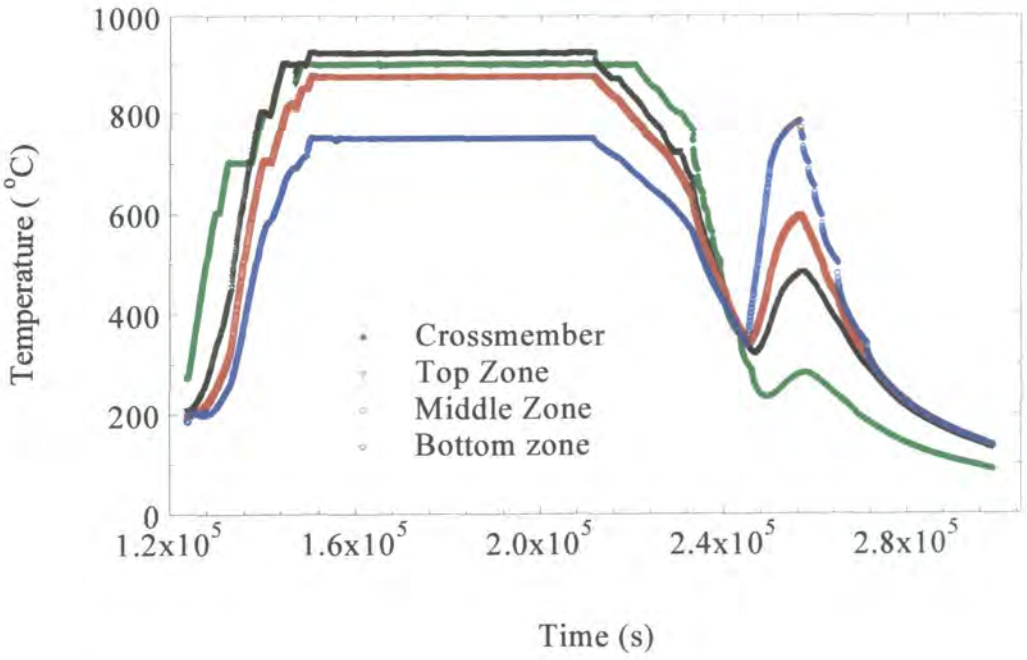

Figure 5a. Source and crossmember temperatures during run 25/26.

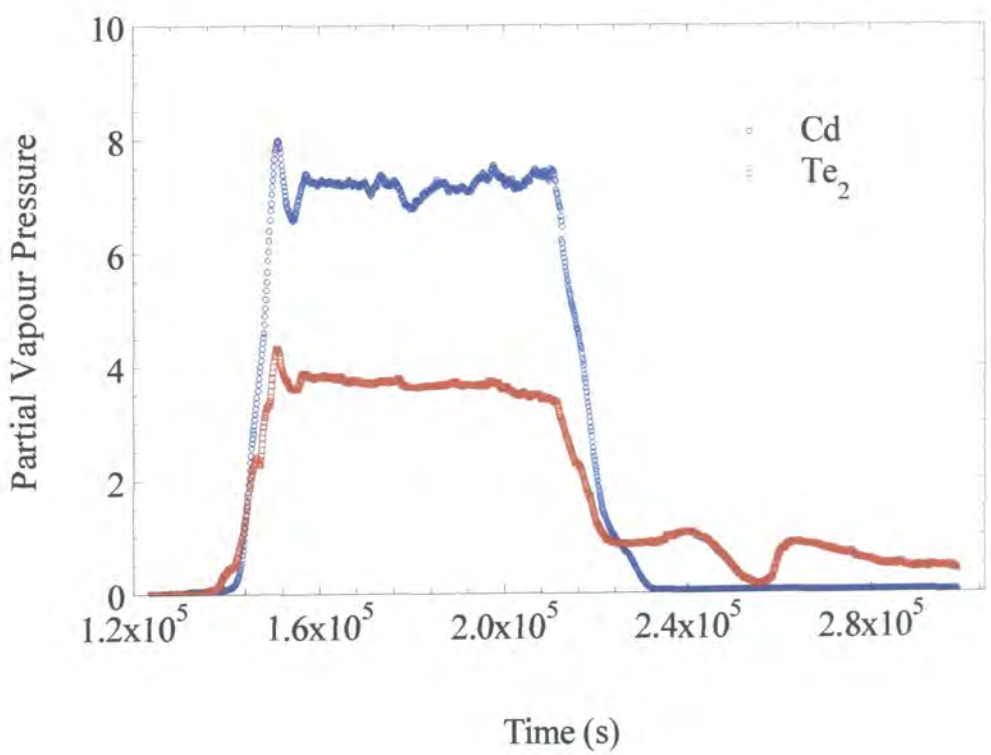

Figure 5b. Cd and Te_2 partial pressures in the source side during run 25/26

the source. This is consistent with the fact that the voltage signal of all three source side detectors increased sharply as the crossmember reached 600 °C temperature as the thin CdTe layer from the previous run which was coating the optical windows was sublimed away. Visual examination of the source windows after the run also indicated the existence of a thin coating of CdTe. The occurrence of these layers was not only due to the smaller heat capacity of the crossmember during the cooling down process, but to the postgrowth process also: as shown in figure 5a, the source zone temperatures were controlled in such a way that the temperature of the bottom heater was higher than that of the top one during cool down, in order to unseal the source/crucible aperture, so that in future runs, the ampoule could be safely evacuated. As indicated in figure 5b, once the ampoule was cooled down, it seems that the tellurium vapour pressure remained constant. As discussed previously, this was probably due to the coating effects; on the other hand, the cadmium vapour pressure appeared to reduce to zero, since even a vapour pressure as small as 0.1 mbar results in a loss of signal of at least 60 % (see figures 13 and 14 of chapter 4).

In the actual configuration, it was not possible to precisely determine the source temperature. Ideally, the three zones should be kept at the same temperature, thus ensuring constant sublimation rates and knowledge of the source temperature. However, the pressure monitoring system allows an estimation of the sublimation temperature to be obtained using equations 2.5 of chapter 2, in particular from the tellurium partial pressure. The cadmium partial pressure might be altered due to preferential transport.

The partial pressure ratio P_{Cd} / P_{Te_2} in the source side is shown in figure 6 and is close to two, as one would expect in a semiopen system with viscous flow. Given the

low vapour pressures encountered here and since such low pressures do not permit viscous flow to be fully established, a partial pressure ratio of 2 should not occur if the modelling of chapter 6 is correct. It is important however to realise that the partial pressure ratio of 1.32-2 can only occur once equilibrium in the source side has become established. The source arrangement in the current MPVT system, together with the use in this experiment of different temperatures in different zones probably caused intense sublimation from the top part of the source ampoule, which would tend to condense in the cooler source/crucible aperture rather than transported through the capillary restrictor. Under these conditions, where the "equilibrium" pressures and more precisely the partial pressure ratio is not set by the flow restrictor, the partial pressure ratio would be expected to be 2.

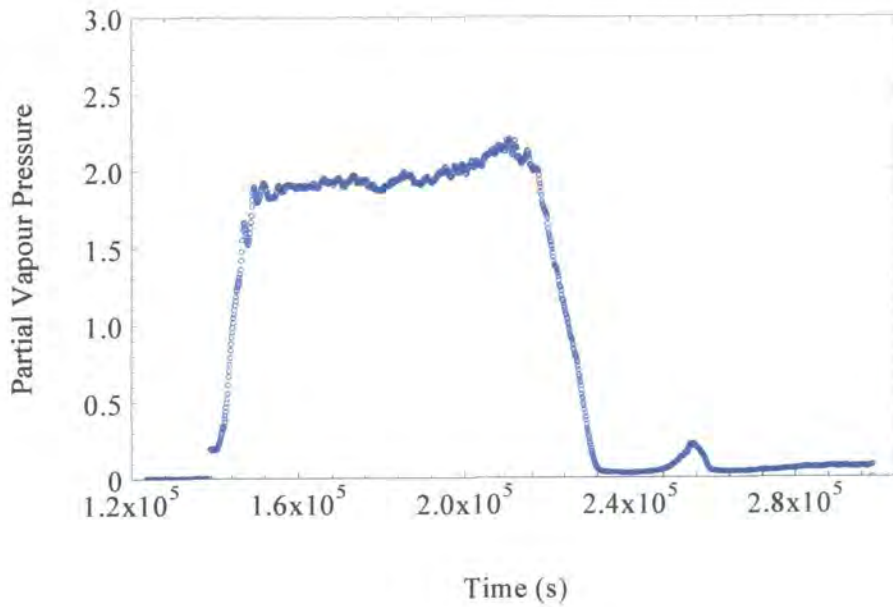

Figure 6. Partial pressure ratio in the source side as calculated from the Cd and Te_2 measured partial pressures during run 25/26.

Several other growth experiments were carried out. Figure 7 shows the temperature profile of run 34. On this occasion, especial care was taken to ensure no

coating of the ampoule optical monitoring windows, by ensuring that the crossmember remained at a higher temperature than the rest of the zones during the cooldown process. Figure 8 shows the partial pressures of Cd and Te_2 throughout the whole experiment. As can be seen, although the temperature of each zone remained constant, the partial pressures of both cadmium and tellurium increased as the growth experiment proceeded. However, this was not a real feature, since in this run, the glass joints in the crossmember were not completely tight and as a result the monitoring windows in the vacuum jacket as opposed to the crossmember became coated with CdTe. This was visible at the end of the run and was confirmed with EDAX by N. M. Aitken. As a result of the progressive coating as growth proceeded, the optical densities were artificially increased, resulting in a fictitious increase of the partial pressures. The final level of the tellurium signal was due to coating of the interior ampoule windows as has been explained before. It is still possible to obtain an idea of the Cd and Te_2 partial pressures by taking the starting portion of the curves in figure 8, where no coating existed yet.

The partial pressure ratio as calculated from the curves in figure 7 is shown in figure 9. As can be seen, the partial pressure ratio at the beginning of the experiment is about ~1.7. This is in agreement with the modelling of chapter 6, were it was seen that a partial pressure ratio between 1.33 and 2 was expected when using a capillary flow restrictor. A partial pressure ratio higher than 1.33 but smaller than 2 denotes that the flow mechanism was of slip type. The increase in the partial pressure ratio is less pronounced than in the case of the actual Cd and Te_2 pressures since as the growth progressed, the "masking effect" of the coating should have affected the optical densities of the Cd and Te_2 lines in approximately equal proportion.

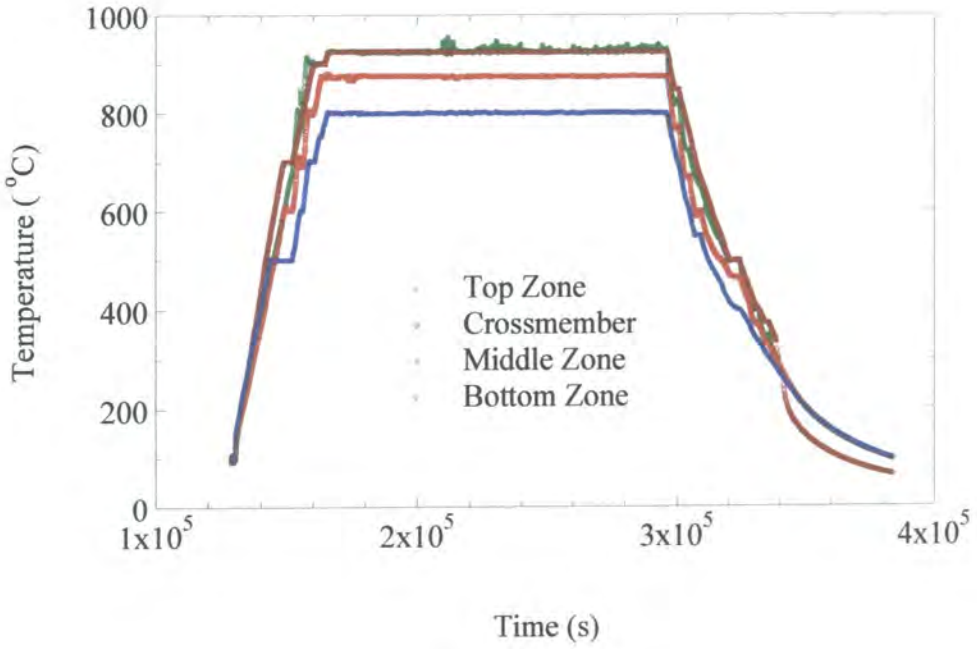

Figure 7. Source zones and crossmember temperatures during run 34.

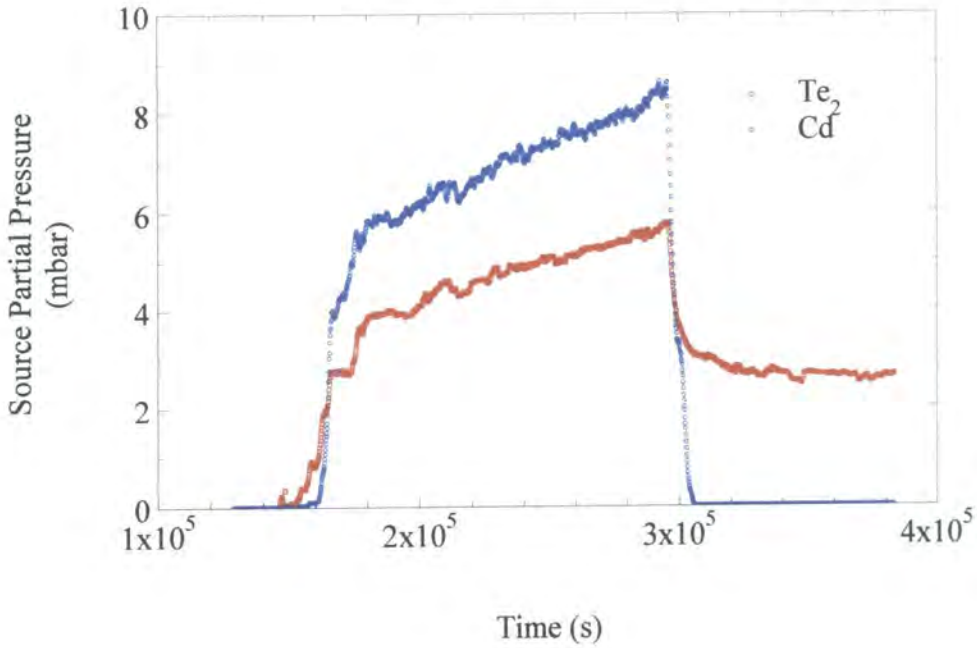

Figure 8. Partial pressures of Cd and Te_2 in the source side during run 34. For an explanation see text.

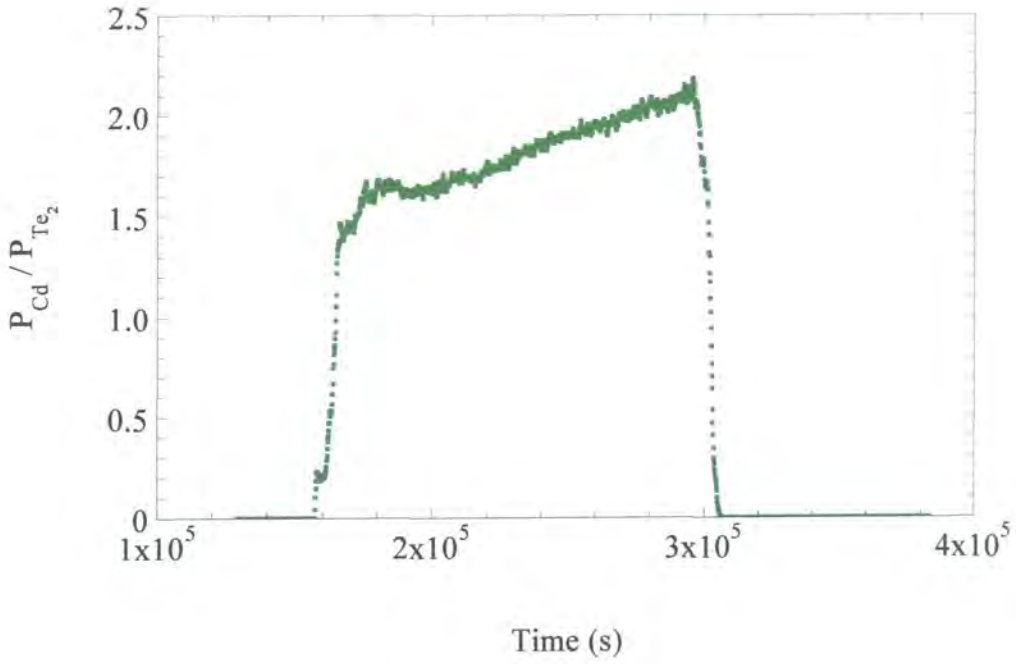

Figure 9. Partial pressure ratio P_{Cd} / P_{Te_2} in the source side during run 34.

The seed temperature at the beginning of the growth run 34 was set to 710 °C. Again, the optical monitoring system in the growth side could not monitor any appreciable vapour pressure, except perhaps for the most sensitive cadmium line. The optical density $D_{326.1}$ was about 0.5, and according to figure 14 of chapter 4, the partial cadmium vapour pressure is about ~ 0.5 mbar. Unfortunately, the predictions obtained in chapter 6 concerning the partial pressure ratio in the growth side cannot be experimentally determined, and more importantly, the degree to which near equilibrium conditions were met during the growth process could not be assessed. However, given that the results obtained in the source side quantitatively agree with the modelling equations, it is expected that a partial pressure ratio close to 1.32 in the growth occurred during the growth.

7.2 DISCUSSION AND CONCLUSIONS.

The optical monitoring data obtained by Dr. J. T. Mullins during growth of CdTe in the MPVT system has been analysed. The vapour pressure optical monitoring is capable of monitoring Cd and Te_2 vapour pressures over the source side, but not in the growth side. It has not been possible to conclude definitively if the vapour pressure over the crystal is set by the temperature of the crystal (in which case, since growth normally takes place at ~700 °C, very low vapour pressures would be expected) or by the flow conductivity of the annular section past the crystal. Obviously, growth at higher seed temperatures should answer this question, although this was not possible at the moment due to technical problems. Correction of the technical problems should allow seeded growth at higher temperatures, and once the vapour pressures at both sides of the restrictor are known, the reliability of the expressions given in chapter 6 may be tested, allowing direct measurement of the growth rate, and once the temperature profile of the growth tube is known, determination of the supersaturation over the crystal. Nonetheless, the fact that the vapour pressure monitoring allowed part of the theoretical modelling of chapter 6 to be tested giving positive results, suggests that the rest of the predictions, particularly the partial pressure ratio in the growth side and the dependency of the transport rate on the pressures, should also be essentially correct.

REFERENCES FOR CHAPTER SEVEN

[1] K. Zanio. *Cadmium Telluride.* Semiconductors and Semimetals Treatise, Volume 13. Edited by R. K. Willardson and A. C. Beer. Academic Press, London (1978).

Chapter Eight

Summary of Conclusions

8.0 SUMMARY OF CONCLUSIONS.

Several diverse lines of research have been presented in this thesis with the aim of improving the growth of high quality, large diameter CdTe crystals from the vapour phase using a new Multi-tube Physical Vapour Transport (MPVT) apparatus.

The MPVT apparatus designed in Durham incorporates several modifications and improvements from previous PVT methods. In particular:

- Growth is based on the seeded Markov Technique which allows crystal growth to take place free from the ampoule walls. This eliminates stresses induced by differential thermal expansion between the ampoule walls and CdTe, which given the low stacking fault energy and critical resolved stress of CdTe is of considerable importance.
- The introduction of the revolutionary U-shaped ampoule serves as a means to decouple temperature control of the source and growth regions, allowing almost independent selection of the source and growth temperature profiles.
- Use of a crossmember is also the key that allows the introduction of a flow restrictor whose flow properties can be modelled accurately hence allowing mass transport control and decoupling of the sublimation and growth processes.
- The crossmember also allows the possibility of using a vapour optical absorption technique as a non-intrusive, *in situ* monitoring partial pressure process control tool.

Other equally important features of the MPVT system include the reusability of the ampoule, the truly semiopen nature of the ampoule, which allows efficient removal

of outgassing and volatile impurities through the use of dynamic pumping and the possibility, not explored in this work of introducing a carrier or inert gas.

This thesis has focused on three main objectives: the study of the optical absorption behaviour of Cd atoms and Te_2 molecules and its application to the measurement of partial pressures during the growth of CdTe in the MPVT system; the quantitative study of the mass transport mechanisms through porous silica discs for use as a mass flow restrictor in the MPVT apparatus, and the global modelling of the flow regimes and mass transport processes in the ampoule under dynamic pumping conditions.

The broad absorption band spectra of Te_2 vapour in the 300-650 nm range and the absorption of the 326.1 nm atomic line in Cd vapour have been extensively studied. It has been shown that optical absorption in any of the wavelengths in the range 470-510 can be used as a non-intrusive tool to measure the partial pressure of Te_2 molecules. Moreover, the relations between Te_2 pressure and absorbance for the 479 and 508 nm have been established. The dependency of the 326.1 nm Cd line absorbance as a function of the Cd pressure has also been established. The non-overlapping of the broad absorption band of Te_2 with the 326.1 nm Cd atomic absorption band for Te_2 pressures lower than 18 mbar allows the partial pressures of Cd and Te_2 over CdTe to be measured simultaneously and independently.

Accordingly, a simple and compact system that uses a Cd hollow cathode lamp as a light source together with a set of suitable interference filters and photodetectors was designed in Durham and used for measurement of Te_2 partial vapour pressures in

the range 0.1 – 18 mbar and of Cd partial vapour pressures in the range 0.01 – 20 mbar over CdTe in the MPVT apparatus. The nature of the apparatus calls for the need of calibration curves (optical density versus vapour pressure). In particular, it has been shown that the 479 and 508 nm Te_2 absorption lines approximately follow the BBL law of absorption, meanwhile the 326.1 nm Cd atomic absorption line does not follow it, as expected (see figures 13 and 14 of chapter 4).

The flow conductivity of porous silica discs as an alternative to capillaries for use as mass transport restrictors during CdTe vapour growth in the MPVT system was studied. In particular, the flow of several gases with a broad range of molecular weights through a silica disc has been studied as a function of the gas and disc temperatures. More importantly the pressure dependency of the gas flow has been quantified both theoretically and experimentally with good agreement. It has been shown that the intrinsic nature of the porous disc sets the flow regime and hence the dependency of the transport rate on pressure as predicted by the Kozeny-Carman equation of flow.

Quantitative analysis using theoretical expressions is used to understand how the flow regime influences the partial pressure ratio of the elemental vapour constituents in a Cd and Te_2 vapour mixture. In particular, it has been shown that for normal vapour growth temperature and vapour pressure conditions the flow regime through the restrictor can be considered to be of slip type only. This has great consequences for the partial vapour pressure ratio over the source, where the ratio P_{Cd} / P_{Te_2} is not 2 as expected but adopts, once equilibrium is established, a value of 1.32. Experiments done in order to confirm this agree with the theoretical predictions.

The porous silica disc replaces the need for a temperature gradient between source and growth locations, since the driving force to transport the vapour is provided by the pressure difference across the silica disc provided by dynamic pumping from the growth side. Modelling of mass transport through a silica disc as a function of its intrinsic parameters and the extrinsic parameters can be used to estimate mass transport rates. The modelling can be used to choose the dimensions of the silica porous disc appropriate to the growth of CdTe in the MPVT apparatus.

The modelling of mass transport rates through a porous silica disc has been extended and applied to the study of the mass transport processes in the MPVT apparatus. Theoretical expressions available from the literature have been used to predict both the influence of the mass flow restrictor in the crossmember (disc or capillary) and the existence of the annular gap past the crystal holder on the mass transport rate, the growth rate and the partial pressure ratio in the source and growth sides. In particular, the model predicts a P_{Cd} / P_{Te_2} ratio in the range 1.32-2 over the source and of 1.32 over the crystal (the latter assuming that the vapour pressure in the growth side is not set by the crystal itself).

Analysis of the little experimental data available as obtained using the optical absorption vapour pressure monitoring system in the MPVT apparatus has shown that the partial pressure ratio in the source side has a value within the range predicting by the flow model. However, the partial pressure ratio in the growth side could not be monitored due to the low growth temperatures used and to the technical problems encountered when trying to obtain higher growth temperatures. Consequently, the

predictions on the mass transport rate, growth rate and yield obtained in the flow model remain for future work.

In conclusion, the MPVT apparatus for CdTe growth, and in particular the mass transport process is well understood. This has been possible largely thanks to the optical absorption monitoring technique used. The conclusions and findings of this thesis should permit future research efforts to be focused on the implementation of the MPVT for CdTe substrate production. In particular,

- The quantitative study of porous silica discs should be used to model mass transport in order to optimise the growth rate in practice and obtain growth under controlled conditions.
- The predictions of the flow modelling of the Multi-tube PVT in chapter seven should be further tested and verified against growth experiments, specially for several growth temperatures.
- The use of another absorption Cd line that behaves more linearly against cadmium vapour pressure, like the 228.8 nm UV line, should be investigated.
- Further partial vapour pressure monitoring experiments should be done in order to obtain for the first time the true supersaturation of the growing crystal as well as to investigate the influence of the vapour stoichiometry on the crystal stoichiometry.

Finally, the possibility of using several source tubes containing II-VI binary compounds in order to grow ternary II-VI compounds should be studied. The resulting *"octopus-like"* PVT system should, with the help of several porous silica restrictors (and not capillaries) be able to produce highly uniform ternary and multinary II-VI compounds.

APPENDIX A

A qualitative estimation of the maximum temperatures within different parts of the crystal that can be tolerated during growth in order to avoid the associated thermal stress can be obtained if plastic behaviour is assumed. Mathematically, the formulation for stress free conditions in a crystal is[1]

$$\nabla^2 T = \frac{\partial^2 T}{\partial x^2} + \frac{\partial^2 T}{\partial y^2} + \frac{\partial^2 T}{\partial z^2} = 0 \qquad \text{(A1)}$$

and hence when the temperature gradients in all co-ordinates are linear, the thermal stress associated is zero, since the crystal only experience free temperature bending[1]. Normally, there is at least one co-ordinate that has a non lineal temperature gradient, which results in an associated stress. An idea of the maximum temperature difference allowed in order to avoid such a stress exceeding the *CRSS* for CdTe can be obtained using the Young's modulus *E*, defined as *E = Stress / Strain,*

$$\Delta T \leq \frac{CRSS}{E\alpha} \qquad \text{(A2)}$$

since the thermal strain is $\delta l / l = \alpha \Delta T$. The modulus *E* does not change much with temperature[2]. The lineal thermal expansion coefficient, as given by 2.8 in chapter 2 also can be considered constant at temperatures above room temperature. Using the values given for E, α and *CRSS* given in section 2.1.2 it can be seen that at room temperature, in order to avoid creation of dislocations,

---

[1] J. Völkl. *"Stress in a Cooling Crystal"*, in *Handbook of Crystal Growth*, volume 2b. Edited by D.T.J. Hurle. North-Holland, Amsterdam (1994).

[2] G. G. Gadzhiev, Sh. M. Ismailov and A. I. Dadashev. *"Thermal Properties of Ceramics Based on $A^{II}B^{VI}$ Compounds.* High Temperature, **3** (1993) 468.

$$\Delta T \leq 20K$$

and for growth temperatures in the range 1000- 1200 K, and since the *CRSS* decreases about one order of magnitude,

$$\Delta T \leq 2K$$

From the above, rather simple, analysis it can be seen that temperature differences as little as ~ 2 K can produce an associated stress that can exceed the *CRSS*, hence allowing dislocations to multiplicate. Although the above is a rough estimation, and more precise calculations should be done where possible, temperature differences (specially radial) between different zones of the crystal should be minimised.

APPENDIX B

The importance of the source stoichiometry was discussed in chapter 2. Here, a simple calculation that delineates the ultimate attainable stoichiometry of the source as determined by the accuracy of the molecular weight (limited by the different abundance of different isotopes) is given. According to the latest available data[1], the atomic weights of cadmium and tellurium are,

$$\begin{aligned} M_{Cd} &= 112.411 \pm 0.008 \\ M_{Te} &= 127.60 \pm 0.03 \end{aligned} \qquad \text{(gm)}$$

and hence, the minimum uncertainties in weighing are,

$$\begin{aligned} \delta x_{Cd} &= 7.1167 \times 10^{-3}\% \\ \delta x_{Te} &= 2.3511 \times 10^{-2}\% \end{aligned}$$

which correspond to 71 and 235 ppm for Cd and Te respectively. It can be seen that the margin of allowed weighing errors is quite broad. In fact, for large source charges, an accuracy of a tenth of a gram might be enough for tellurium, for example, since any further accuracy would not guarantee a perfect stoichiometry. Given the above levels of uncertainty, figures 6a and 6b in chapter 2 can now be fully appreciated. Although nominal stoichiometry might be achieved, there is a fundamental limit to the achievable accuracy due to the uncertainty in the atomic weights as shown above. In addition, there will be errors and uncertainties due to the presence of oxide monolayers[2] on the surface.

Since the partial pressure ratio and transport rates can vary by several orders of magnitude with stoichiometry variations of the order calculated above, closed ampoule techniques are obviously not a good choice for quantitative growth rate studies.

---

[1] *Pure & Appl. Chem.* **60** (1988) 841.
[2] M. M. Faktor and I. Garret. *Growth of Crystals from the Vapour.* Chapman & Hall, London (1974).

Publications and Conference Attendances During the Course of This Work

Publications

1.- J. Carles, J. T. Mullins and A. W. Brinkman. *"Partial Pressure Monitoring in CdTe Vapour Growth"* published in the Journal of Crystal Growth, 1997, Vol. 174 p.740-745.

2.- J. T. Mullins, J. Carles and A. W. Brinkman. "*High Temperature Optical Properties of CdTe*", published in the Journal of Applied Physics, 1997, Vol. 81, p.6374-6379.

3.- University of Durham.UK Patent Application No. 9717726.5 *"Improvements in and related to Crystal Growth"*.

4.- N. M. Aitken, M. D. G. Potter, J. T. Mullins, J. Carles, D. P. Halliday, K. Durose, B. K. Tanner and A. W. Brinkman *"Characterisation of Cadmium Telluride Bulk Crystals Grown by a Novel "Multi-tube" Vapour Growth Technique"* submitted to the Journal of Crystal Growth.

5.- J. T. Mullins, J. Carles, N. M. Aitken and A. W. Brinkman. *"A New Multi-tube Vapour Growth Apparatus and Its Application to CdTe Growth"* in preparation.

6.- J. Carles, J. T. Mullins and A. W. Brinkman *"Vapour Flow through Porous Silica at Elevated Temperatures"* in preparation.

Conferences and Seminars

The 7th International Conference on II-VI Compounds, August 1995, Edinburgh, UK

II-VI UK Interaction Meeting, March 1996, Durham, UK. *"Vapour Pressure Monitoring by Optical Absorption"* J.Carles.

Materials and Crystal Growth Seminar, NASA Marshall Space Flight Center, Space Sciences Laboratory, August 1996, Hunstville, AL. "*The Optical Monitoring of Cd and Te_2 Vapour Partial Pressures and the Optical Properties of CdTe at Elevated Temperatures*". J.Carles, J.T.Mullin and A.W.Brinkman.

ACCG-10/ICVGE-9. The Tenth American Conference on Crystal Growth and The Ninth International Conference on Vapour Growth and Epitaxy, August 1996, Vail, CO.

MRS 1997 Fall Meeting. December 1997, Boston, MA.